Aachener Verfahrenstechnik Series
AVT.CVT – Chemical Process Engineering
Volume 44 (2024)

Tobias Harhues

Process Integration and Intensification of Electrochemical Reactions for Biomass Valorization

DOI: 10.18154/RWTH-2024-06302

Process Integration and Intensification of Electrochemical Reactions for Biomass Valorization

Prozessintegration und -intensivierung von elektrochemischen Reaktionen zur Verwendung von Biomasse

Von der Fakultät für Maschinenwesen
der Rheinisch-Westfälischen Technischen Hochschule Aachen
zur Erlangung des akademischen Grades
eines Doktors der Ingenieurwissenschaften
genehmigte Dissertation

vorgelegt von

Tobias Harhues

Berichter:
Univ.-Prof. Dr.-Ing. Matthias Wessling
Assoc. Prof. Dr.Ir. David A. Vermaas

Tag der mündlichen Prüfung: 13.06.2024

Diese Dissertation ist auf den Internetseiten der Universitätsbibliothek online verfügbar.

Parts of this thesis have been published. Reproduced with permission from:

Tobias Harhues, Lukas Portheine, Cathleen Plath, Joern Viell, Robert Keller, Jochen Büchs, and Matthias Wessling
Direct Electrosynthesis of 2-Butanone from Fermentation Supernatant, acs sustainable chemistry & engineering, 2022 DOI: 10.1021/acssuschemeng.2c01971

Carolin Grüntering, Tobias Harhues, Fabian Speen, Robert Keller, Martin Zimmermann, Peter R. Jensen, Matthias Wessling and Lars M. Blank
Acetoin production by resting cells of Lactococcus lactis for direct electrochemical synthesis of 2-butanone, Green Chem., 2023, DOI: 10.1039/D3GC02513F

Tobias Harhues, Maria Padligur, Franziska Bertram, Daniel Matthias Roth, John Linkhorst, Andreas Jupke, Matthias Wessling and Robert Keller
Integrated Biphasic Electrochemical Oxidation of Hydroxymethylfurfural to 2,5-Furandicarboxylic Acid, ACS Sustainable Chem. Eng., 2023, 11, 23 8413-8419 DOI: 10.1021/acssuschemeng.3c01403

Titel: Process Integration and Intensification of Electrochemical Reactions for Biomass Valorization
Prozessintegration und -intensivierung von elektrochemischen Reaktionen zur Verwendung von Biomasse

Autor: Tobias Harhues

Reihe: Aachener Verfahrenstechnik Series
AVT.CVT - Chemical Process Engineering
Volume: 44

Herausgeber: Aachener Verfahrenstechnik
Forckenbeckstraße 51
52074 Aachen
Tel.: +49 (0)241 8095470
Fax.: +49 (0)241 8092252
E-Mail: secretary.cvt@avt.rwth-aachen.de
http://www.avt.rwth-aachen.de/AVT

Volltext verfügbar: 10.18154/RWTH-2024-06302

Acknowledgement

Die fünf Jahre, die es brauchte, um diese Dissertation zu vollenden, waren eine auf vielen Ebenen herausragende Zeit. Ich blicke zurück auf vielfältige Aufgaben und Herausforderungen, die durch äußere Umstände wie die pandemiebedingten Einschränkungen nicht unbedingt leichter wurden. Dass ich diese schlussendlich bewältigen konnte, verdanke ich zu einem großen Teil den Menschen, die mich auf diesem Weg begleitet haben.

Zunächst möchte ich meinem Doktorvater, Prof. Matthias Wessling, danken, der mir vor mehr als 5 Jahren das Vertrauen geschenkt und im Anschluss die Freiheit gelassen hat, meine Ideen zu verwirklichen und an den Herausforderungen zu wachsen. Außerdem möchte ich meinem Zweitprüfer Prof. David A. Vermaas danken, der meine Dissertation wohl strenger unter die Lupe genommen hat als viele andere.

Ich danke der DFG, die meine Forschung im Excellenzcluster „*Fuel Science Center*“ gefördert hat und viele Kooperationen ermöglicht hat. Den Kooperationspartnern innerhalb des FSCs und außerhalb möchte ich für den Austausch danken.

Eine wichtige Säule in meiner Forschung waren die mehr als 30 Studierenden, die ich in verschiedenen Arbeiten und Projekten betreuen durfte. Ohne eure Hands-On Forschung wäre der Inhalt meiner Arbeit wohl nicht so zustande gekommen.

In den vergangenen fünf Jahren haben mich zudem viele Kolleginnen und Kollegen begleitet. Ihr habt mich erst an der CVT willkommen geheißen haben dann meine Forschung fachlich mit lebhaften Diskussionen sowie meinen Alltag an der CVT freundschaftlich bereichert. Hier möchte ich insbesondere meinen langjährigen Bürokolleginnen und Kollegen Anna, Maria, Mojtaba, Yannick und später Jan und Matthias danken. Natürlich auch allen anderen, meinen FSC-Kollegen Alexander und Nils, dem ZAL Team und Susi, die mich alle bei verschiedensten Aufgaben unterstützt haben. Außerdem Robert, der seinen vielen Aufgaben zum Trotz immer wieder Zeit für meine Fragen gefunden hat.

Neben dem Kollegium möchte ich meiner Familie danken. Ihr habt mich schon im Studium, aber auch den darauf folgenden Zeiten unterstützt und wart immer für mich da. Darüber hinaus möchte ich meinen Freunden danken, insbesondere Dominik. Ihr habt meine Erfolge mit mir geteilt, mir Ausgleich verschafft und meine Misserfolge ertragen. Zu guter Letzt möchte ich noch Sarah danken. Du hast mir in leichten und schweren Zeiten Halt und Unterstützung gegeben und ohne dich hätte ich die vergangene, intensive Zeit nicht überstanden.

Contents

Abstract

The consumption of fossil resources as the carbon feedstock for the chemical industry is a major source of the global CO_2 emissions that can be counteracted by replacing fossil carbon with sustainable sources such as hemicellulosic biomass. However, the replacement requires novel processes and, in part, products that have been proposed with the concept of the biorefinery. Yet, these processes do not include electrochemical conversion methods, as research on electrochemical reactions has mostly been limited to the catalyst and reactor levels. Their implementation into process chains still needs to be demonstrated.

This work aims to integrate electrochemical processes into two process chains to yield 2,5-furandicarboxylic acid (FDCA) and 2-butanone. It reveals the possibility of eradicating intermediate purification steps when integrating electrochemical conversion with the preceding chemocatalytic or microbial processes. Additionally, a structured approach towards paired electrolysis for biomass valorization is presented and implemented to combine the two reactions and show the potential to increase the energy efficiency of paired electrolysis.

For the reduction of acetoin to 2-butanone, the fermentation supernatant from the microbial synthesis of acetoin was directly used as the electrolyte without intermediate purification. The pH in the electrochemical cell was adapted to the fermentation supernatant, which resulted in a yield of 45%. To increase the yield further, the fermentation was carried out in a minimal medium, leading to a yield of above 50% 2-butanone in the electrochemical conversion step. Similarly, for the synthesis of FDCA, hydroxymethylfurfural (HMF) was supplied to the electrochemical cell via the organic product mixture of its synthesis. In the cell, it was oxidized to FDCA in the biphasic electrolytic system with a yield of over 70%. A so-called swiss roll reactor increased the space-time yield by more than one order of magnitude compared to a planar reactor at only very little loss of yield. Lastly, a structured approach to pair the two electrochemical reactions was developed. A a stable process could be established through the choice of a bipolar membrane and appropriate reaction conditions. The product concentration could be increased to industrially relevant values of up to 0.5 mol L^{-1} FDCA and 2-butanone at a yield above 90% for FDCA and 35% for 2-butanone at a current density of 150 mA cm^{-2}.

With the integration of the electrochemical processes with chemocatalytic and microbial process steps, this work demonstrates that electrochemical reactions can be integrated into process chains to valorize biomass. Moreover, electrochemical processes offer the possibility to mitigate intermediate purification and increase the efficiency of the process chain. The intensification of these reactions through paired electrolysis can further increase process efficiency so that the products and processes based on sustainable carbons can contribute to the defossilization of the chemical industry.

Zusammenfassung

Fossiler Ressourcen als Kohlenstoffquelle der chemische Industrie sind eine der Hauptursachen der weltweiten CO_2-Emissionen. Der Austausch von fossilen durch nachhaltigen Kohlenstoffquellen wie hemizellulosehaltige Biomasse kann diese drastisch reduzieren. Dafür sind neuartige Verfahren und Produkte notwendig, die sich im Konzept der Bioraffinerie bündeln. Darin finden sich aber keine elektrochemischen Umwandlungsmethoden, da die Forschung zu elektrochemischen Reaktionen bisher auf Katalysator- und Reaktorebene beschränkt ist.

Diese Arbeit beschreibt die Integration elektrochemischer Prozesse in zwei Prozessketten zur Herstellung von 2,5-Furandicarbonsäure (FDCA) und 2-Butanon. Sie zeigt, dass durch die Integration mit vorangehenden chemokatalytischen oder mikrobiellen Prozessen Aufreinigungsschritte in den Prozessketten eliminiert werden können. Darüber hinaus wird ein strukturierter Ansatz für die gepaarte Elektrolyse zur Verwertung von Biomasse entwickelt und umgesetzt. Diese demonstriert das Potential zur weiteren Steigerung der Energieeffizienz der elektrochemischen Prozesse.

Für die elektrochemische Reduktion von Acetoin zu 2-Butanon wurde der Fermentationsüberstand aus der mikrobiellen Synthese von Acetoin direkt als Elektrolyt verwendet. Der pH-Wert im Elektrolyseur wurde an den Fermentationsüberstand angepasst, womit eine Ausbeute von 45% erreicht wurde. Anschließend wurde die Fermentation in einem Minimalmedium durchgeführt, um die Ausbeute der elektrochemsichen Reduktion weiter zu erhöhen, die daraufhin auf über 50% gesteigert werden konnte. Zur Synthese von FDCA wurde Hydroxymethylfurfural (HMF) über die organische Produktphase aus der HMF Synthese ohne Aufreinigung genutzt. In der Zelle konnte einem zweiphasigen Elektrolysesystem eine Ausbeute von über 70% erreicht werden. Ein Swiss-Roll-Reaktor erhöhte die Raum-Zeit-Ausbeute um mehr als eine Größenordnung im Vergleich zu einem planaren Reaktor bei sehr geringen Ausbeuteverlusten. Schließlich wurde ein strukturierter Ansatz zur Paarung der beiden elektrochemischen Reaktionen entwickelt. Nach der Etablierung eines stabilen Prozesses durch die Wahl einer bipolaren Membran und geeigneter Reaktionsbedingungen konnte die Reaktantenkonzentration auf industriell relevante Werte von bis zu 0.5 mol L^{-1} FDCA und 2-Butanon bei einer Ausbeute von über 90% für FDCA und 35% für 2-Butanon bei einer Stromdichte von 150 mA cm^{-2} erhöht werden.

Durch die Integration der elektrochemischen Prozesse mit der Synthese der Edukte zeigt diese Arbeit, das Potential von elektrochemische Reaktionen in Prozessketten zur Verwertung von Biomasse. Darüber hinaus konnte diese Arbeit zeigen, dass elektrochemische Prozesse die Möglichkeit bieten, Zwischenreinigungen zu umgehen und so die Effizienz der Prozesskette zu erhöhen. Die Prozessintensivierung durch gepaarte Elektrolyse kann die Energieeffizienz weiter erhöhen, so dass die auf nachhaltigen Kohlenstoffen basierenden Produkte und Prozesse zur Defossilisierung der chemischen Industrie beitragen können.

1 Introduction

Climate change is among the mayor threats for our society today and the chemical industry is a major contributor to the still rising CO_2 emissions that fuel the man-made increase in global temperatures [Meys2021]. To reduce the CO_2 emissions, fossil carbon and energy sources have to be replaced with net-zero alternatives. This can be achieved by harvesting renewable energy sources such as wind and solar and replace the fossil carbon feedstock with sustainable carbon sources [Wint2022]. While current research is often focused on carbon capture and utilization technologies (CCU) for the future, the utilization of biomass poses a readily available carbon alternative as biomass binds CO_2 from the atmosphere through photosynthesis. As depicted in Figure 1.1, the ultimate release of the carbon from biomass as CO_2 does not contribute to an increasing CO_2 concentration in the atmosphere since the carbon cycle is closed. Notably, the prospective demand for renewable carbon in the chemical industry surpasses the availability of biomass, so that CCU will be inevitable in the future. In the meantime, conversion of biomass in efficient processes that provide a high yield and conversion of the renewable carbon available is required [Shin2020]. Additionally, supply of renewable energy remains a limiting factor for the near future so that energy efficiency is crucial for biomass conversion processes [Bidd2023]; [Meys2021].

Electrochemical processes have the potential to achieve efficient biomass conversion. They utilize electrical energy directly as the driving force for the conversion and can operate at ambient temperature and pressure, which leads to a potentially low energy demand. Additionally, they have the potential for highly selective reactions through catalyst design and power control [Schm2003]. A further increase in efficiency

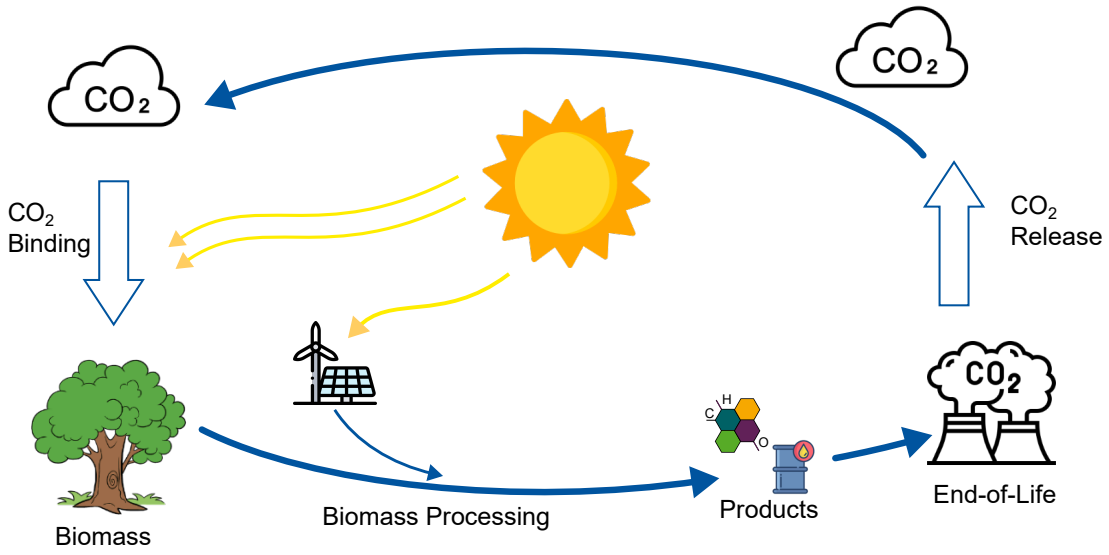

Figure 1.1: Closed carbon cycle based on renewable carbon from biomass valorization powered by renewable energy.

can be achieved through process integration and intensification. On the one hand side, process integration can be conducted on a horizontal level to mitigate energy intense and loss-associated intermediate purification steps. On the other hand, process intensification can be introduced on a vertical level, interlinking two complementing processes, in case of electrochemical processes via paired electrolysis of an oxidation and a reduction reaction. Yet, research in the field of electrochemistry often focuses on catalyst development and reaction optimization in ideal systems under ideal conditions [Tanb2020]. While fundamental research is invaluable, it leaves a wide gap towards its application. To bridge this gap and drive electrochemical biomass valorization towards its application, findings from research need to be incorporated in processes and process chains. Therefore, they need to be operated under realistic conditions and feature a high degree of integration, ideally coupling consecutive process steps. Further, downstream processing has to be considered when arranging these reactions, which calls for high product concentrations and high degree of conversion.

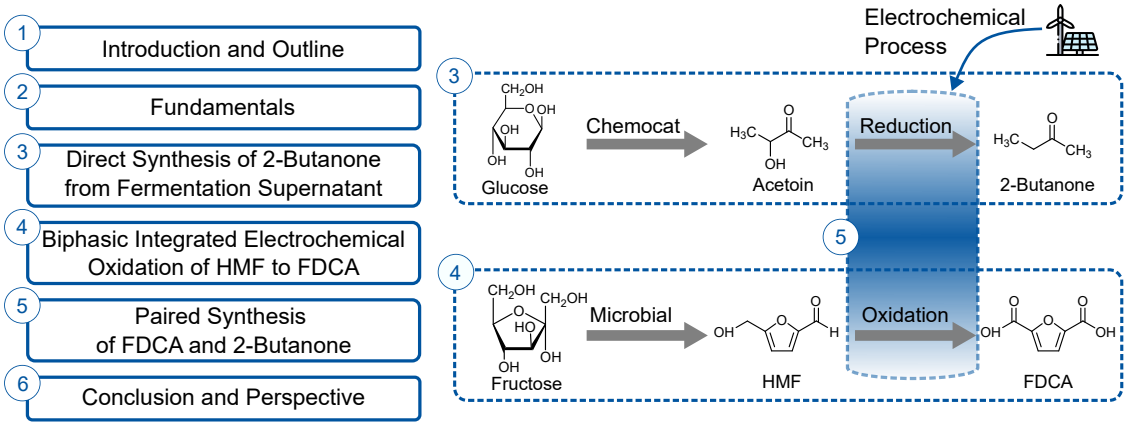

Figure 1.2: Outline of this thesis with its respective chapters.

Scope and Outline of the Thesis

This thesis aims to push electrochemical processes for biomass valorization towards their application in highly integrated and efficient processes along the process chains from fructose to 2,5-furandicarbioxylic acid (FDCA) and glucose to 2-butanone, as depicted in Figure 1.2.

Chapter 2 presents the governing principles in an electrochemical cell and presents the characteristics of biobased carbon sources in the context of the biorefinery. It closes with an overview on the reactions and processes within the biorefinery concept, and the process chains and products FDCA and 2-butanone, this thesis is concerned with.

Chapter 3 presents the horizontal process integration of the microbial fermentation from glucose to acetoin and its electrochemical reduction to 2-butanone. The chapter showcases how the integration can mitigate the need for intermediate purification from the complex fermentation broth. Subsequently, it highlights how the fermentation can be modified to increase the overall process yield and efficiency.

Chapter 4 demonstrates horizontal process integration of the synthesis of 5-hydroxymethylfurfural (HMF) from glucose and its subsequent electrochemical oxidation to FDCA in a biphasic process. The biphasic process mitigates intermediate purification and simultaneously protects the reactive intermediate from degradation. Subsequently, two different tubular reactors with different electrode geometries are introduced to increase mixing and

active surface area in the reactor.

Chapter 5 presents a structured approach to integrate the individual electrochemical reduction and oxidation reaction to 2-butanone and FDCA in a paired electrolysis process. It showcases the impact of the membrane on the paired electrochemical process and subsequently moves the process towards industrially relevant conditions.

Chapter 6 summarizes the results of the previous chapters and underlines the most important findings. It gives a perspective on how electrochemical reaction engineering can be integrated successfully into the toolkit of the biorefinery towards the efficient valorization of biomass in a closed carbon cycle.

The content of this thesis and the results presented therein originate in part from student theses that have been supervised by Tobias Harhues within in his position as a research assistant and PhD candidate at the Chair of Chemical Process Engineering:

- Lukas Portheine, bachelor thesis, 2021, Continuous synthesis of acetoin to 2-butanone from a fermentation broth - an integrated approach
- Cathleen Plath, master thesis, 2021, Electrochemical bio-hybrid fuel production – from batch to continuous synthesis of acetoin to 2-butanone
- Prasath Paskaran, bachelor thesis, 2022, Integrated electrochemical synthesis of the bio-hybrid fuel 2-butanone from fermentation supernatants - Characterization of the influence of different fermentation media
- Johanna Güttler, bachelor thesis, 2021, Biphasic reaction system for the electrochemical synthesis of 2,5-furandicarboxylic acid
- Katharina Weis, bachelor thesis, 2022, Scale-up of the biphasic electrochemical synthesis of 2,5-Furandicarboxylic acid from 5-Hydroxymethylfurfuran
- Benjamin Zemlin, master thesis, 2022, Design and performance analysis of a tubular reactor for the biphasic electrochemical oxidation of 5-hydroxymethylfurfural to 2,5-furandicarboxylic acid
- Max Horn, bachelor thesis, 2022, Parameter study of a biphasic electrochemical reaction system for the synthesis of 2,5-furandicarbooxylic acid from hydroxymethylfurfural
- Saskia Inge Sabine Fischer, master thesis, 2022, Reactor design for the simultaneous electrochemical production of 2-butanone and 2,5-furandicarboxylic acid
- Hasan Erguvan, master thesis, 2023, Simultaneous electrosynthesis of 2-butanone and 2,5-furandicarboxylic acid from biobased resources

1

2 Fundamentals in Electrochemical Biomass Valorization

2.1 Electrochemical Processes

Electrochemistry describes the phenomena that revolve around the conversion of electrical energy into chemical energy and vice versa. One way to classify electrochemical processes is by the direction of energy transfer. When chemical energy is converted into electrical energy as for example when discharging batteries, these processes are called galvanic processes. When electrical energy is converted to chemical energy, these processes are called electrolytic [Schm2003]; [Pere2016]. This thesis describes the refinement of biobased chemicals with the utilization of electrical energy. Therefore, only electrolytic reactions, also called electrolysis, and the accompanying processes are elaborated further. This chapter presents the fundamentals of electrochemical reactions, reactors, and the governing phenomena within. A separate section is reserved for membranes in electrochemical reactors as they are of particular interest in this thesis.

2.1.1 Electrochemical Reactions

Electrochemical reactions are the centerpiece of electrochemical processes. The conversion of electrical into chemical energy in these reactions requires the transfer of charge, which comprises an electron and an ion transfer. The transfer of electrons is conducted by an external conductor circuit and ions are transferred through an electrolyte. In electrolytic reactions, the driving force necessary for this reaction is supplied via the electrons as a voltage, ions close the electrical circuit. In contrast to conventional redox reactions, the distinct charge transfer spatially separates the oxidation and the reduction reaction. Nevertheless, the oxidation and the reduction reaction are still coupled by the amount of charge transferred.

The equation for such a reaction pair is given below:

$$\text{Reduction:} \quad Ox + ze^- \rightarrow Red \tag{2.1a}$$

$$\text{Oxidation:} \quad Red \rightarrow Ox + ze^- \tag{2.1b}$$

Here, *Red* is a reduced component, Ox is an oxidized component, and z is the number of electrons exchanged in the individual reaction. Obviously, the real species are usually different in the oxidation and the reduction reaction. Each reaction exhibits a change in Gibbs free energy. Its relation to a potential in the equilibrium state, in which no current is flowing, can be expressed through the Nernst equation [Schm2003], presented for the reduction reaction from 2.1a:

$$E_{Red} = E_{Red,0} - \frac{RT}{zF} - ln(\frac{a_{Red}}{a_{Ox}}) \tag{2.2}$$

E_{Red} is the resulting potential of the reduction reaction and $E_{Red,0}$ is the standard potential of the reaction at standard conditions. *R* is the universal gas constant, T the temperature, and F the Faraday constant. The activities a_{Red} and a_{Ox} are the activities of the oxidized reactant and the reduced product. The equilibrium potential E for the coupled oxidation and reduction reaction is the sum of the two half-cell potentials E_{Ox} for the oxidation and E_{Red} for the reduction reaction in Equation 2.1a. When no current is flowing, it is also called the open circuit potential (OCP).

$$E = E_{Ox} + E_{Red} \tag{2.3}$$

In case of electrolytic reactions, the overall potential is negative, which describes a non-spontaneous reaction with a positive change in Gibbs energy. While the potential of an individual reaction can be calculated theoretically, it can only be measured to a reference. To compare different potentials measured, half-cells with defined potentials have been developed [Smit2007]. The most prominent example is the Standard Hydrogen Electrode (SHE), which describes the potential of the hydrogen evolution reaction (HER) in equation 2.4 at an hydrogen pressure of 1013 hPa and a

proton concentration of 1 mol L^{-1} on a platinum electrode.

$$2\,\mathrm{H}^{+} + 2\,\mathrm{e}^{-} \longleftrightarrow \mathrm{H}_2 \tag{2.4}$$

However, these standard conditions are hard to realize in a practical setup. Therefore, the normal hydrogen electrode (NHE) is defined with a concentration of HCl of 1 mol L^{-1} and ambient conditions. The difference can be calculated via the Nernst equation but is negligible for most applications. A common alternative is the reversible hydrogen electrode (RHE), which describes the potential of the HER at ambient conditions and the apparent pH of the electrolyte. Thus, the potential is pH dependent. At 25 °C, the Nernst equation for the RHE can be simplified to:

$$E_{RHE} = E_{SHE} - 0.059\,V \cdot \mathrm{pH} \tag{2.5}$$

Calculations from the Nernst equation are valid for the equilibrium, when no current is flowing. However, when a current is applied, the measured potential deviates. The relation of the potential difference to the current density can be calculated via the Bulter-Volmer or the Tafel equation [Schm2003]; [Tafe1905]. It is particularly relevant when modeling electrochemical reactions but as such, it is beyond the scope of this thesis.

Apart from the electrical approach, electrochemical reactions can be described analogously to conventional chemical reactions. Figures of merit for the efficiency of reactions can be derived from reactant concentrations. Analogue to conventional reactions, the efficiency of electrochemical reactions can be evaluated by similar key indicators. These are the conversion of the reactant (X), the selectivity of a specific reaction (S), and the yield of a reaction or process (Y).

$$X = \frac{n_{i,0} - n_i}{n_{i,0}} \tag{2.6a}$$

$$S_P = \frac{n_{Product} - n_{Product,0}}{n_{Reactant,0} - n_{Reactant}} \cdot \frac{|\nu_{Reactant}|}{|\nu_{Product}|} \tag{2.6b}$$

$$Y = X \cdot S_P = \frac{|\nu_{Reactant}|}{|\nu_{Product}|} \cdot \frac{n_{Product} - n_{Product,0}}{n_{Reactant,0}} \tag{2.6c}$$

Additionally, a key indicator to describe the selectivity of the charge supplied to the reaction can be derived. Therefore, Faraday's law relates the amount of substances to the charge exchanged in the reaction in Equation 2.7. Here, *n* is the amount of product, *Q* is the amount of charge, *z* the number of electrons involved in the reaction according to the reaction equation, and *F* the Faraday constant [Schm2003]; [Bard2000].

$$n = \frac{Q}{z \cdot F} \tag{2.7}$$

The comparison of the charge ($Q_{product}$) that would have been necessary for a certain amount of product ($n_{product}$) to the overall charged passed in the reaction (Q_{total}) yields the Faraday efficiency (FE) :

$$FE = \frac{Q_{product}}{Q_{total}} = \frac{z \cdot n_{product} \cdot F}{Q_{total}} \tag{2.8}$$

Faraday's Law further allows to calculate the amount of charge necessary to potentially convert all reactants submitted in a batch reaction. When a constant current I is applied, Equation 2.8 can be rearranged to yield the time t_{FC}, at which sufficient charge for a full conversion has been supplied:

$$t_{FC} = \frac{(c \cdot V) \cdot z \cdot F}{I} \tag{2.9}$$

In the batch reaction, c is the initial concentration of the reactant, V is the electrolyte volume, z is the number of electrons transferred in the reaction according to the reaction equation, and F the Faraday constant.

All figures of merit described above are heavily influenced by various parameters beyond the reaction. Many of these, such as kinetics, mass transport, and stability are governed by the conditions in the electrochemical reactor, which is subject of the following section [Schm2003].

2.1.2 Electrochemical Reactors

Electrochemical reactions take place in electrochemical cells, the centerpiece of every electrochemical reactor. Figure 2.1 depicts the sketch of an electrochemical cell and its key components.

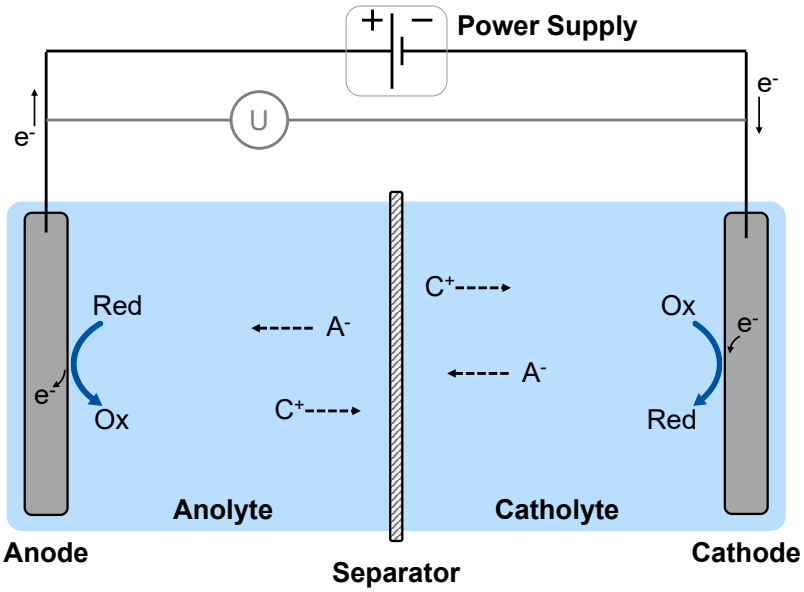

Figure 2.1: Schematic of a divided electrochemical cell and the main components depicted with the reaction from Equation 2.1. The electrolyte is divided by a separator into the anolyte at the anode and the catholyte at the cathode site. C^+ represents cations and A^- represents anions present in the solution with their respective direction of migration. Adapted from [Schm2003].

The reactions occur at the interface of the electron-conductive electrodes with the ion-conductive electrolyte. Per definition, the oxidation takes place at the anode, while the reduction takes place at the cathode. The electrons are transferred through the outer conductor circuit, where the cell potential can be measured; in electrolytic reactions, a power supply provides the electrical energy necessary. Accordingly, ions transfer the charge in the electrolyte, corresponding to the electrons in the outer circuit, to maintain electroneutrality. When a separator divides the electrolyte in the anolyte and catholyte, the ions have to migrate through the separator. Within the scope of this thesis, different membranes are considered as separators and their influence on the process will be discussed in Chapter 2.1.3. Evidently, the oxidation and reduction reaction are coupled by the charge transferred.

One way to categorize coupled reactions is by their respective reactants and the products, displayed in Figure 2.2.

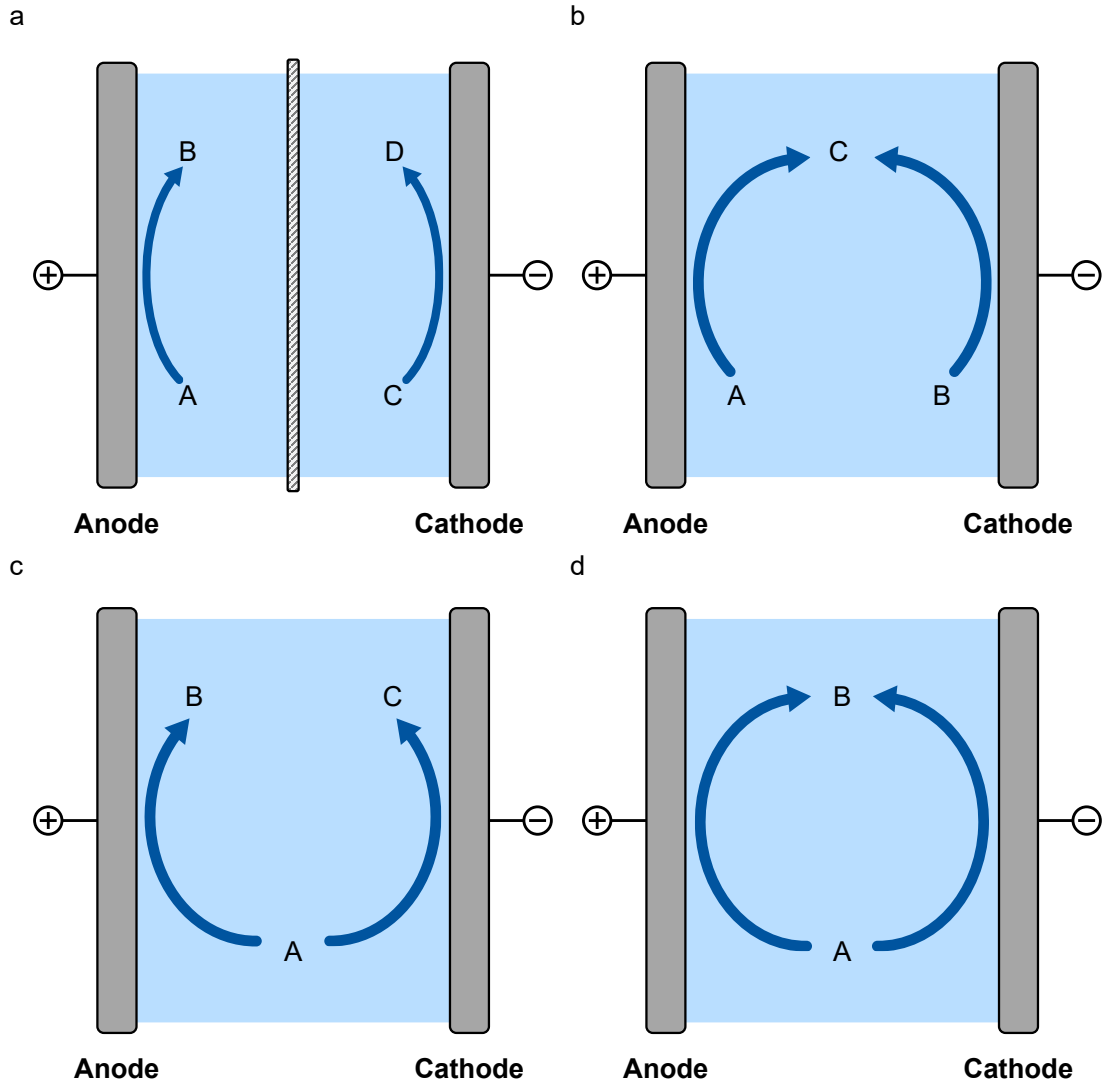

Figure 2.2: Schematic of the four different categories of paired electrolysis, categorized by the relation of product and reactant. a: parallel paired electrolysis; b: convergent paired electrolysis; c: divergent paired electrolysis; d: linear paired electrolysis without the display necessary intermediate reactions. Adapted from [Iban2016]

.

A parallel paired electrolysis is displayed in Figure 2.2a, where the reactants are not interconnected. Such coupling is often used in research, when only one reaction is of interest and, in aqueous electrolytes, it is mostly complemented by water splitting on the counter electrode. How-

ever, a parallel paired electrolysis can yield two value added products, as Chapter 5 demonstrates. In a convergent electrolysis, a single product is formed in two different reactions (Figure 2.2b and a divergent electrolysis reduces and oxidizes the same reactant to two different products (Figure 2.2c. Lastly, the linear paired electrolysis yields the same product on the anode and the cathode (Figure 2.2d. This can be achieved through intermediate redox mediator reactions, a detailed description can be found in literature [Iban2016].

Electrolytic reactions convert electrical energy into chemical energy. The electrical power (P_{El}) supplied is the product of current (I) and the voltage (U) in Equation 2.10a. Further, the voltage relates to the current and the resistance of the total resistance (R_{Total}) via Ohms Law in Equation 2.10b.

$$P_{El} = U \cdot I \tag{2.10a}$$

$$U = R_{Total} \cdot I \tag{2.10b}$$

$$R_{Total} = R_{Reaction} + R_{Electrolyte} + R_{Membrane} \tag{2.10c}$$

R_{Total} in Equation 2.10c is comprised of the resistance of the reaction, $R_{Reaction}$, the resistance from ion transfer in the electrolyte, $R_{Electrolyte}$, and through the membrane, $R_{Membrane}$. The ohmic resistance in the electrodes and the outer circuit can often be neglected [Schm2003]. $R_{Membrane}$ is governed by the material's property. The resistance of the electrolyte is proportional to the distance of the electrodes and inversely proportional to its conductivity, which is a result of the mobility and concentration of ions in the electrolyte [Schw2022]. Next to the ion conductivity, aqueous electrolytes often serve as proton and hydroxide ion donors. They constitute the pH in the electrolyte, which often governs a reactions performance and the stability of reactants and products [Venn2019]. Buffered systems can stabilize the pH during the operation. Additionally to aqueous electrolytes, this thesis deals with biphasic electrolytes that consists of an aqueous phase and an organic phase. These can influence the solubility and distribution of the reactants between the two phases [Di M2017].

Mass transport in the electrolyte serves to supply reactants to and trans-

ports products from the electrode. The general nature and boundaries of mass transfer is governed by the electrochemical reactor, similar to conventional reaction engineering. Beakers or H-cells are similar to stirr-tank reactors, while flow-cells resemble plug flow reactors, in which the electrolyte is constantly pumped through the electrolyte compartments. The governing mass transport principles are convection and diffusion for all species, and migration for charged species. Convection can be controlled by stirring in the batch reactor or manipulation of the volume flow in a flow cell. It is caused by a pressure gradient which results in a flow of the electrolyte and can be described according to Equation 2.11b, where J_i is the convective flux, u is the velocity of the electrolyte and c_i is the concentration of a species i [Schm2003]. There are two governing flow-regimes: laminar and turbulent flow. They can be distinguished by the apparent Reynolds number Re in Equation 2.11a, where u is the velocity of the electrolyte, ρ_{EL} is the density, L the characteristic length and η_{EL} the viscosity of the electrolyte [Schm2003].

$$Re = \frac{u \cdot \rho_{EL} \cdot L}{\eta_{EL}} \tag{2.11a}$$

$$J_{i,convection} = u \cdot c_i \tag{2.11b}$$

$$J_{i,diffusion} = D_i \cdot \frac{dc_i}{dx} \tag{2.11c}$$

$$J_{i,migration} = -F \cdot u_i \cdot c_i \cdot \frac{dE}{dx} \tag{2.11d}$$

Diffusion, based on Brownian molecular motion is dependent on the reactant concentration gradient, the diffusive flux can be described by Fick's law in Equation 2.11c, where D_i is the Diffusion coefficient and $\frac{dc_i}{dx}$ is the spatial concentration gradient of a species i [Schm2003]. In electrochemical reactors, the Nernst diffusion layer with the thickness δ_N describes the boundary layer on the surface of an electrode, in which diffusion is the governing mechanism.

Migration describes the movement of charged species due to an externally applied electrical field in Equation 2.11d, where F is the Faraday con-

stant, u_i is the mobility, c_i is the concentration of the species i and $\frac{dE}{dx}$ is the gradient of the electrical field. In an electrochemical cell, the field forms between the electrodes and the ion migration closes the electrical circuit [Schm2003]. Additionally, migration is accompanied by the so-called electro-osmotic drag, which describes the co-movement of the hydration shell of an ion through a membrane [Drio2016]. This is especially relevant, when an ion moves through an ion-exchange membrane (IEM). The IEMs further govern the direction of migration, which is elaborated further in the following chapter.

2.1.3 Membranes in Electrochemical Reactors

IEMs are used as separators in electrochemical cells, when a separation of anolyte and catholyte is beneficial for the process. IEMs can either be selective for cations, so-called cation exchange membranes (CEMs) or for anions, so-called anion exchange membranes (AEMs). Further, bipolar membranes (BPMs) exist as an assembly of an AEM and a CEM. These IEMs are dense membranes and inhibit convective mass transport between the analoyte and the catholyte. Thus, different electrolyte compositions and reactants at the anode and cathode are possible, and products from the cathodic reduction reaction can be protected from a possible reoxidation on the anode and vice versa. This drastically increases the freedom of design for electrochemical processes and for example enables parallel paired synthesis in Figure 2.2. However, IEMs can exhibit diffusive mass transport, depending on the membrane thickness, backbone polymer, solubility of the diffusing species in the membrane phase etc.. The selective permeability for cations in CEMs and anions in AEMs governs the overall ion transport in the electrochemical cell, as displayed in Figure 2.3 for ideal membranes.

When a CEM is used as in Figure 2.3a, anions cannot permeate the membrane, which enforces the exclusive migration of cations. In turn, this enforces the overall water dissociation on the anode side, either through auto dissociation in the anolyte or within the anodic oxidation, since only

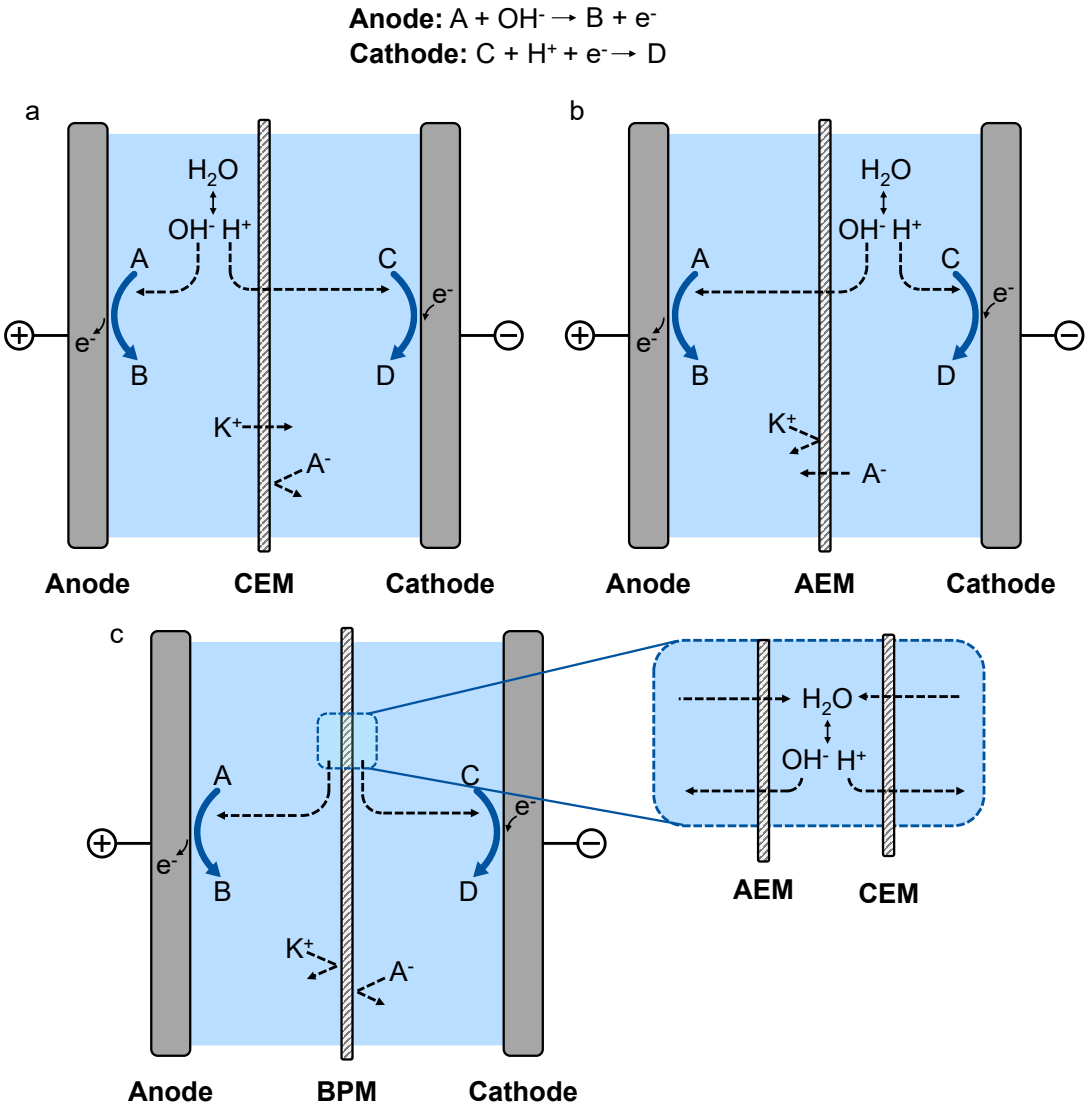

Figure 2.3: Autodissociation of water and ion migration in electrochemical cells when a: a CEM is used, b: an AEM is used, or c: a BPM is used. Reaction equations are given above. K^+ represents cations and A^- represents anions present in the solution.

protons can permeate the membrane to react on the cathode surface. However, if other cations are present in the anolyte, they can also migrate through the membrane, depending on their mobility and their charge. Some membranes show selectivity towards the ion's valency [Drio2016].

The AEM in Figure 2.3b reverses the direction of charge transfer, so that hydroxide ions and, if present, other anions can permeate the membrane. Equation 2.11d shows the dependence of migration flux of a species on

concentration and mobility of the ion. While the mobility of protons and hydroxide ions is higher than that of other ions, their concentration is often smaller, as electrolytes require dissolved ions to ensure sufficient conductivity. Electrolyte concentrations often range between 0.05 mol L^{-1} and 1 mol L^{-1} [Schm2003]. Thus, the majority of charge is often transported by these ions instead of hydroxide ions or protons. However, most reactions in electrosynthesis and all reactions within the scope of this thesis consume protons or hydroxide ions. If other ions resupply the charge to the electrolyte compartment, this leads to a drastic change in the concentration of hydroxide ions and protons. Thereby, the pH changes in both compartments and needs to be accounted for when designing a process [Xu2023]. In contrast to AEMs and CEMs, bipolar membranes offer a possibility to inhibit the crossover of anions or cations. As depicted in Figure 2.3c, they are an assembly of AEM and CEM. The excerpt depicts the ion migration within the membrane in the so-called reverse bias: Water diffuses into the membrane where it dissociates, facilitated by a catalyst. The protons and hydroxide ions migrate towards the cathode and anode, respectively. In forward bias, hydroxide ions and protons migrate into the membrane and form water, which diffuses out of the membrane. However, other ions in the electrolytes also migrate into the membrane in forward bias, where they can accumulate and lead to its deterioration [Pärn2021]. In both cases, a fully selective BPM would inhibit the crossover of cations and anions from one compartment to another. Yet, real bipolar membranes exhibit ion crossover with an increasing impact of migration over diffusion at higher current densities [Blom2020]. Commercially available BPMs suffer from a high resistance at elevated current densities due to the limitation of water dissociation sites within the membranes and resupply of water [Xu2023]. A detailed overview on BPMs, the transport phenomena within and their applications can be found in literature [Pärn2021].

So far, CEMs and AEMs are readily available for large-scale commercialization in the field of electrolysis [Pärn2021]. In contrast, BPMs are only readily available for application in electrodialysis (ED), coining the term bipolar membrane electrodialysis (BPMED), where they are operated at

low voltage and current [Pärn2021]. For application in electrolysis, BPMs are still under development [Xu2023]. They often exhibit a higher voltage drop over the membrane due to a higher thickness of the individual layers. Further, the charge transport can be limited by the dissociation rate of at the interface of AEM and CEM or the diffusive transport of water to the interface at current densities that can lead to membrane degradation beyond 600 mA cm^{-2} [Blom2021]; [Krol1998].

2.2 Biomass Valorization

Biomass can be utilized as a sustainable carbon source, with carbon bound from atmospheric CO_2 by photosynthesis as depicted in Figure 1.1. However, CO_2 neutral utilization is only possible if additional materials and energy for the cultivation and processing are not associated with CO_2 emissions [Wint2022]. Such processing is especially challenging since biomass is structurally more diverse and oxygen-rich than fossil resources.

This section characterizes the different biobased carbon feedstock. Subsequently, it gives an overview on current and perspective products and processes from biobased carbons within the concept of the biorefinery and elaborates its current state.

2.2.1 Feedstock

Biomass is the umbrella term for a wide variety of plant matter from for example crops or trees, but also marine organisms and plant-based waste from food production, households or animals. [Shin2020] Obviously, the wide spectrum of sources is composed of different molecular structures with different functional groups in various quantities, of which some are more suitable as a feedstock for the chemical industry than others. Most accessible for the conversion to value added products are crops with either a high starch content, which can be readily converted to ethanol or methane, or with a high content of fat, which can be converted to biodiesel.

These substrates are called first generation substrates and were mainly harvested for their energy content and their convertibility to biofuels. However, they compete directly with food supply [Kiat2022]; [Aziz2020]. Processes that use 2nd generation feedstock from non-edible plants do not resolve the conflict per se as the competition is often merely shifted from a competition for the edible plant to a competition for land and water usage [Aziz2020]. To resolve this conflict, current research is focused on lignocellulosic biomass, which is a byproduct from biomass processing, e.g. the wood industry, as the feedstock for biorefineries. Lignocellulosic biomass consists of three mayor components: 40 - 50% cellulose, 20 - 30% hemicellulose and 10 - 25% lignin, with their molecular structures are displayed in Figure 2.4 [Cher2010].

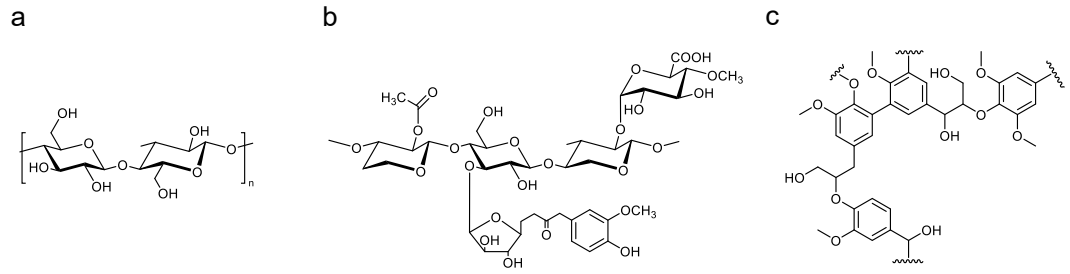

Figure 2.4: a: Chemical structure of cellulose; b: exemplary structures of hemicellulose and c: lignin. [[Sun2020]; [Shin2020]

Lignin is prospected to be the largest source of biobased aromatics and specialty chemicals such as vanillin. Despite extensive research on electric and conventional lignin depolymerization to value-added products, no selective catalysts and efficient processes were established and the majority of lignin is still burned despite its rather low heating value [Shin2020]; [Sun2020]; [Du2020]. In contrast, processes for the conversion of hemicellulosic and cellulosic biomass have been established and are ready to be employed. Both are naturally polymerized structures; cellulose is composed of D-glucose monomers, while hemicellulose consists of various C5 and C6 sugars with more functional groups than cellulose [Shin2020].

Compared to fossil based carbon sources, especially naphta and natural gas, biomass is a highly diverse feedstock, with the varying composition and diverse structure of hemicellulose and lignin. They can differ in functional groups, chain length of the polymerized units and even nature of the polymerized units [Rait2022]. These depend on the plant, but can also show a time dependency from climatic conditions, which makes processing challenging and requires robust and flexible processes. On the other hand, the variety of functional groups constitutes a potential for their selective extraction and utilization. Independent of the source, biomass and hemicellulosic biomass in particular, exhibit a far greater oxygen content than fossil based carbon sources, that are nearly deprived of oxygen. These different properties require different processing methods but also translate to different products that can be generated efficiently in terms of energy input and carbon efficiency. The potential of this diverse biobased feedstock is undisputed, if efficient processes for the conversion of biomass to novel products can be established [Shin2020].

2.2.2 Processes and Products from Biomass Valorization

Bioethanol and biodiesel are the most prominent products from biobased resources; yet, they exhibit a strong competition to the food industry, as elaborated above. Other products have the potential to utilize biobased resources beyond their energy content, such as biopolymers or biobased solvents. Several prospectful biobased platform chemicals have been identified as early as 2004 [Werp2004]; [Shin2020]. For an efficient production of such products, the different biomass fractions need to be converted in an holistic approach that minimizes waste production. Such a holistic approach constitutes the biorefinery as a concept to process and valorize complex substrate to a wide spectrum of products [Cher2010]; [Thon2022]; [Jong2012b].

In a first step, the substrate is mechanically processed and the shredded pulp is subsequently hydrolyzed and fractionated, mostly in aqueous me-

dia, catalyzed by a base, acid or by microorganisms [Bhow2018]. Here, the reaction conditions, such as temperature or a degree of acidity or alkalinity determine the degree of hydrolyzation. An additional organic phase can be introduced to either extract the far less polar lignin, which is mostly insoluble in water, or valuable intermediates such as hydroxymethylfurfural (HMF). The biorefinery aims to assign different products to each fraction so that the overall efficiency of the multi product process is optimized and all fractions can be valorized. Several concepts that link the different prospected platform chemicals to the different biomass fractions can be found in literature [Cher2010]; [Thon2022]; [Wint2022].

Depending on the desired product and the quality of the feedstock, the process chains feature multiple processing steps, combining various unit operations and disciplines with intermediates such as C5 and C6 sugars or other platform chemicals. Yet, the matrix of products and processes is still changing, as new processes are developed or products with superior characteristics emerge. Lately, several electrochemical reactions have emerged in the field of biomass valorization, inspiring the term "e-refinery" [Tang2021]. They use electricity directly as the driving force for the reactions and enable for example the conversion of carboxylic acids in (Non-)Kolbe-electrolysis [Holz2020] or highly selective oxidation and reduction reactions [Bend2022]. The incorporation of these reactions in the concept of biorefineries will further refine the fraction and product matrix [Luo2023]; [Meys2021].

Figure 2.5 gives a schematic overview on two possible processes from hemicellulosic biomass to Polyethylene furan-2,5-dicarboxylate (PEF) and 2-butanone. 2-Butanone is a widely used solvent, produced from fossil resources; the production from biobased carbon could extend its usage into the carbon neutral era. A more detailed analysis of its potential is given in Chapter 3. PEF, on the other hand, is a novel, biobased polymer, capable of replacing polyethylene terephthalate (PET) and has the potential to be employed as a high performance polymer. A more detailed description is given in Chapter 4.

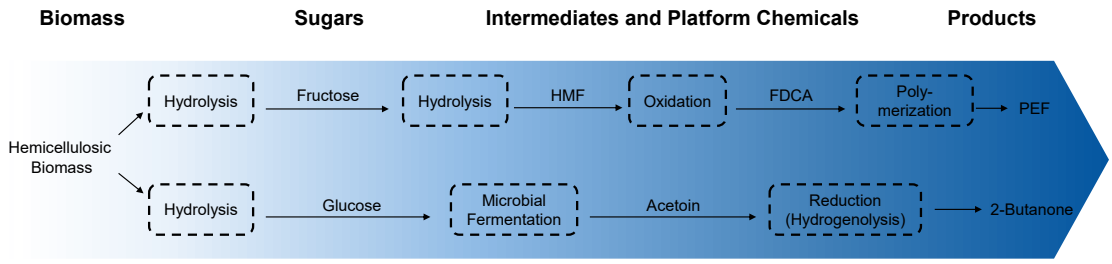

Figure 2.5: General value chains for 2-butanone and FDCA from hemicellulosic biomass without display of purification steps and accompanying substances.

Both require the hydrolysis of hemicellulosic biomass to C6-sugars, fructose or glucose, and diverge in the subsequent processing. For PEF synthesis, fructose is further hydrolyzed to HMF and subsequently oxidized to FDCA, which serves as a monomer for a wide spectrum of biobased polymers, such as PEF. For 2-butanone synthesis, glucose is processed to acetoin in a microbial process, which is reduced to 2-butanone. All the individual process steps are conducted with different techniques, catalysts, solvents, and oxidizing or reducing agents. These consecutive steps require different intermediate and product purification. Often, they determine the economic feasibility and energy intensity of the production cascade [Shol2016]. This is especially true for electrochemical reactions and microbial processes. Both take place in aqueous environments with limited product concentrations. Further, research on electrochemical applications often suffers from low reactant concentrations and is conducted with ideal solutions without impurities or fluctuations in reactant purity, as it would be expected from biobased resources.

The limited or non-existent experimental data from research that incorporates these non-ideal but realistic conditions limits model based approaches to asses these value chains. Therefore, experimental assessment of entire process chains from biobased substrates to sustainable products needs to be conducted to extend the promising concepts of biorefineries beyond the existing products and efficiently valorize all biomass fractions.

2

3 Direct Electrosynthesis of 2-Butanone from Fermentation Supernatant

Parts of this chapter have been published as:
Tobias Harhues, Lukas Portheine, Cathleen Plath, Joern Viell, Robert Keller, Jochen Büchs, and Matthias Wessling *Direct Electrosynthesis of 2-Butanone from Fermentation Supernatant*, acs sustainable chemistry & engineering, 2022 DOI: 10.1021/acssuschemeng.2c01971
and
Carolin Grüntering, Tobias Harhues, Fabian Speen, Robert Keller, Martin Zimmermann, Peter R. Jensen, Matthias Wessling and Lars M. Blank *Acetoin production by resting cells of Lactococcus lactis for direct electrochemical synthesis of 2-butanone*, Green Chem., 2023, DOI: 10.1039/D3GC02513F

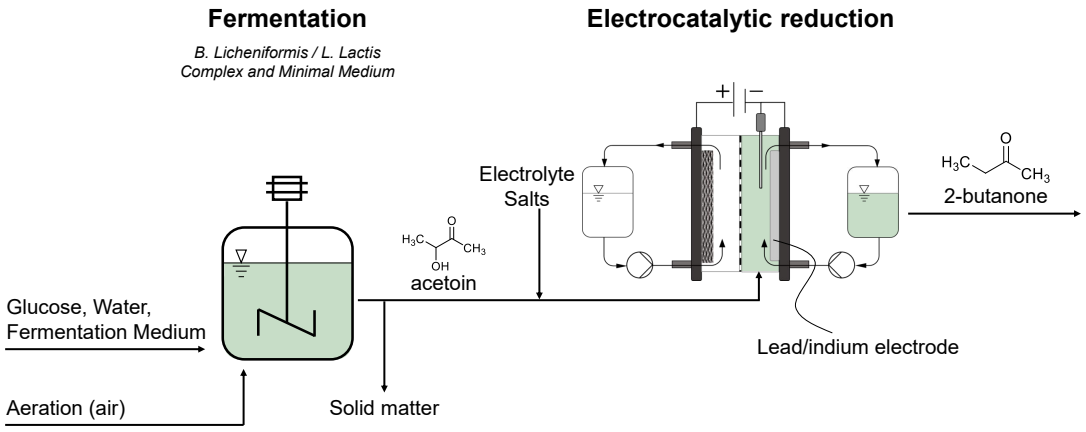

3.1 Introduction

Solvent production and utilization strongly contribute to the CO_2 footprint of the chemical industry. It can be reduced by replacing the basis of abundantly used solvents from the current fossil to a biobased feedstock and implementing a sustainable energy-efficient production pathway. The existing guidelines for green chemistry offer a basis for the evaluation of these processes [Anas2010].

2-Butanone, commonly known as methyl ethyl ketone (MEK), is a commonly used solvent with an over 1.3 million metric tons market size in 2015 that is expected to grow up to 1.754 million tons by 2020 [Kim2016]; [LIU2006]. It is an environmentally friendly solvent due to its low acute toxicity and eco-toxicity compared to other commonly used solvents [Hege2018]; [Hege2021]. Applications are in the paint industry or as a plastic wielding agent [Thio2017]; [Mehr2019]. Further, 2-butanone has shown good properties as a possible energy carrier or biofuel [Dahm2016]; [Hopp2016]. Today, more than 92% of 2-butanone is produced from fossil resources via reduction of 2-butanol, mainly from butylene which originates from C-4 oil cuts [Hoel2011]; [Torr2020]. Azapagic et al. [Azap2013] summarized the global warming potential in CO_2-emission equivalents of fossil 2-butanone from different life cycle assessment(LCA) tools, which showed

an average CO_2-equivalent of 1.47 ton CO_2-eq per ton 2-butanone. The carbon footprint can be decreased to 0.798 ton CO_2-eq per ton 2-butanone, if 2-butanone is recycled. The report only covers cradle-to-gate emissions, so that emissions from, e.g., thermal recycling are not covered. The large scale production and application of this solvent come with a strong lever to decrease CO_2-emissions when replacing its feedstock and production route with a sustainable alternative.

Several routes for the sustainable production of 2-butanone from a biological feedstock are possible. Production based on microbial processes has been theoretically investigated [Toki2018] and experimentally conducted with, e.g., modified *E. coli* with glucose [Mult2012]; [Yone2014] or levulinic acid as substrate [Mehr2019], and with *Klebsiella pneumoniae* [Chen2015] with the substrate glucose. However, with a maximum titer of 160 mg L^{-1}, 900 mg L^{-1} and 450 mg L^{-1} respectively, the product concentration remained low and did not move towards a quantitative production.

More promising results were achieved on a different route via 2,3-butanediol (2,3-BD) fermented from biomass, where titers of the fermentation already reach up to 150 g L^{-1} [Ma2009], with a subsequent chemical conversion [Mult2012]; [Wang2014]; [Penn2017]; [Ronc2017]; [Main2021b]; [Cui2018]. Yet, the high boiling temperature and affinity to the aqueous fermentation broth of 2,3-BD lead to a demanding and highly complex intermediate purification. The intermediate purification of highly polar and low vapor pressure platform molecules such as 2,3-BD or 3-hydrox-2-butanone (acetoin) has been identified as one of the key challenges in biomass utilization [Deli2014]; [Penn2017].

Different approaches for an efficient purification of 2,3-BD from a fermentation medium, such as distillation, pervaporation, solvent extraction and reverse osmosis have been analyzed [Xiao2014]; [Main2021a]. Lately, even more complex processes such as anionic extraction based on the formation of reversible complexes [Drab2017], extraction and subsequent purification with ionic-liquids [Dai2021] or liquid-liquid extraction coupled with a thermal approach [Sánc2021b] were analyzed and further optimized to increase the efficiency [Sánc2021a]. In the process models, the environmental impact

of the separation could be decreased by 14%.

Recently, the acid-catalyzed dehydration of 2,3-BD to 2-butanone in an aqueous environment has been investigated [Main2021c]. While the study showed promising results, the catalytic reaction did not move beyond a simulation, based on model solution experiments from literature [Emer1982].

A different route to produce 2-butanone has been presented in 1984: In a two stage process, 2,3-BD was first electrochemically oxidized to acetoin, which was subsequently reduced to 2-butanone [Baiz1984]. However, this route was not pursued to technical maturity, because of the competing cost-efficient synthesis of 2-butanone from fossil-based 2-butanol. In search for a sustainable production route, Ochoa-Gómez et al. [Ocho2019] reintroduced the reductive electrochemical production route in 2019: Building on the advances in the microbial production of acetoin, they reduced acetoin to 2-butanone using different electrode materials [Ocho2019]. Promising figures of merit were achieved with an overall 2-butanone yield of 60% at an acetoin conversion of 72% and a Faraday efficiency (FE) of 77% for an initial concentration of 200 g L^{-1} on a lead electrode with a selectivity of more than 80% toward 2-butanone. Unfortunately, the study did not show the feasibility of the process chain but worked on synthetic model solutions from purified acetoin.

The electrochemical synthesis route was only of interest through the advances in acetoin fermentation. For the microbial synthesis of acetoin, various microorganisms, wild types as well as genetically modified have been employed. Among them the *B. Subtilis*, the *Bacillus Licheniformis* and the *L. Lactis*. A wide variety of substrates have been utilized as feedstock, such as glucose [Heym2020] and galactose, mannitol and xylose as carbon sources [Xiao2012], but also less valuable compounds such as hemicellulose/cellulose in a SSF (simultaneous saccharification and fermentation) process [Jia2017]. From glucose, the highest reported titer known to the author reached 100.1 g L^{-1} acetoin [Bae2016], with 2,3-BD as a substrate, 165.9 g L^{-1} was reported [Zhou2018]. Acetoin was also synthesized from mixed sugar substrates and oil palm fiber, or lignocellulosic hydrolysate [Mohd2017]; [Zhan2016a]; [Zhan2016b], lactose [Kand2016] and bakery

waste with a titer of up to 65.9 g L^{-1} [Main2021a]. A more detailed overview on different microorganisms forming acetoin can be found in the literature [Xiao2014]; [Main2021c]; [Yang2017].

These advances in substrate range, microbial productivity, and scalability of the fermentation process, paired with the promising results of Ochoa-Gomez et al. [Ocho2019] with synthetic model solutions, indicate the high potential of a sustainable production route for 2-butanone via acetoin. Yet, an efficient synthesis of 2-butanone via acetoin requires a highly efficient intermediate purification from the fermentation media. With the rather similar physicochemical properties of acetoin and 2,3-BD (high miscibility with water and boiling point), the separation is similarly challenging [Xiao2014]; [Main2021b]. Further, the fermentation to acetoin takes place in a complex fermentation medium, which includes trace metals, proteins, cellular matter and salts. Further, most of the fermentations yield not one, but a spectrum of intermediate and final products, often including acetoin and 2,3-BD.

In other systems, the separation of intermediate products from a fermentation broth has also been identified as crucial, and different strategies were demonstrated. For carboxylic acids, for example, a sequence of fermentation and subsequent electrochemical conversion with intermediate membrane purification has been presented [Urba2017]. Other approaches couple electrochemical reactions into the fermentation in so-called bioelectrochemical systems [Schr2015]. For the production of methylsuccinic acid from itaconic acid, Holzhäuser et al. showed a electrochemical reduction in the fermentation medium [Holz2017]. They reported a nearly unchanged selectivity and yield compared to a model solution in small scale batch experiments at a decreased FE, which they mainly attributed to reduction reactions with residual sugar. Recently, de Smit et al. [Smit2023] showed that trace metals from fermentation media facilitated the parasitic HER, which might also decrease the FE for an electrochemical conversion in the fermentation medium.

This chapter shows the coupling of the biotechnological synthesis of acetoin with the subsequent electrochemical 2-butanone production. It circumvents the complex intermediate separation of acetoin as the acetoin-rich

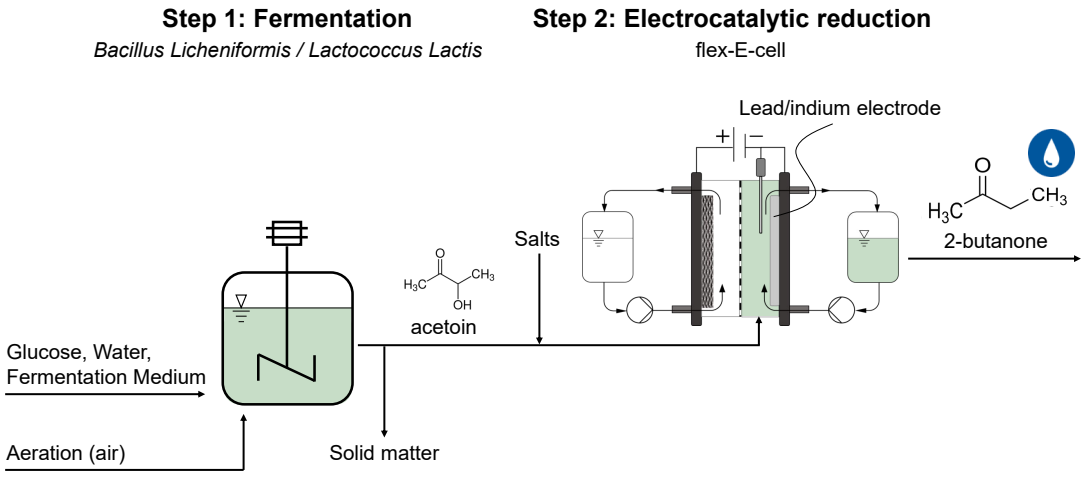

Figure 3.1: Process scheme of the coupling of biotechnological and electrochemical conversion. Glucose is fermented to acetoin in step 1 by two different organisms in different fermentation media and subsequently reduced electrochemically to 2-butanone in step two. The fermentation broth is not elaborately purified. Only solids are removed and a salt is added as supporting electrolyte prior to the electrochemical conversion.

fermentation supernatant with added salts is directly employed as the electrolyte for the electrochemical conversion of acetoin to 2-butanone as depicted in Figure 3.1. To assess the feasibility of the integrated process, two catalyst materials are screened for their catalytic activity with a model solution and the supernatant from fermentation with the robust *B. Licheniformis* in linear sweep voltammetry (LSV). Next to lead, known from Ochoa-Gómez et al. [Ocho2019], indium is proposed as a non-toxic alternative. After assessing the activity, quantitative acetoin conversion is conducted in an electrochemical flow cell. The reaction pathway is displayed in Figure 3.2. The influence of the initial acetoin concentration and pH value is analyzed with a model solution and the supernatant from *B. Licheniformis* fermentation, revealing the different effects of the pH in the model solution and the supernatant. While the *B. Licheniformis* is a very robust organism that yields a high acetoin titer, the carbon efficiency from glucose to acetoin is inherently limited by the intermediate 2,3-BD. It consists of two isomers, of which only one can be converted to acetoin [Heym2020]. To explore

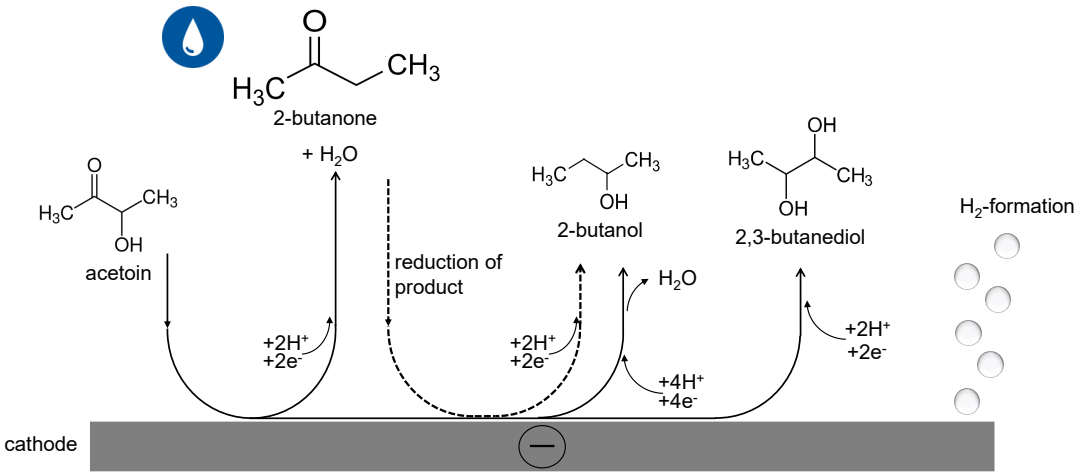

Figure 3.2: Reaction mechanism observed on lead and indium cathodes in this work. Acetoin is reduced to 2-butanone and can be further reduced to 2-butanol. 2,3-BD is formed as side product from acetoin.The hydrogen evolution reaction (HER) occurs as a parasitic reaction.

a potentially more carbon efficient route, a genetically modified strain of *Lactococcus Lactis* is used to produce acetoin. The fermentation is conducted different complex media and the influence of these media on the subsequent electrochemical conversion is analyzed. To increase the overall process efficiency, the amount of dissolved species in the fermentation supernatant is reduced by conducting the *L. Lactis* fermentation in a resting cell essay. Finally, the supernatant is employed for the electrochemical conversion to assess the advantages of this approach for the integrated process.

3.2 Experimentals

3.2.1 Materials

Indium and lead electrodes were purchased at Evochem and Alfa Aesar, respectively, with a purity of 99.99%. Counter electrodes were titanium mesh electrodes, coated with iridiumoxide, purchased from Umicore

Electroplating. All experiments were conducted with a PGSTAT302N from Metrohm Autolab. Fumapem F-14100 cation exchange membranes were used for flow cell experiments. Acetoin and potassium dihydrogen phosphate (K_2HPO_4) were purchased from Sigma-Aldrich (purity 96% and >98% respectively), potassium hydrogen phosphate (KH_2PO_4) and 1 M H_2SO_4 were purchased from Carl Roth (purity >99%).

3.2.2 Fermentation

Fermentation with *B. licheniformis*

Fermentation with *B. licheniformis* was carried out according to Heyman et al. [Heym2020] in Nakashimada medium [Naka1998]. The substrate was glucose. To increase the acetoin yield, fermentation was prolonged to 110 h. The resulting broth was centrifuged at 11000 rpm for 10 min to ensure a solid-free supernatant. High performance liquid chromatography (HPLC) analysis revealed a complex mixture of different products (acetoin, 2,3-butanediol, and 2-butanone).

Fermentation with *L. Lactis*

Fermentation with a modified strain of *L. Lactus* was carried out according to Grütering et al. [Grüt2023] in M17, Herstrin Schramm (HS), Lysogeny Broth (LB), and Yeast Extract Peptone (YEP) complex medium. The substrate in all complex media was glucose. Further, fermentation was conducted in a so-called minimal medium in a phosphate buffer. A pre-culture of *L. Lactus* was cultivated for cell-growth, then the medium was exchanged to a minimal medium consisting of a phosphate buffer and glucose as substrate. The resulting broth was centrifuged at 11000 rpm for 10 min to ensure a solid-free supernatant. The supernatants were subsequently analyzed via HPLC.

3.2.3 Electrochemical Experiments

Electrolyte Solutions

Experiments were conducted with model solution and fermentation broth supernatant. The model solution was prepared from DI water by adding salt (7 g L^{-1} K_2HPO_4 and 5.5 g L^{-1} KH_2PO_4) and acetoin with the desired concentrations from 5 to 75g L^{-1}. The acetoin concentration of the fermentation broth was adjusted by diluting the original fermentation broth with the K_2HPO_4-KH_2PO_4 containing electrolyte solution. The same phosphate buffer was added to the fermentation broth to ensure sufficient conductivity. H_2SO_4 (1 M) was added dropwise to adjust the pH value whenever necessary.

Electrochemical Characterization

Measurements were performed at different acetoin concentrations for both the model solution and fermentation broth. All LSV measurements were compensated for 80% of the iR drop, which was measured via EIS prior to each experiment. Electric impedance spectroscopy (EIS) was measured at the respective open circuit potential (OCP) from 1 mHz to 1 Hz with an amplitude of 10 mV. LSV measurements were performed with a scan rate of 0.05 V s^{-1}. A HgE11 ($Hg/HgSO_4$ with sat. K_2SO_4) reference electrode from Meinsberg was used as reference electrode.

Product Analysis

Liquid samples were analyzed via Agilent 1200 HPLC, equipped with an organic acid resin column (CS - Chromatographie Service GmbH, Germany) at 70 °C, with 0.5 mL min^{-1} flow rate of 2.5 mmol H_2SO_4 in H_2O at a pressure of 45 bar. Detection was done via a refractive index detector (RID) for 2,3-BD, 2-butanone and 2-butanol. Acetoin was analyzed with a variable wavelength detector (VWD) at 190 nm wavelength. Gaseous samples were analyzed for some experiments to account for the residual charge that

liquid products cannot account for with HER as the parasitic reaction. The analysis was conducted on an Agilent 8860 GC equipped with two consecutive Haysep Q and a mole-sieve MS5A from Agilent. Helium was used as the carrier gas with a flow of 5.745 mL min^{-1}. The oven temperature was held at 50 °C for 7 min and increased to 150 °C with 15 °C min^{-1}.

3.2.4 Flow Cell Experiments

Flow cell experiments were conducted with the commercial flex-E-cell (flex-X-cell, Germany). The active electrode area was 35 cm^2 for experiments with the supernatant from *B. Licheniformis* fermentation and 25 cm^2 for experiments with the supernatant from *L. Lactis* fermentation. The electrolyte gap was 2 mm. Electrolytes were pumped by gear pumps (MCP-Process, Colepalmer) with a flow rate of 100 mL min^{-1} and recycled in the electrolyte tank. Samples were taken from the anolyte and catholyte tanks periodically and analyzed via HPLC. All experiments with supernatans from fermentation with *B. Licheniformis* were conducted at a current density of 50 mA cm^{-2}. Due to the lower acetoin concentration, the current density for experiments with supernatants from fermentation with *B. Licheniformis* was adjusted to 10 mA cm^{-2} when the acetoin concentration was below 10 g L^{-1} and 25 mA cm^{-2} when it was above. This was done to avoid mass transport limitations. The apparent voltage on the working electrode was measured with a mini HydroFlex® reversible hydrogen electrode (RHE) from Gaskatel.

Experiments were evaluated for conversion of acetoin, selectivity toward 2-butanone, 2,3-BD and 2-butanol, as well as FE. Because the individual experiments were conducted with varying initial amounts of acetoin, all results were compared at the time of 100% theoretical conversion of acetoin. Here, the 100% theoretical conversion is defined as the time t_{FC}, when sufficient charge has passed the electrode to convert all acetoin to 2-butanone according to Faraday's law. t_{FC} is calculated from Equation 2.9, with the process specific parameters in Equation 3.1. Here c is the initial concentration of acetoin, V the Volume of the electrolyte, $M_{Acetoin}$ the molar mass of acetoin, z the number of transferred electrons (2), F the Faraday constant,

and I the applied current.

$$t_{FC} = \frac{(c \cdot V)}{M_{Acetoin}} \cdot \frac{zF}{I} \tag{3.1}$$

Reactants crossing the membrane during the experiments were included in the experiment's evaluation, so that e.g., 2-butanone in the anolyte is included in selectivity and yield. Conversion, selectivity and yield were calculated after Equations 2.6a-c. Changes in electrolyte volume due to osmotic drag were measured and accounted for when evaluating concentrations in the electrolyte.

3.3 Results and Discussion

3.3.1 Catalyst Analysis

Two different catalysts were characterized for electrochemical 2-butanone synthesis: lead has yielded promising results in a study by Ochoa-Gómez et al. [Ocho2019] and indium was additionally chosen due to its high overpotential for the hydrogen evolution reaction. Figure 3.3 displays LSV measurements with varying acetoin concentrations in the model solution and in the fermentation broth.

As expected, the LSV measurements show a remarkable onset potential difference with and without acetoin in the solution. The onset potential decreases from about -1.5 V vs SHE (standard hydrogen electrode) for HER to -1.25 V vs SHE when acetoin is present in the solution with a lead electrode in the model solution in Figure 3.3a. It decreases further with 50 g L^{-1} initial acetoin concentration. Additionally, the current density increases significantly with increasing acetoin bulk concentration after the onset potential is surpassed. Similar results are visible for LSV measurements with the indium electrode in Figure 3.3c. The onset potential decreases from the HER at -1.4 V vs SHE to -1.1 V vs SHE when acetoin is present in the solution, and it decreases further with increasing acetoin concentration. The high

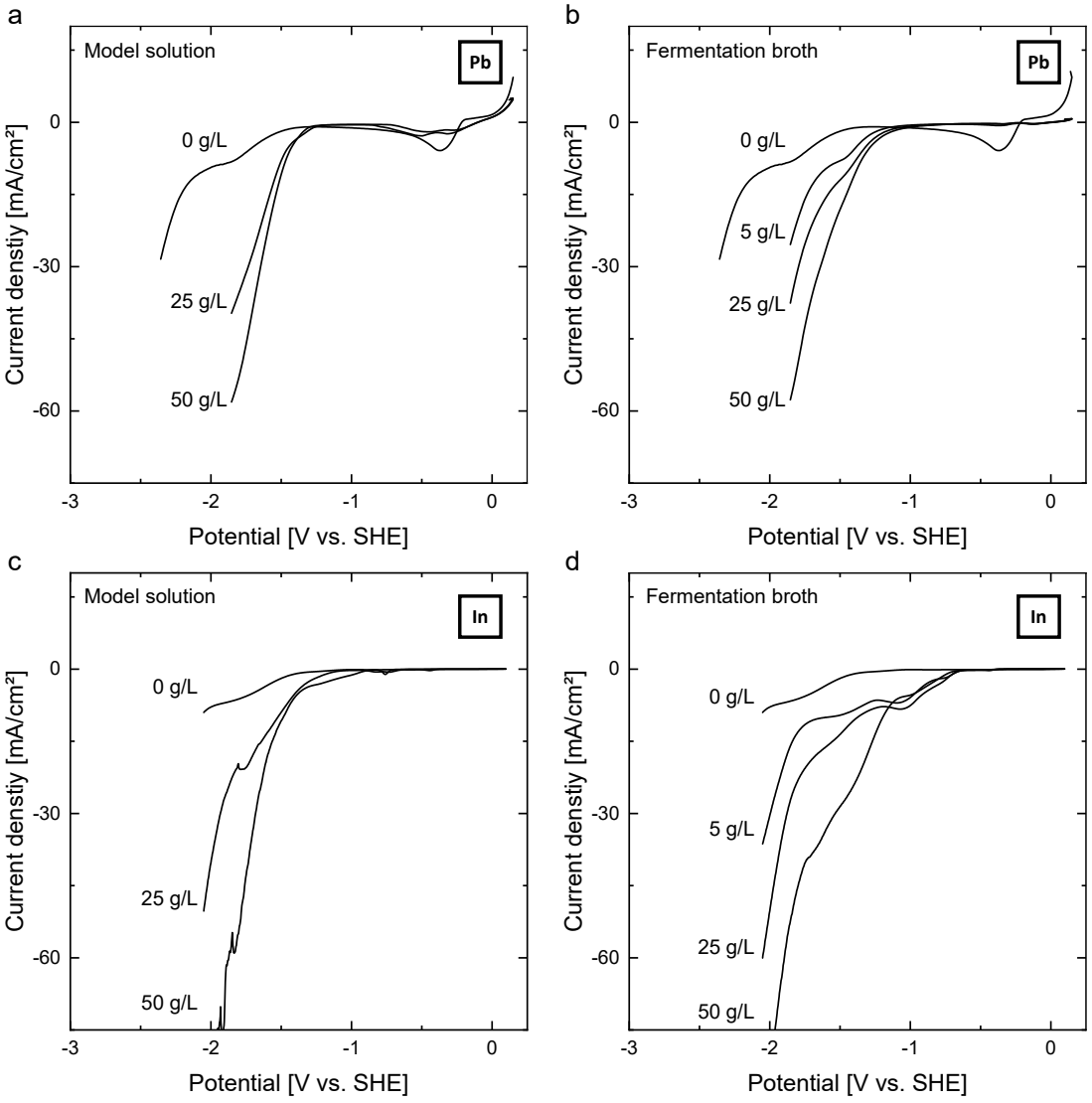

Figure 3.3: LSV on a lead electrode in a: the model solution and b: the fermentation broth. LSV on an indium electrode in c: the model solution and d: the fermentation broth with increasing acetoin concentration at pH 3.2. The scanrate was 50 mV s^{-1}.

overpotential of lead for the HER opens a potential window for acetoin reduction.

LSV measurements were also conducted with the supernatant from fermentation with the *B. Licheniformis*. The results are displayed in Figure 3.3b and 3.3d for lead and indium, respectively. The general course of the current is similar for measurements conducted with the model solution. However, a notably lower onset potential is visible on both electrodes in

the fermentation broth. At this onset potential, the initial increase in current is less steep compared to the model solution and a plateau-like region is apparent. This behavior can be attributed to side-reactions of species in the fermentation broth, which are not present in the model solution. Also, the HER can be catalyzed by the various trace metals from the fermentation medium. The composition of the fermentation broth prior to the fermentation with the various trace components can be found in the literature [Naka1998]. Nevertheless, beyond this plateau-like region around the onset potential in the model solution, a steep increase in current can be seen. The apparent current density is similar to the respective current density in the model solution, which indicates similar reaction rates in the model solution and the fermentation broth. This is attributed to a predominant reduction of acetoin on both electrode materials. Quantitative product analysis needs to be conducted in flow cell experiments to give insight into product selectivity and to asses the catalyst's suitability.

3.3.2 Flow Cell Experiments with Supernatant from *B. Licheniformis* Fermentation

Quantitative analysis of the conversion, selectivity, and FE was conducted in flow cell experiments. To assess the influence of an increasing acetoin concentration, experiments were initially conducted with diluted fermentation broth and model solution. The degree of dilution was subsequently decreased, until the non-diluted fermentation broth was employed. Figure 3.4 depicts the concentrations of acetoin, 2-butanone, 2-butanol, and 2,3-BD over time for the model solution and fermentation broth with 5 g L^{-1} initial acetoin concentration on indium electrodes. The reaction pathways including the side products 2-butanone, 2-butanol, and 2,3-BD are displayed in Figure 3.2. The qualitative trends are similar for other initial acetoin concentrations and the lead electrode.

In both experiments, the conversion of acetoin is apparent. In Figure 3.4a about 37% of the initial acetoin is converted in the model solution at 100% theoretical conversion t_{FC}, as indicated by the dashed line. Bubble

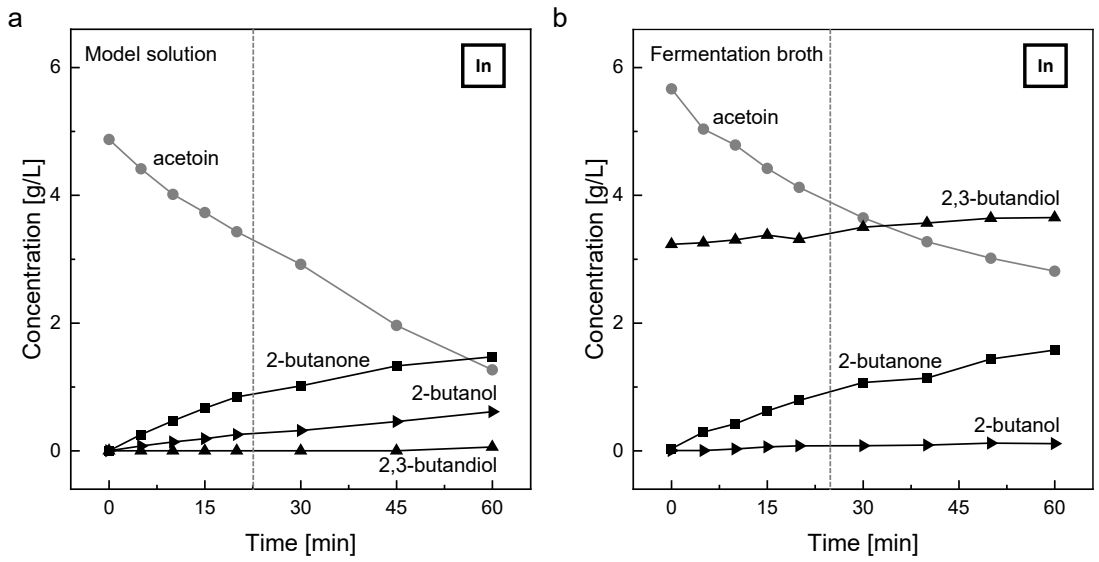

Figure 3.4: Concentration of reactants over the reaction time in a: the model solution and b: the fermentation broth at 50 mA cm^{-2} with an indium electrode. The dashed vertical line indicates the time of 100%. theoretical conversion (t_{FC}).

formation was observed on the cathode, indicating the HER as a parasitic reaction. Due to the low initial acetoin concentration, side reactions dominate and the FE is low (26%). The reaction yields predominantly 2-butanone with a selectivity of 71% and the side product 2-butanol. The 2,3-BD concentration remains close to zero over the entire time course.

In the diluted fermentation broth, the conversion of acetoin is 31% at t_{FC} and lower as compared to the model solution. The main product of the acetoin reduction is again 2-butanone. Its selectivity of 61% is close to the selectivity in the model solution experiment. 2,3-BD is present from the start of the experiment as a byproduct of the fermentation. In contrast to the model solution, 2,3-BD is formed as the secondary product at a low rate. As in the model solution experiment, bubble formation indicates the HER as a parasitic reaction. Acetoin is depleted linearly over the course of the experiment in the model solution while the conversion decreases over time in the fermentation broth. Generally, the findings from these experiments at a low acetoin concentration match indications from LSV experiments, especially the more pronounced HER or sidereactions in the experiments with the fermentation broth.

Influence of the Acetoin Concentration

Further experiments were conducted at higher acetoin concentrations of up to 50 g L^{-1}. All experiments are benchmarked for conversion, selectivity, yield, and FE at the t_{FC}, so that the FE equals the yield. These indicators are displayed for indium in Figure 3.5 and for lead in Figure 3.6.

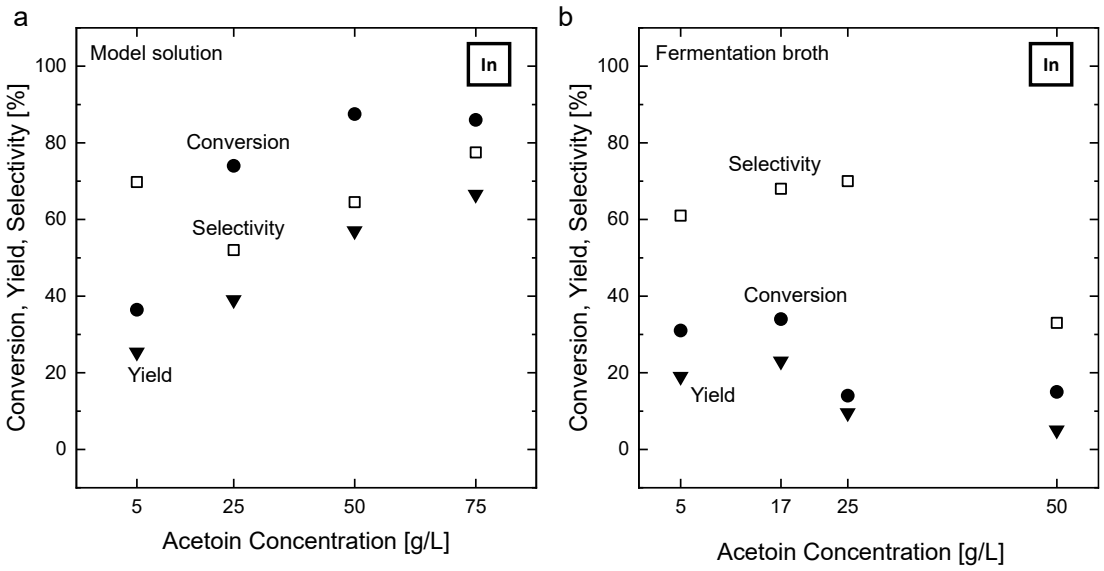

Figure 3.5: Conversion (●), selectivity (□), and yield (▼) of acetoin reduction to 2-butanone at different initial acetoin concentrations in 7 g L^{-1} K_2HPO_4 and 5.5 g L^{-1} KH_2PO_4 at pH 3.2 in a: model solution and b: fermentation broth experiments on an indium electrode. Characteristic values are given at 100% theoretical conversion (t_{FC}).

Figure 3.5a displays the influence of an increasing acetoin concentration on the selectivity, conversion, and yield (FE) of model solution experiments with an indium electrode. All indicators benefit from an increasing acetoin concentration in the model solution. At an initial acetoin concentration of 50 g L^{-1}, experiments show a selectivity of 64.5% and a yield and FE of 57.5% at a conversion of 87.5%. A further increase in concentration to 75 g L^{-1} further increases selectivity to 77.5% and yield to 66.5%, while the conversion ratio of acetoin slightly decreases to 86%.

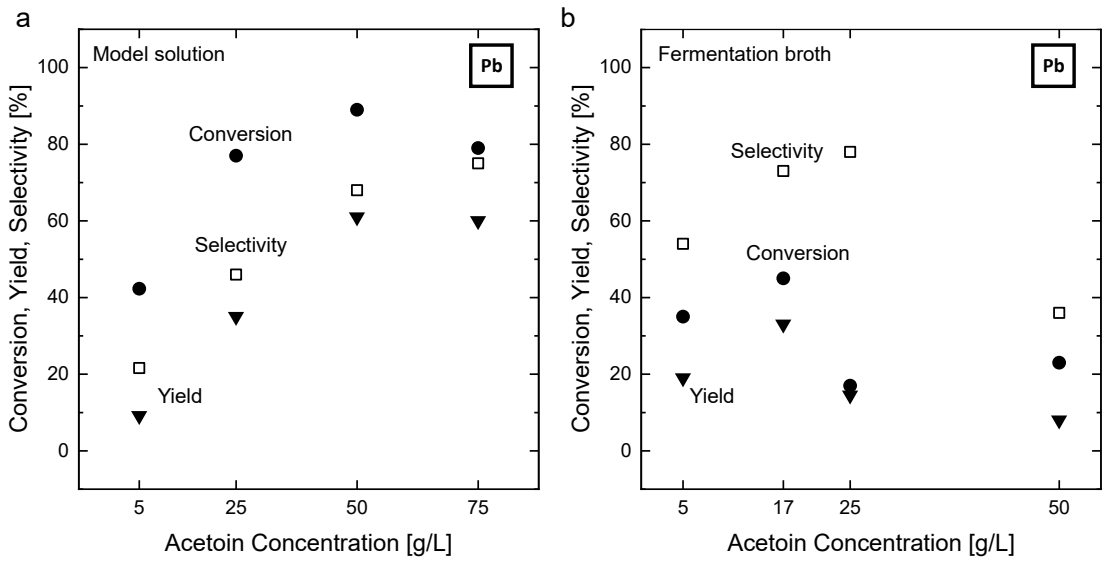

Figure 3.6: Conversion (●), Selectivity (□), and Yield (▼) of acetoin reduction to 2-butanone at different initial acetoin concentrations in 7 g L^{-1} K_2HPO_4 and 5.5 g L^{-1} KH_2PO_4 at pH 3.2 in a: model solution and b: fermentation broth experiments on a lead electrode. Characteristic values are given at 100% theoretical conversion (t_{FC}).

The results of conversion from the gradually less diluted fermentation broth are depicted in Figure 3.5b. The trend of increasing efficiency with an increasing reactant concentration does not extend to the fermentation broth, so that the highest selectivity, conversion, and yield are achieved at 17 g L^{-1}. At 50 g L^{-1} the yield is as poor as 5%. Figure 3.6 shows the corresponding measurements with lead as the cathode and display a nearly identical trend.

On both electrodes, the acetoin concentration on the electrode's surface seems to be the limiting factor for a concentration below 50 g L^{-1} at the given current density in the model solution without impurities. Next to the process indicators, a decreasing selectivity and FE over the course of the experiments has to be noted, as acetoin is gradually depleted.This fits findings from LSV-experiments, which show an increasing activity with increasing reactant concentration.

In the fermentation broth experiments, the low overall conversion rate of acetoin at a concentration above 17 g L^{-1} indicates more pronounced par-

asitic reactions, most likely a predominant HER. This is further supported by the increased bubble formation on the cathode, which further increased formation of foam. Above 25 g L^{-1}, the selectivity decreases drastically, diminishing the overall process yield. At 50 g L^{-1}, more than 80% of the electrical charge can be attributed to the HER, which is apparent from gas phase analysis for the model solution at a pH of 3.2 in Figure 3.8c. Next to the decreased product yield, the resulting foaming makes process control complex. Most likely, the increased HER in the fermentation broth can be attributed to the increased catalytic activity of various trace metal components in the mixture. The Energy-dispersive X-ray spectroscopy (EDX) images in Figure 3.7 show copper and zink on the electrode after the experiments Therefore, the reaction conditions chosen here seem to be unfavorable for conversion in a non-diluted fermentation broth.

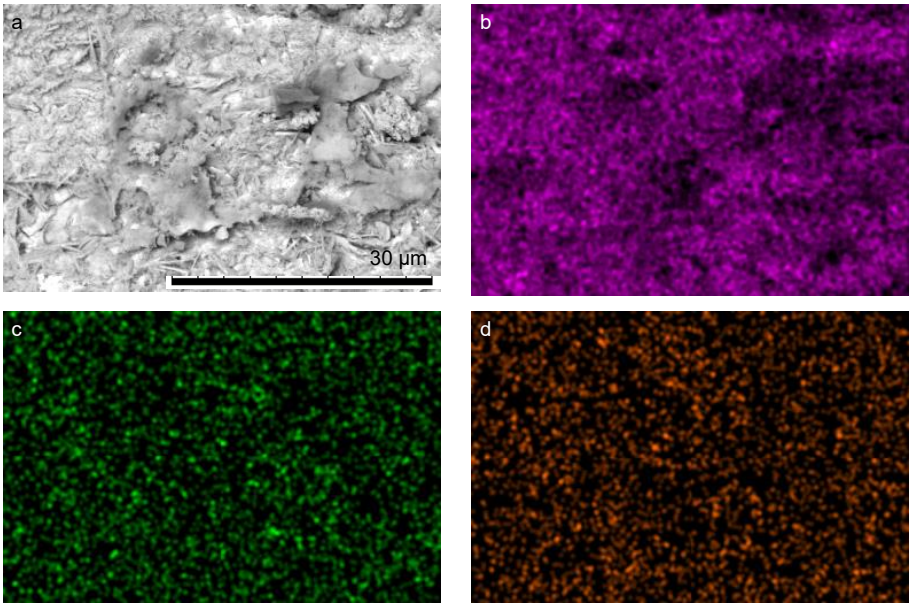

Figure 3.7: SEM (a) and EDX (b-d) analysis for lead (b), zinc (c) and copper (d) of the lead electrode after acetoin reduction in the non-diluted FB.

Influence of the pH Value

Originally, the pH was chosen in accordance with Ochoa-Gómez et al. [Ocho2019] from model solution experiments. To suppress the undesired

HER in the fermentation broth, the pH adjustment was omitted and experiments were continued at the original pH of the fermentation supernatant of 6.5. This decreased the intermediate treatment steps further. To show the influence of the pH on the model solution, experiments with the model solution were conducted accordingly.

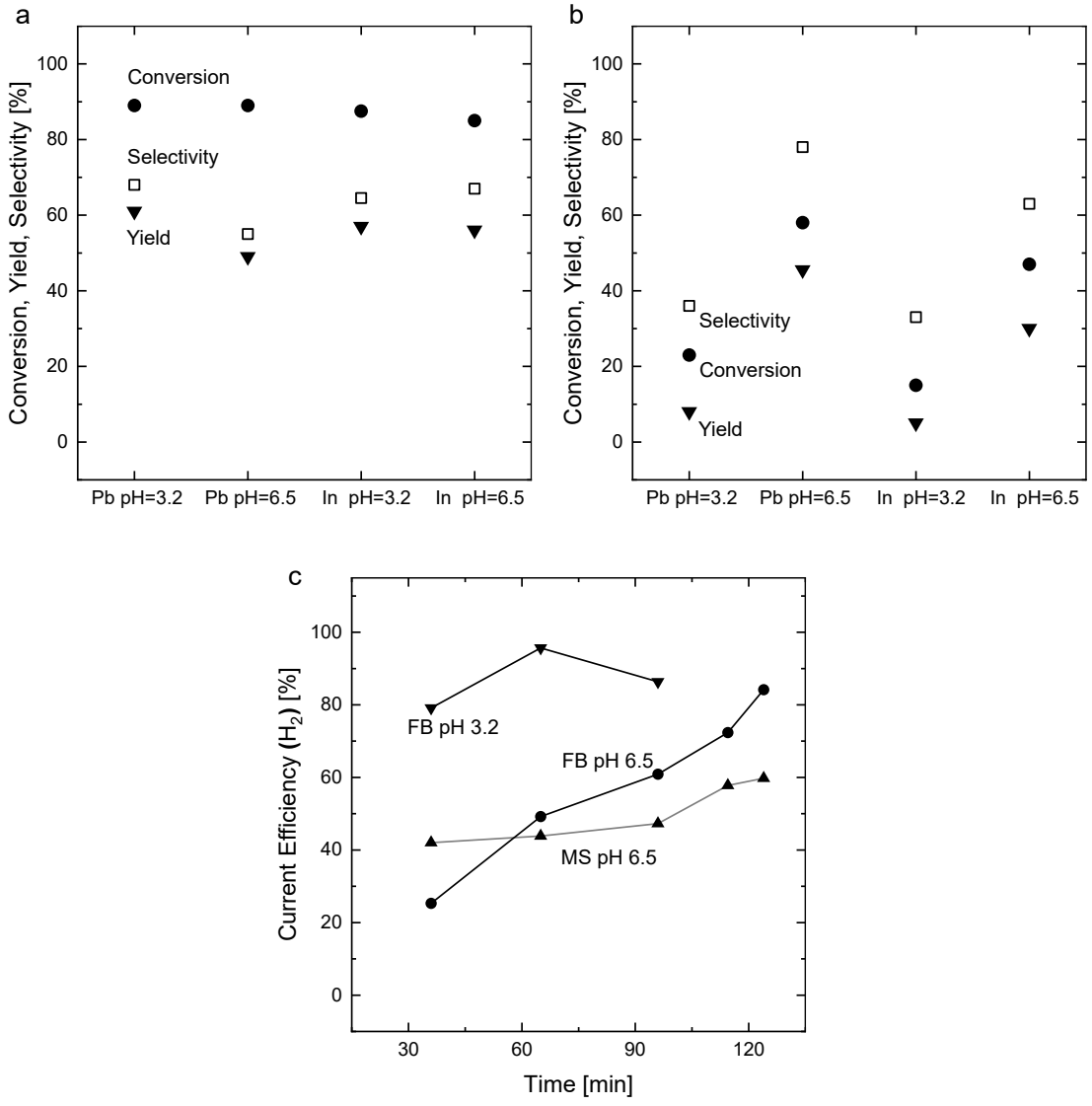

Figure 3.8: Conversion (●), selectivity (□), and yield (▼) of acetoin reduction to 2-butanone at different pH values in 7 g L^{-1} K_2HPO_4 and 5.5 g L^{-1} KH_2PO_4 in a: model solution and b: fermentation broth experiments on a lead electrode at 50 g L^{-1} initial acetoin concentration. Characteristic values are given at 100% theoretical conversion (t_{FC}). c: Current efficiency for the undesired HER on a lead electrode.

Ochoa-Gomez et al. [Ocho2019] describe the pH as a minor factor for the characteristic performance indicators and find the best performance at pH values between 3 and 5.5. Below a pH of 3 HER increases significantly [Ocho2019] and above a pH of 7, aldol condensation is reported in literature [Zhu2016]; [Ocho2019]. Results for the model solution in Figure 3.8a show, that reaction at a pH of 6.5 does not impair yield or selectivity on the indium electrode, while the selectivity on the lead electrode is slightly lower than at a pH of 3.2.

The influence of the pH on the reaction in the fermentation broth is displayed in Figure 3.8b. In contrast to the model solution, the pH has a major impact on the performance in the fermentation broth. All characteristic values, especially on the lead electrode, increase dramatically at this elevated pH, resulting in a yield and FE of 47%. For indium, the increase in performance is less pronounced but still notable, with a yield and FE of 30%. Figure 3.8c also shows the decrease in hydrogen evolution at pH of 6.5. The reduced gas evolution also results in a dramatically decreasing bubble formation, which simplifies the process control significantly by decreased foaming.

As discussed before, the HER was far more pronounced in the fermentation broth than in the model solution at the pH of 3.2. This might be due to active sites that might stem from deposited trace metals in the fermentation broth with a low overpotential for the HER. The pH dependence appears to be stronger for the HER than for the acetoin reduction. The concentration of acetoin is significantly larger than the proton concentration, which leads to an increased acetoin reduction compared to the HER. The impact of trace metals promoting the HER seems less pronounced at the higher pH. This enables an enhanced conversion of acetoin in the fermentation broth at elevated pH values. The selectivity towards 2-butanone in the fermentation broth is again higher than in the model solution. Hereby, the high selectivity appears independent of the current acetoin concentration and remains more or less constant over the course of the experiment. The HER increases with decreasing acetoin concentration over the course of the experiment and the FE for 2-butanone drops from nearly 80% after 15 min to

47% at the t_{FC} and further to 25% after 240 min. At t_{FC}, the conversion of acetoin is lower with 85% in the fermentation broth compared to 89% in the model solution on lead. Next to the pH, this could be further tackled by the adjustment of other reaction parameters such as a lower current density, for example, or better mixing by an increased flow rate. A removal of metal ions via ion exchange or electrodeposition could also prevent the HER due to the elimination of active sites from trace components. Nevertheless, with a not yet optimized process resulting in a yield of 47% and a high selectivity of 78%, these results demonstrate the feasibility of the electrolysis directly in the fermentation broth.

Prolonged Experiments

Experiments with the model solution with acetoin concentration in the range of the fermentation broth were additionally conducted until acetoin was converted completely. The resulting concentrations are depicted in Figure 3.9.

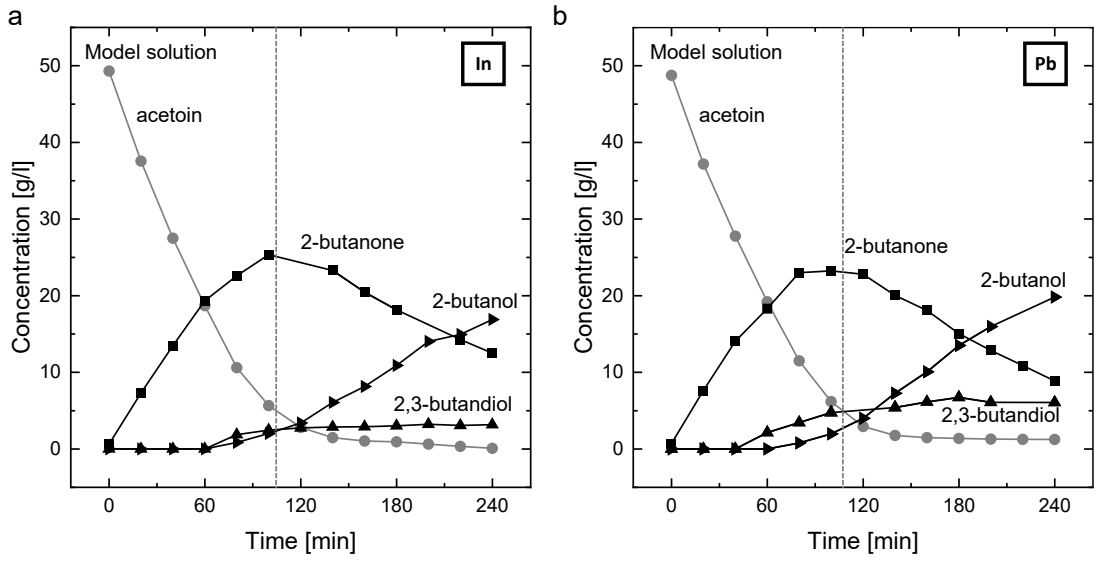

Figure 3.9: Course of the concentration of reactants over the reaction time from the model solution on a: indium and b: lead at 50 mA cm^{-2}. The dashed vertical line indicates the time of 100% theoretical conversion (t_{FC}).

When prolonging the experiment well beyond t_{FC}, the 2-butanone

concentration decreases and 2-butanol is formed. This appears slightly more pronounced on the indium electrode in Figure 3.9a than on lead in Figure 3.9b. Both show a previously unreported electrochemical reduction of 2-butanone to 2-butanol, rather than a direct reduction from acetoin to 2-butanol. In Figure 3.4a 2-butanol was also formed. However, at this low concentration, acetoin is depleted over the length of the electrochemical cell, which enables reduction of 2-butanone to 2-butanol. No 2-butanol is apparent in experiments with the fermentation broth, as the lower overall conversion prevents the reduction of 2-butanone because acetoin is not depleted during the experiment, even at lower initial concentration.

The unwanted reduction of 2-butanone could be prevented by continuous product removal. It could be achieved by gas-stripping, as 2-butanone has a far higher vapor pressure at ambient conditions than acetoin, 2,3-butanediol, or water, or by other separation techniques such as liquid-liquid extraction or simulated moving bed chromatography. The choice should be guided by the influence on the electroreduction and economic feasibility. Alternatively, a lower current density and higher flow rate of the electrolyte could decrease the formation of 2-butanol until nearly all acetoin is depleted. However, a full conversion of acetoin at a reasonable current density would not be possible without continuous product removal.

3.3.3 Flow Cell Experiments with Supernatant from *L. Lactis* Fermentation

To increase the potential carbon efficiency of the process chain, the *B. Licheniformis* was exchanged with the more carbon efficient *L. Lactis*. The modified organism was kindly provided by Kandasamy et al. [Kand2016]. A detailed evaluation of the acetoin production of the organism is reported in Literature [Grüt2023]. Fermentation supernatants from different complex media and a resting cell fermentation were used as the electrolyte for subsequent 2-butanone synthesis after the removal of solids without further purification. Figure 3.10 shows the resulting yield for 2-butanone

synthesis. The current density was adjusted to the acetoin concentration in the different fermentation supernatants.

The yield in the different complex media (M17, HS, LB and YEP) is

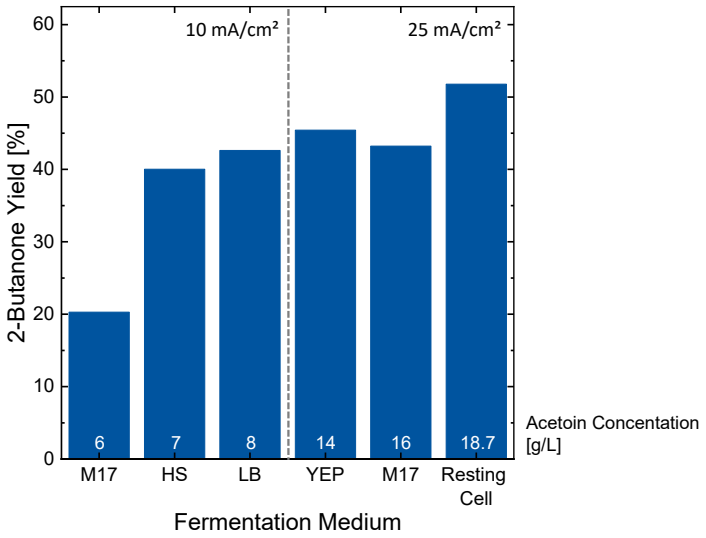

Figure 3.10: 2-butanone yield after electrochemical reduction on the lead cathode of supernatants from fermentation with *L. Lactis* in different complex media: (M17, Herstrin Schramm (HS), Lysogeny Broth (LB), and Yeast Extract Peptone (YEP)) and the resting cell cultivation. The current density was adjusted to the acetoin concentration in the fermentation supernatant, which is indicated in white in g L^{-1}

around 40 to 45% in most cases. Only the yield of the conversion in M17 complex media at a low acetoin concentration is lower at 20%, most likely due to the low initial concentration. The reproducibility of the results indicate that conversion in the different complex media is not hindered by specific components, unique to a specific complex medium, but by the overall amount of ions and organic substances in the complex media. This observation is underlined by the similar yield in the fermentation broth in Figure 3.8 on the lead cathode at pH 6.5.

In contrast, 2-butanone synthesis in the supernatant from the resting cells reaches a yield well above 50%. It surpasses the yield from conversion in the different complex media, as well as the yield of the synthesis in the fermentation supernatant from *B. Licheniformis* fermentation, displayed in Figure 3.8. This indicates that the lower concentration of dissolved

species in the supernatant from the resting cells benefits the subsequent electrochemical conversion, which is in agreement with the recent findings from de Smit et al. [Smit2023]. The improved yield in the electrochemical conversion step in combination wit a more efficient microorganism for the initial acetoin synthesis showcase the potential of the integrated process. Further, the result illustrates that experimental assessment of process chains under realistic conditions is essential, to efficiently coordinate subsequent processes and determine the feasibility of process integration.

3.4 Conclusion and Outlook

This chapter demonstrated a promising sustainable production route for 2-butanone from glucose in a two-stage process: a fermentation with subsequent electrochemical reduction of the supernatant without further intermediate purification. Acetoin was directly converted in the fermentation broth supernatant after the addition of a supporting electrolyte in an electrochemical cell. Lead and indium were analyzed for their activity in a model solution and the supernatant from fermentation with a *B. Licheniformis* in LSV experiments. Then, labscale experiments with 35 cm^2 electrode area at 50 mA cm^{-2} current density yielded a quantitative analysis of the 2-butanone production. There, the influence of the acetoin concentration was analyzed in a model solution and by gradually decreasing the dilution of the fermentation supernatant. Reaction conditions that proved suitable for reduction in the model solution initially showed a poor yield in the fermentation supernatant. By adjusting the pH in the electrolysis cell to the pH of the fermentation supernatant, selective reduction was achieved with a yield and FE of 47%, and a selectivity of 79% from a non-diluted fermentation supernatant on a lead electrode. While indium showed a better performance in model solution experiments, it showed a lower conversion and selectivity in experiments with the fermentation broth. On both electrodes, the HER appeared to be the predominant competing reaction, likely due to trace metal components in

the complex fermentation medium.

While fermentation with the *B. Licheniformis* is robust and yields high acetoin titers, the maximum carbon efficiency is limited intrinsically. Therefore, a genetically modified strain of *L. Lactis* was employed for acetoin synthesis. Acetoin conversion in the supernatants from different complex media showed a nearly identical yield to those from the *B. Licheniformis* supernatant. Then, the supernatant from a resting cell fermentation with a lower amount of dissolved ions was employed. The 2-butanone yield was above 50%, outperforming all previous electroreductions in fermentation supernatants. The result underlines the hypothesis that dissolved ions and organic species have a detrimental effect on the subsequent electrochemical conversion. Further, it highlights the importance of experimental process coupling under real conditions to coordinate subsequent processes towards a feasible process chain. The resulting combination of the highly efficient acetoin production with the *L. Lactis* and the improved yield of the subsequent electrochemical conversion in the supernatant of the resting cell essay supernatant showcases the potential of such an integrated process.

Future work should assess the entire process chain to analyze the energy input and the resulting CO_2-equivalent for 2-butanone synthesized via this route. This should include the feedstock for the fermentation and the final product separation after the electrochemical conversion. Subsequently, a techno-economic assessment (TEA) can reveal the market potential of this production route. To further increase the energy efficiency of the process, the oxidation of water to oxygen that accompanies the reduction reaction to 2-butanone in the electrochemical cell could be replaced by a value adding reaction, such as the oxidation of hydroxymethylfurfural (HMF) to 2,5-furandicarboxylic acid (FDCA).

4 Integrated biphasic electrochemical oxidation of HMF to FDCA

Parts of this chapter have been published as:
Tobias Harhues, Maria Padligur, Franziska Bertram, Daniel Matthias Roth, John Linkhorst, Andreas Jupke, Matthias Wessling and Robert Keller
Integrated Biphasic Electrochemical Oxidation of Hydroxymethylfurfural to 2,5-Furandicarboxylic Acid, ACS Sustainable Chem. Eng., 2023, 11, 23 8413-8419 DOI: 10.1021/acssuschemeng.3c01403
Parts of this chapter are in preparation for publication:
Tobias Harhues, Benjamin Zemlin, Matthias Wessling, Robert Keller

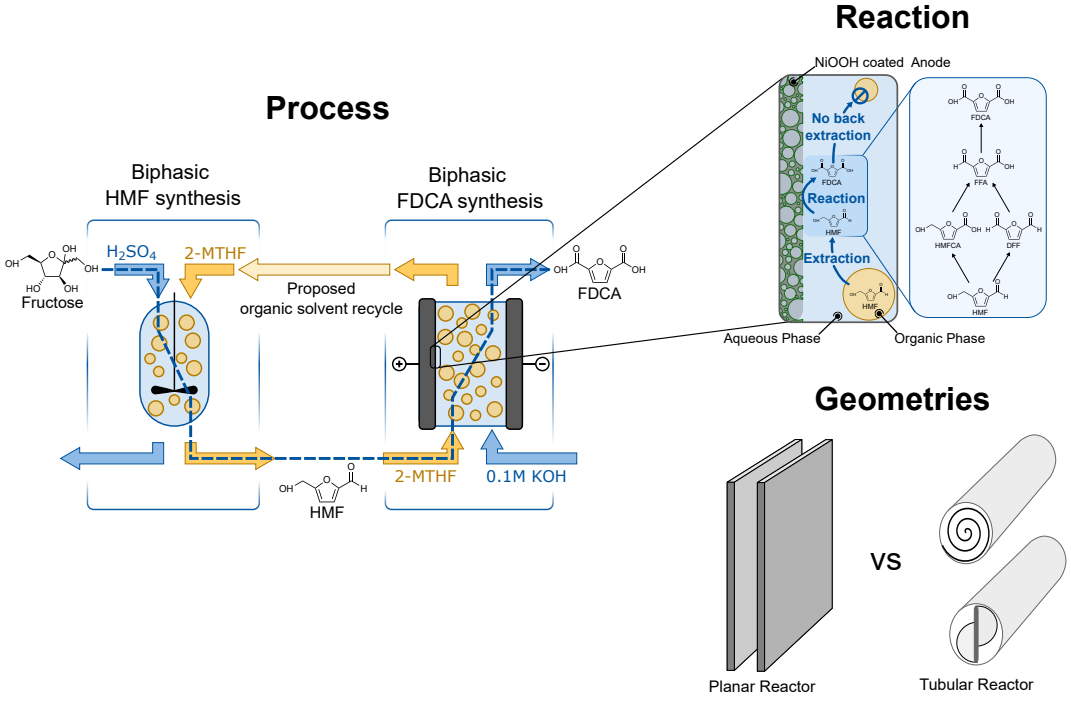

4.1 Introduction

Production of polymers accounts for a significant amount of CO_2 emissions, and is expected to increase from 380 million metric tons (Mt) in 2015 to approximately 1100 Mt per year by 2050 [Geye2017]; [Meys2021]. Further, it led to the emission of 1.8 billion tons of CO_2-equivalent in 2019, and will reach up to 4.3 billion tons in 2060 [Fuhr2019]. This environmental impact can be decreased significantly, when sustainable carbon sources like biomass are employed to produce so-called biopolymers in efficient processes [Meys2021]; [Anas2010]; [Zhen2019]. Monomers for the synthesis of such biopolymers can be produced in electrochemical processes. These monomers often are oxygenates and their electrochemical synthesis has been identified as a key factor to decrease CO_2 emissions in the chemical industry [Leow2023]. 2,5-Furandicarboxylicacid (FDCA) is such an oxygenate and a promising biobased platform chemical and monomer for the chemical industry [Werp2004]. It was among the twelve top value added chemicals, selected by the US Department of Energy as early as 2004 [Werp2004]. FDCA can be polymerized to different polyesters, polyamides or other polymers [Zhan2021]; [Jong2012b]; [Shen2022], with polyethylen furonat (PEF) as the most prominent example [Jong2022].

FDCA can be synthesized from C6-sugars, mainly fructose, via different routes, for example via 5-(hydroxymethyl)furfural (HMF) [Rose2020]. To synthesize HMF, fructose is dehydrated with an acid-catalyzed reaction in aqueous environment. However, HMF is highly reactive and its stability is the main limiting factor of the HMF yield during fructose dehydration [Mukh2015]. The *in situ* extraction of HMF into an organic phase stabilizes the product and increases the HMF yield [Mukh2015]; [Saha2014]; [Aign2020].

Different routes exist to subsequently oxidize HMF to FDCA, for example chemocatalytic, biocatalytic and electrochemical routes [Jens2020]; [Saji2018]. Due to the toxic nature of higher HMF concentrations, no robust bio-catalytic route exists to date and chemo-catalytic oxidation requires elevated temperature and pressure [Yuan2020]; [Hame2020]. In

contrast, electrochemical oxidation of HMF to FDCA is possible at ambient conditions and can reduce the specific carbon footprint of the oxidation significantly [Pate2022]; [Mass2022]. For the electrochemical oxidation, catalysts have been researched extensively [Jens2020]; [Ge2022]. Transition metal catalysts such as $Ni(OH)_2$/NiOOH exhibit good selectivity [Grab1991]; [Tait2019] and have been researched in depth [Bend2022]. Latsuzbaia et al. [Lats2018] demonstrated the potential of the synthesis route with a $Ni(OH)_2$/NiOOH catalyst in a lab-scale pilot plant with a yield of 70%. For an overall process from the raw material (fructose) to the desired product (FDCA), the purification of HMF and the stability of HMF during oxidation are the most limiting steps [Pate2022]; [Mass2022]; [Bell2019]; [Al G2021]. An approach to integrate these processes has been proposed by Liu et al. [Liu2020]. However, it requires dilution of the organic product phase from HMF synthesis to a single aqueous phase, which impairs subsequent product separation and limits the reactant concentration. An alternative could be the direct application of the organic intermediate phase in a biphasic electrochemical reactor.

Biphasic electrochemical synthesis has been successfully employed to extract the product *in-situ* into a second phase to protect it from further oxidation [Stie2015]; [Di M2017]. However, biphasic systems can be accompanied by additional drawbacks such as reactions of the organic solvent and the decreased conductivity of the electrolyte. Therefore, these complex electrolytes have been subject to in depth analysis in the literature [Liu2017]; [Deng2016]; [Dick2014].

Outside of electrochemical applications, biphasic processes are well known in thermal processes, such as extraction, and are mostly carried out in tubular reactors. They offer more favorable flow conditions and are generally easier to scale up towards industrial applications. To decrease mass transport limitations in tubular structures, static mixer elements are employed and have been thoroughly researched [Armb2020]. Recently, additive manufacturing of metal enabled Limper et al. [Limp2022] to deploy a metal static mixer as the working electrode for improved mass transfer in a tubular electrochemical reactor. In a different approach, a high packing

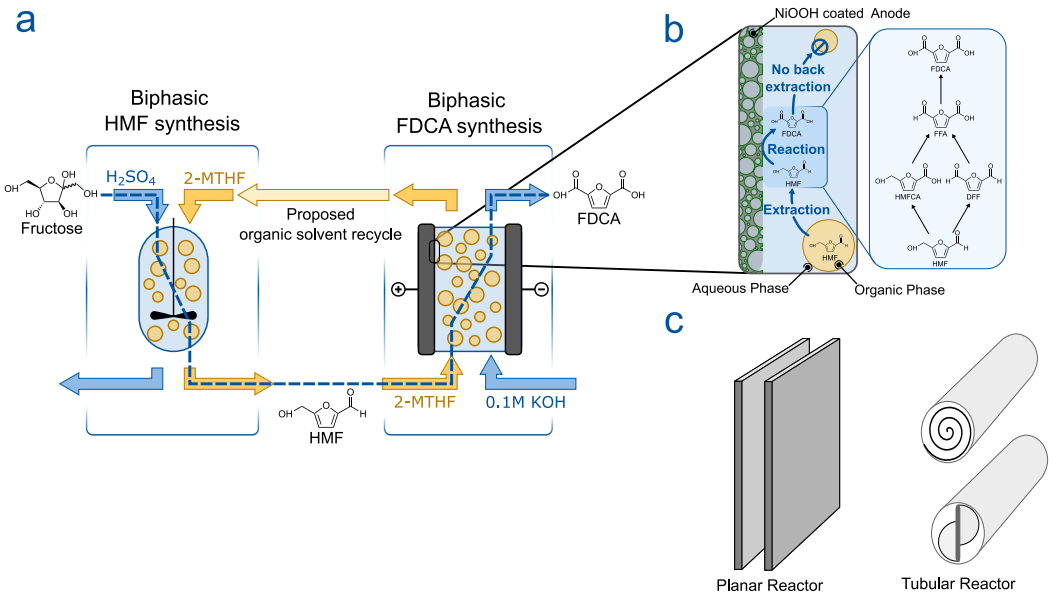

Figure 4.1: a: Process scheme of the integrated two-step synthesis. Fructose is dehydrated and extracted *in-situ* into an organic phase (2-methyltetrahydrofuran (2-MTHF)), which is fed into the electrochemical reactor, where HMF is oxidized to FDCA. b: Schematic of the *in-situ* extraction of HMF into the aqueous phase in the electrochemical cell and the oxidation mechanism on the electrode. c: Different reactor geometries tested for this process.

density of the electrodes was achieved in a tubular so-called swiss roll reactor [Bawa2018].

This chapter studies the biphasic electrosynthesis to couple the electrochemical oxidation of HMF to FDCA and the hydrogenation of fructose to HMF to mitigate intermediate HMF separation as depicted in Figure 4.1. It focuses on the biphasic electrochemical oxidation, where the raw organic product phase of a HMF synthesis is fed directly into an electrochemical flow-cell which mitigates the need for intermediate separation processes. In the reactor, HMF is continuously extracted into the aqueous phase and oxidized with a $Ni(OH)_2$/NiOOH-coated nickel-foam electrode. After the synthesis, FDCA is only found in the aqueous phase, from which it can be separated via different crystallization techniques [Lats2018]; [Gaus2020].

This chapter demonstrates the feasibility of the process and subsequently analyzes the influence of the flow rate and current density for the biphasic electrochemical oxidation with a synthetic model solution in the planar flex-E-cell. Subsequently, it focuses on the energy efficiency

of the electrochemical oxidation by reducing the gap width of the planar flow-cell. The concept is transferred to a tubular reactor geometry to exploit the benefits of the flow distribution in a tubular structure and enable the prospective scale up in the tubular geometry. 3D-printed static mixer electrodes with different structural properties introduce passive mixing to improve the process yield. Further, a swiss roll reactor with an unprecedented volume-specific electrode surface explores the feasibility of such a reactor concept for a future scale up of the biphasic FDCA synthesis. Closing, both concepts are compared to the conventional planar reactor geometry.

4.2 Experimentals

4.2.1 Materials

Nickel foam (grade 4753) was purchased from Recemat NL, HMF (>99%) from AVA-Biochem. Nickelnitrate hexahydrate ($Ni(NO_3)_2 \cdot 6H_2O$) and titanium foil (thickness 0.89 mm, 99.7% purity) were purchased from Alpha Aesar. Sulfuric acid (H_2SO_4, 1 mol L^{-1}), nitric acid (HNO_3, 65 wt%), hydrochloric acid (HCL, 1 mol L^{-1}), FDCA (97%), 5-Hydroxymethyl-2-furancarboxylic acid (HMFCA) (>95%) and Furan-2,5-dicarbaldehyde (DFF) (97%) were purchased from Sigma-Aldrich. Acetone (technical), 2-MTHF (>99%), trifluoroacetic acid(TFA) (≥99.9%) and Acetic Acid (glacial, 100%) were purchased from CarlRoth. 2-formyl-5-furancarboxylic acid (FFCA) (<98%) was purchased from TCI chemicals. Nickelsulfate hexahydrate ($Ni(SO_4)_2 \cdot 6H_2O$) (99%) was purchased from Thermo Scientific. All chemicals were used as received without further purification.

4.2.2 Preparation of Electrodes for the Planar Reactor

Electrodes for the planar electrochemical cell were cut to a geometrical surface area of 35 cm^2. Prior to the deposition of the $Ni(OH)_2$/NiOOH catalyst, nickel foams were etched according to the procedure from Grden et al. [Grde2012] to remove any contamination or oxide layers and increase the adhesion stability of the catalyst coating. After rinsing with deionized water (DI-water), the nickel foam electrodes were immersed in the etching solution for 10 min. The etching solution consisted of 40 mL DI-water, 50 mL 65 wt% nitric acid, 60 mL 1 mol L^{-1} sulfuric acid and 50 mL acetic acid. Subsequently, electrodes were rinsed with DI-water and cleaned in 1 mol L^{-1} hydrochloric acid and aceton in an ultrasonic bath for 15 min each and dried.

$Ni(OH)_2$/NiOOH catalyst coating was deposited following a procedure from Aghazedeh et al. [Agha2014]. The cleaned electrodes were wetted with DI-water and subsequently immersed in a 1 mol L^{-1} solution of $Ni(NO_3)_2$. Then, a constant current of 4.29 mA cm^{-2} was applied for 15.5 min. A platinized titanium mesh (Umicore, Germany) with a surface area of 35 cm^2 was used as the counter electrode.

4.2.3 Preparation of Electrodes for the Tubular Reactors

Electrodes for the tubular mixer electrode reactor were prepared from 3D-printed stainless steel and nickel foam. The 3D-printed electrodes were produced with a MySint 100 PM, (Sisma, Italy) from stainless steal (AISI 316L) with a particle mean diameter below 60 μm, after [Limp2022]. The electrodes were designed as so-called twisted tape static mixer electrodes with a length of 100 mm and a pitch length of 40 mm. The nickel foam based electrodes were shaped by hand, accordingly. All electrodes had a similar outer shape but featured a different structure and porosity. The electrodes are presented in Figure 4.3a, the respective cross sections in Figure 4.3b. The 3D-printed electrodes had to be printed as two separate pieces due to the height limitation of the 3D-printer. The electrodes

produced feature a geometrical surface area of 48 cm^2

To coat the catalyst layer, the electrochemical method used for the planar electrodes was not feasible, as it led to a non-uniform coating. This can be attributed to the non-planar shape which causes shadowing effects during the coating procedure. Instead, a chemical bath deposition known from literature was applied to the electrodes, after etching according to the procedure described for the planar electrodes [Alhe2013]. The electrodes were then immersed in the coating bath of 90 mL DI-water, with 10.4 g $NiSO_4 \cdot 6H_2O$, 2 g $K_2S_2O_8$ and 10mL NH_3 (30-33%) for 2 h. They were subsequently dried at 60 °C for 1 h.

In addition to the mixer electrodes, electrodes for the swiss roll reactor were prepared. For this purpose, nickel foam sheets of 96 mm x 100 mm were cut and subsequently etched and coated according to the mixer electrodes.

4.2.4 Setup of Planar Reactors

For all experiments with planar geometries, the commercially available flex-E-cell (flex-X-cell GbR, Germany) was used. The flex-E-cell was assembled the following way: Two layers of catalyst coated foam with a geometrical area of 35 cm^2 each were placed in the flow cell and contacted on the backside with a titanium plate. The electrolyte gap between anode and cathode was filled with a poly-propylene mesh spacer with a width of 0.8 cm. The counter electrode was a platinum coated titanium mesh (Umicore, Germany) on a titanium plate. Unless stated otherwise, the gap-size was 3 mm. If necessary, the electrolyte gap-size was adjusted via the number of spacers and flow-frames.

4.2.5 Setup of Tubular Reactors

The reactor for the mixer electrodes is displayed in Figure 4.2. It had an active length of 100 mm, an outer diameter of 40 mm, and an inner

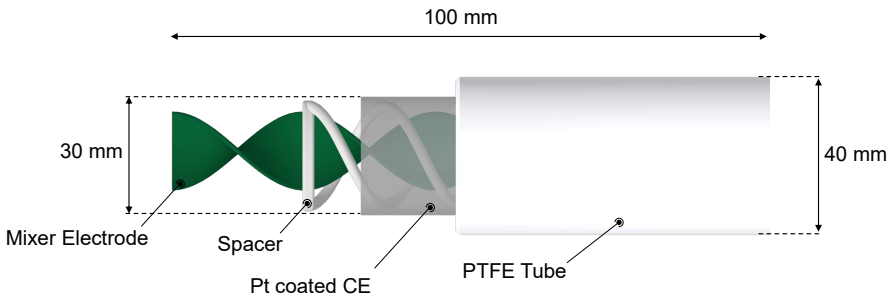

Figure 4.2: Schematic of the mixer electrode reactor and its dimensions.

diameter of 30 mm. It was made of poly(tetrafluoroethylene) (PTFE). The caps were 3D-printed on an EDEN 260V (Stratasys). The mixer electrodes were centered in the reactor, the counter electrode was a platinum coated titanium felt (Fuel Cell Store, US). The working electrodes had a geometric surface area of 49 cm^2. A 3D-printed spacer was used to separate the electrodes. One electrode that was hand crafted from nickel foam (NF) and three 3D-printed electrodes (E01-E03) with different geometric features were used. They are displayed in Figure 4.3a, their respective cross sections are shown in Figure 4.3b.

The swiss roll reactor is displayed in Figure 4.4, the working electrode and counter electrode were separated by a polypropylene mesh spacer with a thickness of 0.8 mm. The active length of the reactor was 100 mm, with an inner diameter of 20 mm and an outer diameter of 22 mm. The electrodes are rolled up to 2.5 windings and contacted with soldered wires. The reactor had a geometric surface area of 192 cm^2. The counter electrode was the same as in the mixer electrode design.

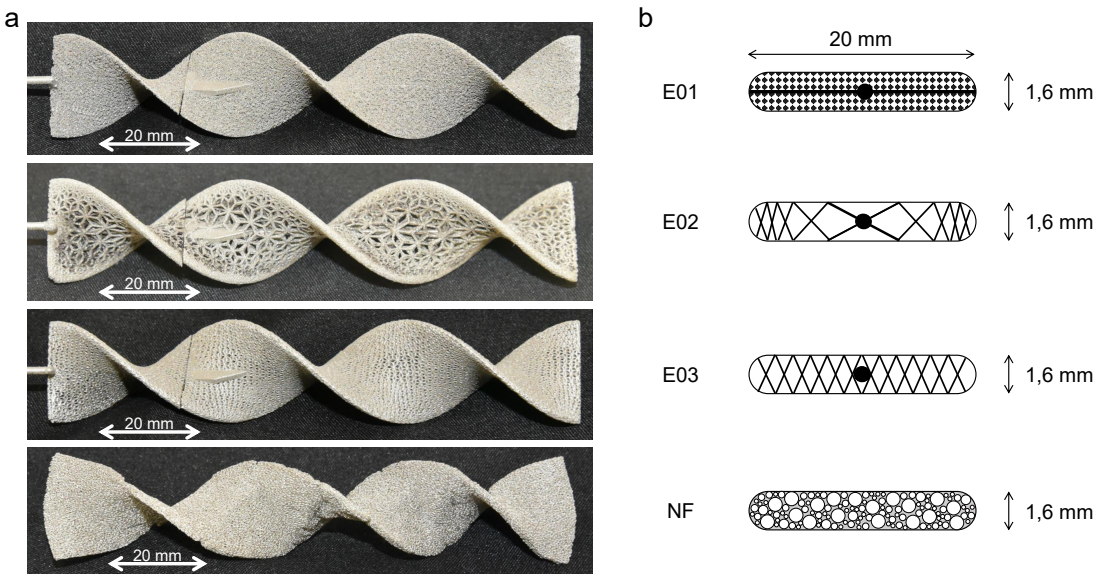

Figure 4.3: a: Images, and b: schematic representation of the cross sections of the different mixer electrodes employed in the reactor, prior to catalyst coating. E01-E03 were 3D printed from stainless steel and the NF electrode was hand crafted from nickel foam. All electrodes were designed with similar outer dimensions.

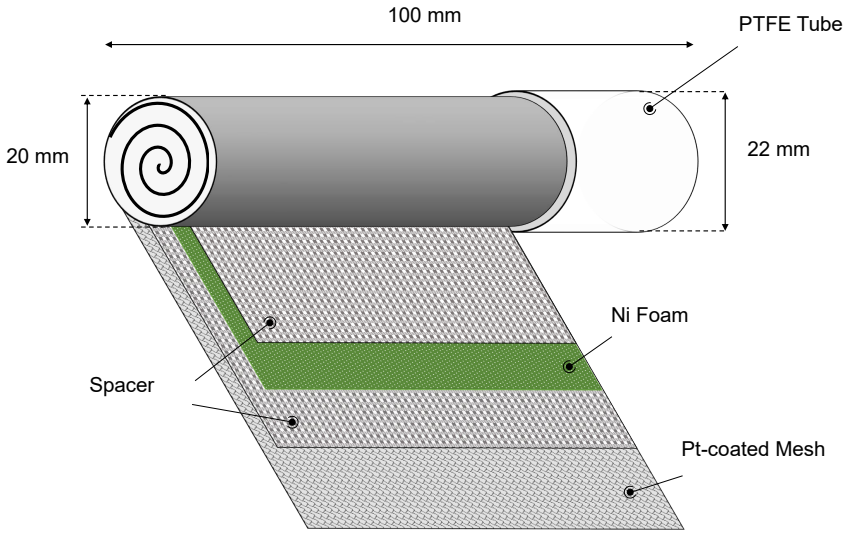

Figure 4.4: Schematic of the swiss roll reactor and its dimensions. The nickel foam is the anode, the platinum coated mesh is the cathode, and the spacer layers establish a constant electrode distance and prevent short circuits.

4.2.6 Flow Cell Experiments

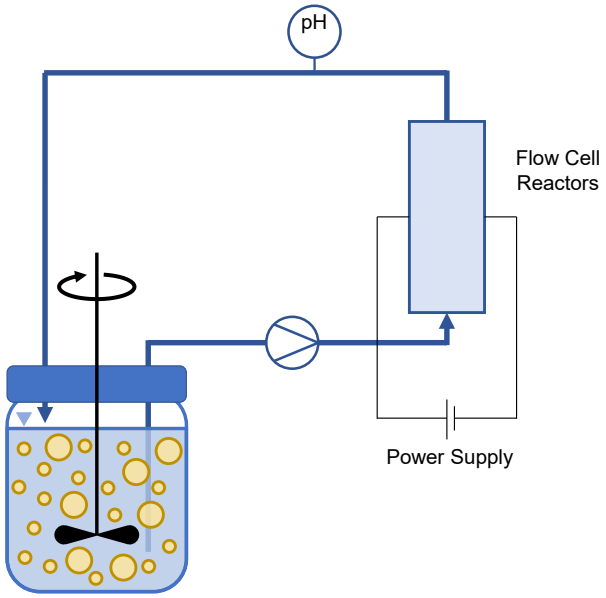

Figure 4.5: Experimental setup used for all flow cell experiments in this work. Different flow cell reactors (planar, tubular mixer electrode reactor and tubular swiss roll reactor) are employed in the setup.

Flow-cell experiments were conducted as single phase (aqueous phase) and biphasic (aqueous and organic phase) systems. The aqueous phase was 0.1 mol L^{-1} KOH in DI-water for experiments in the planar setup and 1 mol L^{-1} KOH in DI-water for experiments in the tubular reactors. The organic phase was 2-MTHF. All experiments were conducted in an undivided cell because of the challenging chemical environment of highly alkaline and organic media where no ion exchange membrane was stable. For the process validation experiments in the planar cell, 300 mL of electrolyte were used, all subsequent experiments were conducted with 450 mL of electrolyte. Reference experiments with the purely aqueous, single-phase electrolyte were conducted with an HMF concentration of 16.66 mmol L^{-1}, which corresponds to the average HMF concentration in the biphasic mixture with a phase ratio of 1:2 ($V_{organic}$ to /$V_{aqueous}$). The setup is depicted in Schematic 4.5.

In the biphasic experiments, HMF was supplied via the organic phase with a concentration of 50 mmol L^{-1} in the organic phase (2-MTHF). The

aqueous phase was mixed with the organic phase at a phase ratio of 1:2 ($V_{organic}$ to $V_{aqueous}$). The mixture was continuously stirred during all experiments with a propeller stirrer (C378-17-A, BOLA, Germany) and a ground clearance of 2 cm^2, powered by a stirrer motor (EUROSTAR 40 from IKA, Germany) at 250 rpm. The emulsion was then pumped through the reactor by a gear pump (MCP-Z-Standart, Ismatec, Germany) at flow rates between 150 and 1000 mL min^{-1}. Although the flow rate did not show an impact on the FDCA yield, the flow rate is increased for experiments at increased current densities to prevent possible mass transport limitations at higher current densities. The electrolyte was recycled during all flow cell experiments. pH and temperature were continuously monitored at the outlet of the flow cell with a pH sensor (SE554, Knick, Germany). Constant current was supplied by a potentiostat (VMP150, VMP 3B-20 (20A/20V), Biologic) and the cell voltage was recorded. A use of a reference electrode was not feasible, most likely due to the discontinuous nature of the biphasic electrolyte leading to highly instable signals. All experiments were carried out at room temperature. At current densities of 45 mA cm^{-2} and above, the reservoir temperature was controlled with a thermostat (CORIO CD-900F).

All experiments were evaluated for conversion (X), yield (Y), selectivity (S) according to Equations 2.6a-c and Faraday efficiency (FE) according to Equation 2.8, when sufficient charge for the complete oxidation of HMF to FDCA was transferred. The reaction time (t_{FC}) was calculated according to Eq. 2.9 with 6 electrons necessary for the oxidation from HMF to FDCA. Consequently, this results in a shorter duration for experiments with higher current and a longer duration for experiments with a higher HMF content.

To evaluate the influence of the electrolyte gap on the cell voltage, the gap width between the anode and the cathode was adjusted via the number of spacers. When the cell voltage is reported as a single value, it is the average value of the experiment, disregarding the first 10% of the duration of the experiment to eliminate the influence of the initial polarization.

4.2.7 Degradation Experiments

HMF-degradation experiments were conducted in a beaker on a stirring plate at room temperature. The mixture was stirred continuously with 300 rpm and samples were taken and processed similarly to the flow-cell experiments. Degradation experiments with the biphasic mixture were conducted with a phase ratio of 1:2. Single phase degradation (aqueous and organic) were conducted with an HMF concentration in the overall system of 16.66 mmol L^{-1}, corresponding to the average concentration in a biphasic mixture with a phase ratio of 1:2.

4.2.8 Preparation of Raw Feed Solution from Fructose Dehydration

HMF synthesis was carried out using the batch reactor used in Aigner et al. [Aign2020]. The reaction was prepared according to the following protocol: 0.1 mol of fructose are dissolved in 0.2 L of 0.2 mol L^{-1} H_2SO_4. In addition, 2.75 mol 2-MTHF were added to the system. The reactor is heated from room temperature to 155 °C over a period of 125 min and the velocity of the lower stirrer is set to 400 rpm. The temperature is maintained for 30 min and quenched directly afterwards to stop the reaction. The organic and the aqueous phase were separated and stored at 4 °C. The HMF-rich product solution used for this work had a HMF concentration of close to 60 mmol L^{-1}. To compare the results of the model solution conducted with 50 mmol L^{-1}, the raw product solution was diluted with 2-MTHF to 50 mmol L^{-1}. In addition to HMF, the organic product solution contained small amounts of levulinic acid (< 0.5 mmol L^{-1}).

4.2.9 High Performance Liquid Chromatography (HPLC)-Analysis and Sampling

Samples were taken via a 3-way valve at the outlet of the flow cell in intervals of 15 min or 7.5 min in experiments with current densities of 60 mA cm^{-2} and above, and for experiments with the swiss roll reactor.

Samples were taken via 3 mL syringes, which were left upright for 5 min to allow for phase separation. Then, the phases where separated, separately diluted and prepared for HPLC analysis. Samples of the aqueous phase were diluted tenfold, and samples from the organic phase were diluted by a 20-fold to ensure full dissolution of the organic phase within the aqueous phase. For the dilution, a phosphate buffer (7.5 g L^{-1} K_2HPO_4 and 5.5 g L^{-1} KH_2PO_4) was used to neutralize the pH and stabilize HMF. As the HPLC, an Agilent 1100 HPLC system with an organic acid resin column at 35 °C with a flow rate of 1 mL min^{-1} at 90 bar column pressure was employed. The eluent was 2 mmol L^{-1} TFA in purified water. Reactant concentrations were analyzed via diode-array detection: HMF and DFF were detected at 300 nm wavelength, FDCA, FFA and HMFCA were detected at 254 nm wavelength.

4.3 Results of HMF Degradation

Costs associated with HMF degradation are one of the critical parameters when processing HMF [Mass2022]. The degradation properties are influenced by the electrolyte, Figure 4.6 shows the degradation of HMF in different solvent mixtures relevant for this work.

In the aqueous medium at pH 13, HMF is degraded nearly linear over the course of the experiment. After 10 hours, more than 20% of the initial HMF is degraded, which is in agreement with literature [Lats2018]. Contrarily in the organic phase, 2-MTHF exhibits no significant degradation over the course of two weeks. In the biphasic mixture, HMF degeneration reduced by more than 50% compared to the single aqueous phase. This shows that storage of HMF is feasible in an organic phase, e.g. the organic product phase of the HMF synthesis. The degradation of HMF in the aqueous phase will limit the performance of the process. Especially in larger plants, where longer retention times in larger tanks and columns are common, degradation will be more prominent, and thus, the forming humins will be even more problematic. In this regard, biphasic electrolytes are attractive as they increase the HMF stability.

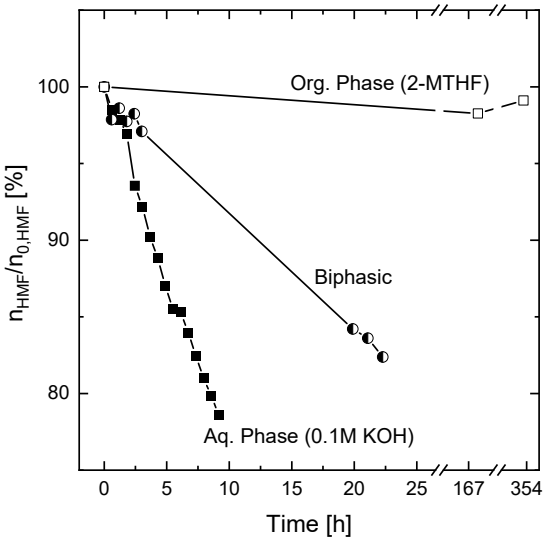

Figure 4.6: Degeneration of HMF in the aqueous electrolyte (0.1 mol L^{-1} KOH) (■), the organic phase (2-MTHF) (□) and a biphasic mixture with a phase ratio of 1:2 ($V_{organic}$ to $V_{aqueous}$) (◐) as used in future experiments. The initial HMF concentration was 16.66 mmol L^{-1}.
This graph is identically used in the dissertation of M. Padligur.

4.4 Results and Discussion of Experiments in the Planar Cell

4.4.1 Process Validation

To show the applicability of the biphasic electrochemical oxidation, Figure 4.7a compares the results of an experiment with the biphasic model solution to an experiment with an aqueous electrolyte with similar reaction conditions. The phase ratio in the biphasic experiment is 1:2 at a current density of 15 mA cm^{-2} and a flow rate of 150 mL min^{-1}. Interestingly, the reaction rate of HMF is similar in both systems. The rate of formation and yield of FDCA is nearly identical, which demonstrates the high potential of the biphasic system. Full HMF conversion is not reached in the biphasic system, when sufficient charge for a full conversion of HMF to FDCA is transferred after 105 min. This is most likely due to mass transport limitations, as HMF needs to diffuse from the organic to the aqueous

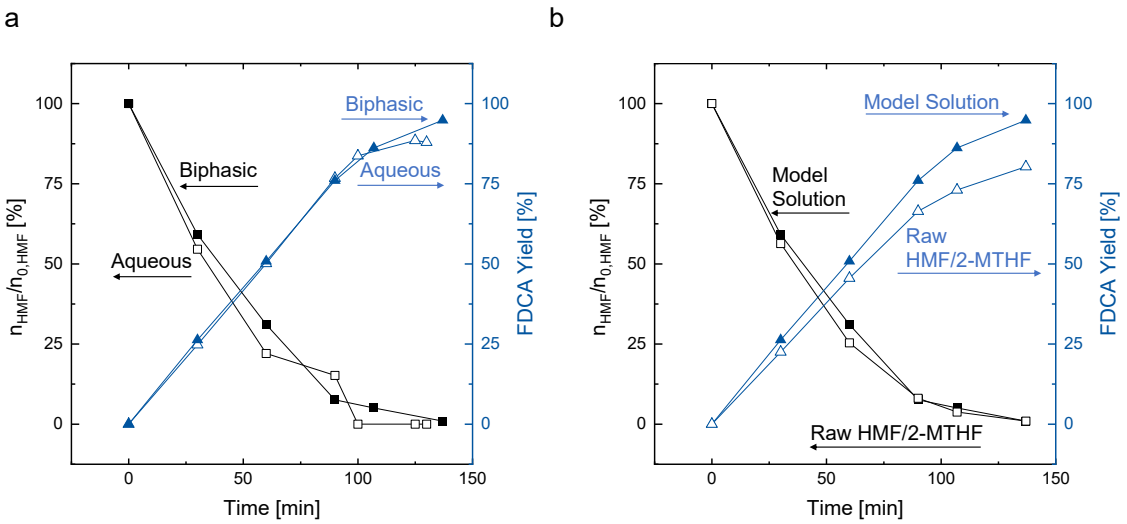

Figure 4.7: a: Comparison of the relative amount of HMF (left y-axis) and yield of FDCA oxidation (right y-axis, blue) in a purely aqueous electrolyte (□, △) and a biphasic model solution (■, ▲).
b: Comparison of the oxidation in the biphasic model solution (■, ▲) and with HMF supplied via the raw HMF/2-MTHF solution from HMF synthesis (□, △). The phase ratio for all biphasic solutions is 1:2 ($V_{organic}$ to $V_{aqueous}$) and the initial HMF concentration in the organic phase is 50 mmol L^{-1}

phase before it can react at the electrode. Especially at low remaining HMF concentrations, mass transport will be low. Further, the electrode surface is always partly in contact with the organic phase, which limits the available surface for the aqueous oxidation. This effect has been described in literature in different systems [Liu2017]; [Zhan2017].

While HMF can be found in both phases with a ratio of 1.4 ($n_{HMF,org}/n_{HMF,aq}$), FDCA is exclusively present in the aqueous phase due to its ionic form, resulting from deprotonation of the two carboxylic acid groups in the alkaline environment. This effect eases the separation task significantly. Moreover, close to full conversion of HMF, enables a high solvent recovery rate of 2-MTHF.

Figure 4.7b compares the biphasic model solution to an experiment with the raw HMF/2-MTHF solution from biphasic HMF synthesis. The raw HMF/2-MTHF solution from HMF synthesis was used without any purification and contained impurities, recognizable by its brown color.

When comparing the results, the HMF conversion is very similar to that of the model solution, but the FDCA yield is decreased by about 10%. The impurities from HMF synthesis could be the main cause for the decreased selectivity, as the synthesis yields a broad spectrum of byproducts which cannot be detected in full, let alone quantified. The brown color of the raw HMF/2-MTHF solution suggests a notable amount of humins, which can have various functional groups. These could interact with the HMF or the intermediates of the oxidation. The amount of humins could not be quantified with the available measurement methods. The results with the raw feed solution show that a direct conversion of HMF from the biphasic synthesis is possible at a high yield. This enables the direct use of the raw feed solution without intermediate purification and establishes a very promising concept for an integrated synthesis of FDCA.

4.4.2 Influence of Process Parameters

Different parameters influence the performance of the electrochemical process. In the following section, the impact of the flow rate of the electrolyte, the current density, and the gap width in the flow cell are analyzed with a synthetic biphasic system.

The flow rate of the electrolyte in Figure 4.8a does not show a distinct impact on the process performance, the yield remains more or less constant around 80%. Likewise, the conversion remained above 90%, which indicates that no mass transport limitation is present at the current density of 15 mA cm^{-2}.

An important parameter for electrochemical process development is the current density as it defines the production rate. Figure 4.8c shows the influence of the current density on the FDCA yield, the HMF conversion and the resulting cell voltage at a volume flow rate of 500 mL min^{-1}. With an increasing current density, the conversion drops from nearly 100% at 15 mA cm^{-2} to 70% at 75 mA cm^{-2}. In alkaline media, $Ni(OH)_2$/NiOOH is also a potent catalyst for the oxygen evolution reaction (OER), so

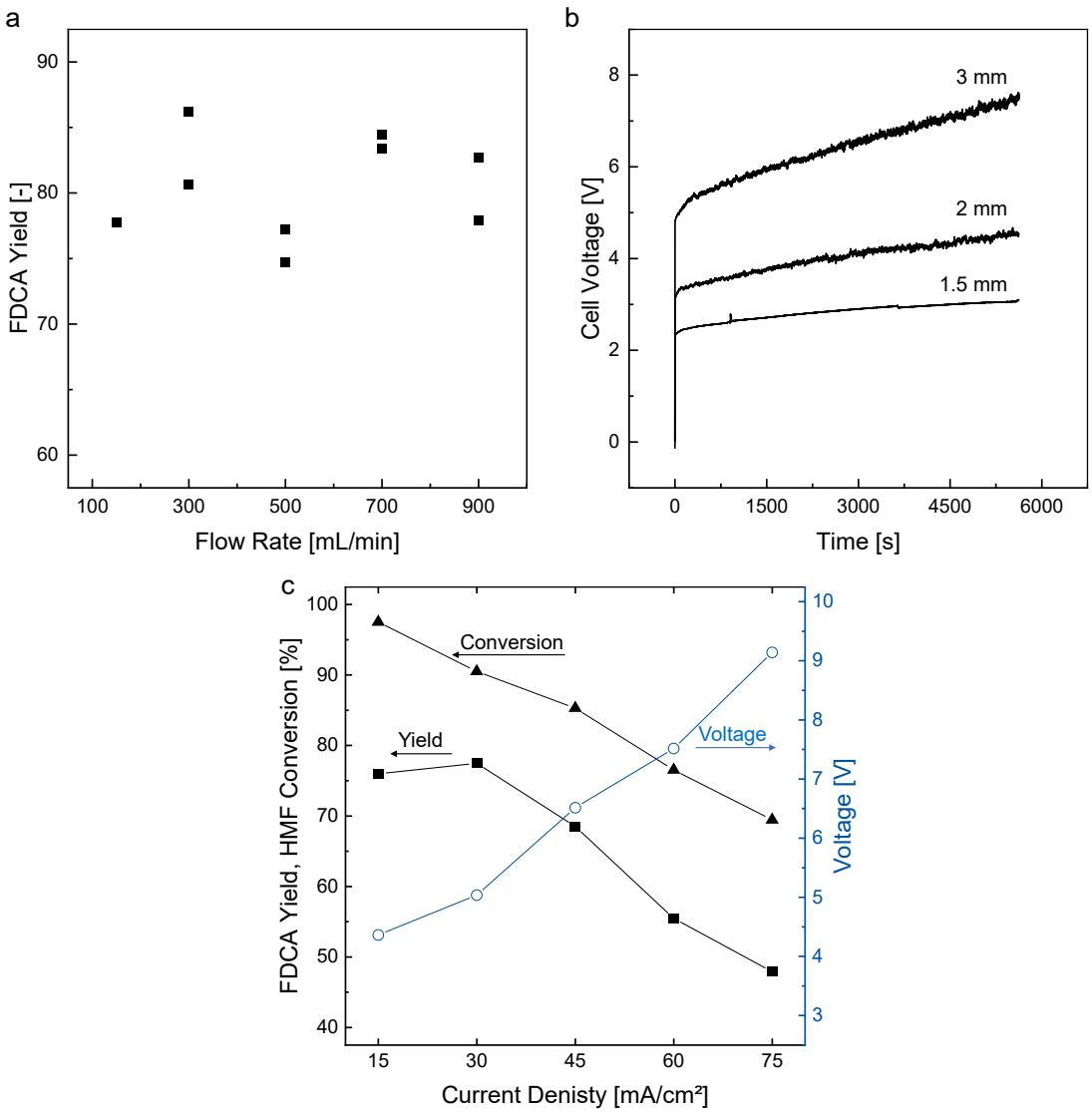

Figure 4.8: a: FDCA yield (■) at different flow rates at a current density of 15 mA cm^{-2}. b: Course of cell voltage over the duration of three experiments for different gap widths of the flow channel at 30 mA cm^{-2} at flow rate of 500 mL min^{-1}. c: HMF conversion (▲), FDCA yield (■) (both on left y-axis) and cell voltage (□) (right y-axis, blue) at different current densities and a flow rate of 500 mL min^{-1}. All experiments in the biphasic model solution with a phase ratio of 1:2 ($V_{organic}$ to $V_{aqueous}$) after t_{FC}.

that at an increasing current density, the OER will become a competing reaction. This is in accordance with a visibly increased gas evolution with increased current density. At 15 mA cm^{-2} and 30 mA cm^{-2}, the yield remains nearly unchanged between 75% and 80%. This can be attributed to the decreased reaction duration, which reduces the extent of the HMF

degradation. At higher current densities, this effect is superimposed by the decreased conversion, resulting in a lower overall yield. In addition to the decreased conversion, the selectivity decreases at higher current densities. The cell voltage increases with the current density, so that HMF could form additional reduction products, as the HPLC analysis detected 2,5-Bis(hydroxymethyl)furan (BHMF) in the aqueous product solution. BHMF has also been detected by Latsuzbaia et al [Lats2018]. In this study, however, the concentration of BHMF was only around 1% of the FDCA concentration. Thus, unidentified products must be present, e.g., oxidation products. In the current experimental setup, a current density of 30 mA cm^{-2} appears to offer a good trade-off between sufficient conversion and short reaction duration.

Further, it can be seen that the cell voltage increases with increasing current density to over 9 V at 75 mA cm^{-2}, which is a consequence of the ohmic resistance of the electrolyte. The overall high cell voltage will impair the economic viability of this process but can be lowered by means of cell design. The gap width of the electrolyte channel is a main factor for the resulting cell voltage.

Figure 4.8b shows the course of the cell voltage over the experiment duration with different gap width at a current density of 30 mA cm^{-2}. Independent of the gap widths, the cell voltage increases over the duration of the experiment. This is partly due to the depletion of HMF, while FDCA accumulates in the system. Further, with decreasing HMF concentration, OER is likely to increase. However, most of the increase in voltage appears to be of an ohmic nature, as it shows a near linear relation to the overall cell voltage. It is far more pronounced at a gap width of 3 mm than at 1.5 mm. This increase likely stems from the acidic nature of the product FDCA. The deprotonation of the two carboxylic acid groups leads to a decrease in hydroxide ions and, in turn, the pH. Yet, due to the logarithmic nature of the pH scale and the difficult measurement of the pH of biphasic electrolyte, the decrease is not visible in pH measurements within the electrochemical experiments. Nonetheless, measurement of the purely aqueous 0.1M KOH solution with and without the addition of

20 mM FCDA confirms the assumption. The pH and conductivity in the solution decreases significantly when FDCA is added. The conductivity decrease by approximately 33% will significantly increase the cell potential as observed in the experiments.

For the gap width of 3 mm, the average voltage is around 6.5 V, which is most likely too high for an economically feasible process. The cell voltage could be decreased tremendously by reducing the gap width, while yield and selectivity remain unaffected. The lowest cell voltage was achieved at a gap width of 1.5 mm which, in turn, leads to a decrease in direct energy consumption by over 50%. A further decrease of the gap width was not possible due to swelling of the ethylene propylene diene rubber (EPDM) frames, used to seal the flow channel. The swelling ultimately lead to blocking of the flow channel at lower gap widths.

4.5 Results and Discussion of Experiments in Tubular Reactors

4.5.1 Static Mixer Electrodes

As an alternative to the conventional planar design, two different tubular reactor concepts are developed and employed in this thesis, the mixer electrode and the swiss roll reactor. Figure 4.9 presents the performance of the four different electrodes employed in the mixer electrode reactor at different applied current densities and flow rates.

At 15 mA cm^{-2} in Figure 4.9a, the conversion is well above 90%, independent of the electrode. However, the yield of the nickel foam electrode (NF) surpasses that of the 3D-printed stainless steel electrodes with a yield of 65% compared to yields between 45% and 50%. Of the 3D-printed electrodes, electrode E02 shows the best yield. When the flow rate is increased to 1000 mL min^{-1} in Figure 4.9b, the yield decreases to 60% for the NF electrode compared to 50% to 55% for the mixer electrodes. The conversion is close to 100%, independent of the electrode. At the

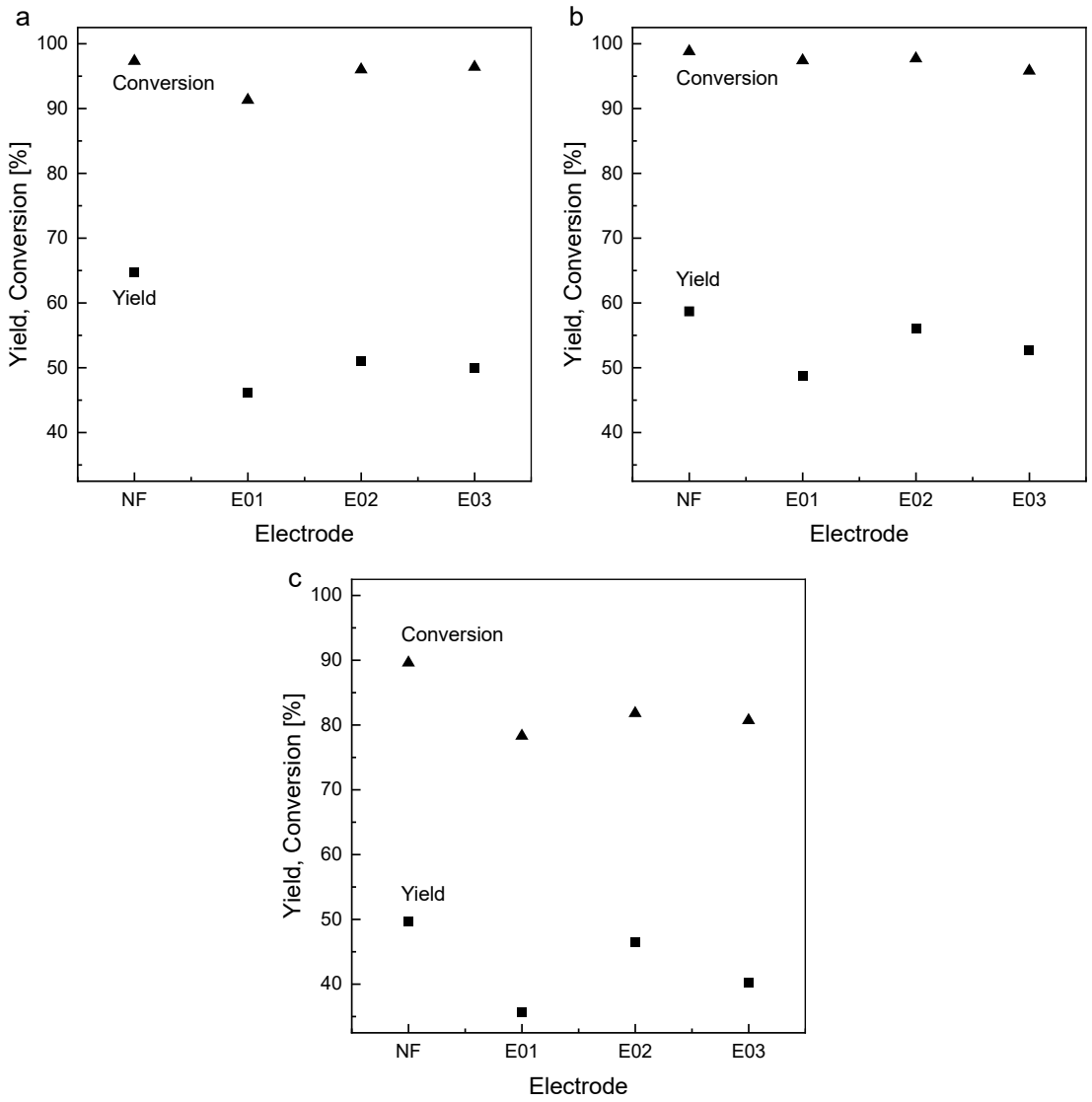

Figure 4.9: FDCA yield (■) and HMF conversion (▲) of different electrode designs used in the tubular reactor setup at a: 15 mA cm^{-2} and 500 mL min^{-1}, b: 15 mA cm^{-2} and 1000 mL min^{-1}, and c: 30 mA cm^{-2} and 500 mL min^{-1} in the biphasic electrolyte.

elevated flow rate, the mixer electrodes seem to benefit from their ability to induce mixing, which is in agreement with literature [Limp2022]. The more open nickel foam electrode does not benefit from the elevated flow rate, as the open foam structure will lead to more flow-through instead of directed mixing. It was not possible to increase the flow rate beyond 1000 mL min^{-1} as the increasing shear forces caused detachment of the catalyst.

At elevated current densities in Figure 4.9c, yield and conversion diminish. A decreased yield was also observed in the planar reactor in Figure 4.8c; yet, it is more pronounced here, already at 30 mA cm^{-2}. The main reason for the decline is most likely the increased oxygen evolution, indicated by the decreased conversion of HMF.

While there is an increasing yield with increasing flow rate, the overall reaction does not benefit from the tubular mixer electrode concept. The enhanced mixing is superimposed by a dominant drawback: the irregular distance of the electrodes. While mixing is generated by the mixer electrodes in the irregular design, it has an adverse effect on the homogeneity of the electric field. In turn, the irregular electrical field results in an inhomogeneous distribution of current so that some areas exhibit a far greater current densities than the average current density. A higher current density is unfavorable for the reaction and leads to more oxygen evolution and side reactions. This is in line with the results of the planar setup, where increasing current density leads to a decreased conversion and selectivity, as shown in Figure 4.8c. Ultimately, the detrimental effect of the irregular distance in the mixer electrode reactor outweighs the benefits of additional mixing, which deems the concept unsuitable.

4.5.2 Swiss Roll Reactor

As an alternative tubular reactor concept, the so-called swiss roll reactor is employed, as depicted in Figure 4.4. Here, the electrolyte flows through the coiled electrodes and the winding arrangement of electrodes leads to a uniform distance between the two electrodes and allows for a higher

volume-specific electrode surface than in the mixer electrode reactor. Figure 4.10a shows yield and conversion at different current densities in the swiss roll reactor at a flow rate of 500 mL min^{-1}. The yield remains at 70% up to a current density of 30 mA cm^{-2} with a conversion of over 90%. Both indicators decrease at current densities above 30 mA cm^{-2}. The course of the yield over the current density is similar to that of the planar reactor in Figure 4.8c. This is consistent, as in both reactor types, the electrolyte can flow through the nickel foam electrode in contrast to the mixer electrode reactor design.

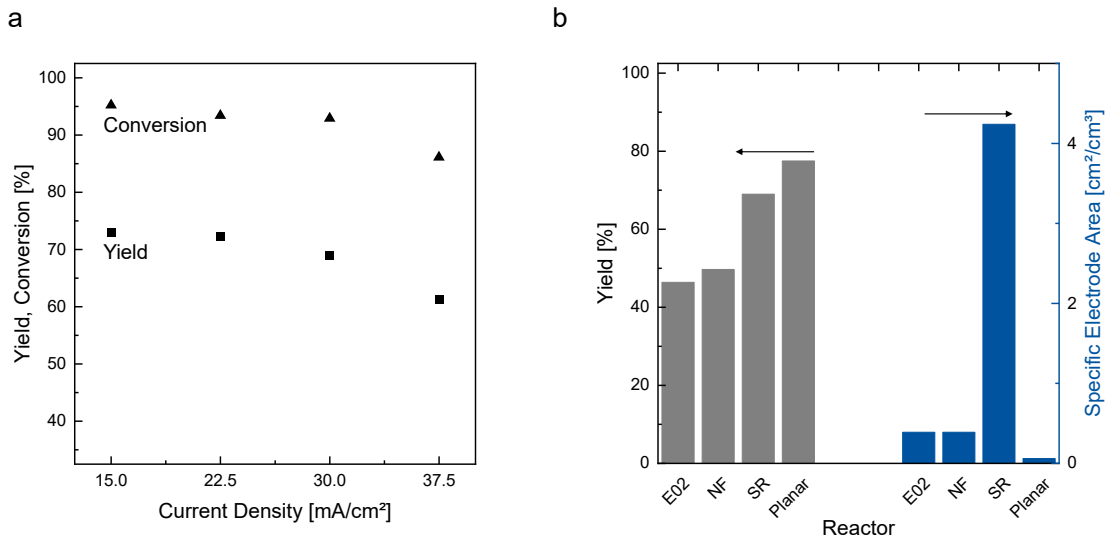

Figure 4.10: a: FDCA yield (■) and HMF conversion (▲) of the swiss roll reactor (SR) over different current densities at 500 mL min^{-1}. b: Comparison of FDCA yield (gray bars, left y-axis) and specific electrode area (blue bars, right y-axis) of the different reactor types at 500 mL min^{-1} and 30 mA cm^{-2}.

Figure 4.10b compares the different reactor designs with respect to the process yield at 30 mA cm^{-2} and 500 mL min^{-1} and their volume-specific electrode surface. The comparison shows that the swiss roll reactor ranks slightly below the planar reactor in terms of FDCA yield, with 69% compared to 77.5%. However, it excels with respect to the volume-specific electrode surface, where it surpasses the other reactors by more than one order of magnitude at 4.24 cm^2 cm^{-3} (geometric electrode area per reactor volume) compared to 0.06 cm^2 cm^{-3} in the planar reactor. In applications

where a high conversion per pass through the reactor is necessary, e.g. for single-pass electrolysis, the high specific surface constitutes a tremendous advantage. Additionally, the scalability of the reactor can be achieved rather simple by increasing the length of the reactor, especially in comparison to the complex stacking of multiple cells in a planar module.

4.6 Conclusion and Outlook

This chapter demonstrated an integrated process combining the biphasic chemo-catalytic synthesis of HMF from fructose with the subsequent biphasic electrochemical oxidation to FDCA to eradicate intermediate purification. Further, it compared three different reactor concepts for the electrochemical oxidation.

The HMF-rich organic product phase was fed directly into the electrochemical flow-cell reactor where HMF was continuously extracted into the aqueous phase and oxidized to FDCA on a $Ni(OH)_2$/NiOOH anode. FDCA accumulated in the aqueous electrolyte, enabling a high degree of recycling of the organic phase. The biphasic electrochemical oxidation showed a yield of 85% with the model solution and close to 80%, when the raw HMF/2-MTHF solution from HMF synthesis was fed to the reactor without any purification. The concept showed an identical yield, compared to conventional, single phase oxidation in the aqueous electrolyte as known from literature, thus, demonstrating the feasibility of the integrated concept.

With a model solution, the influence of different process parameters was analyzed in the electrochemical flow cell. The flow rate did not show a significant influence on the process at a current density of 15 mA cm^{-2}. An increased production rate was subsequently achieved by increasing the current density. However, at higher current densities above 30 mA cm^{-2} the process suffered from an increased cell voltage and decreased FDCA yield. This chapter also showed that the reaction time influences the yield significantly, due to the constantly ongoing degradation of HMF. This demonstrates the trade-off between yield and space-time yield in the electrochem-

ical cell, which leaves room for process optimization. Initially, the biphasic process suffered from poor energy efficiency due to high ohmic resistance in the electrolyte, which resulted in a high cell voltage. In this chapter, the cell voltage was successfully decreased with smaller electrolyte gaps which, in turn, decreased the direct energy input by over 50%.

Additionally, two different tubular reactors for the biphasic electrochemical synthesis were employed to determine if mass transport could be improved by controlling mixing and flow conditions in the reactor and to increase the volume-specific electrode area. The first concept focused on intensifying mixing with mixer electrodes as the working electrodes, formed from nickel foam or 3D-printed from stainless steel. Ultimately, the irregular distance between the working electrode and the counter electrode had a detrimental effect on the process which outweighed the potentially improved mixing. In contrast, the swiss roll reactor excelled with an unprecedented ratio volume-specific electrode surface. It retained a yield of close to 70% at a current density of 30 mA cm^{-2}, which is only slightly decreased compared to the planar design. The main benefit is the production rate, which was more than 10 times higher then the planar design in a comparable reactor volume. With the highest yield in the planar design and the highest space time yield in the swiss-roll reactor, both reactor designs are promising concepts to advance the integrated process for FDCA synthesis.

This chapter delivers data which could be used to optimize the process on a process level and identify most favorable operation conditions. The process chain could be expanded from glucose as a substrate to hemicellulosic biomass. Further, a single-pass electrolysis might be possible with the swiss roll reactor design, which could pave the road towards a continuous process. The flow conditions could be optimized, when grasping the promising opportunity to scale up the design.

Additionally, the reaction mechanism in the biphasic electrolyte could be examined on a mechanistic level, starting with the identification of byproducts from FDCA synthesis from the raw HMF/2-MTHF solution. These could be unidentified oxidation products from e.g. ring-opening reactions but also unwanted products from a reduction reaction on the platinum cath-

ode. The separation of the reactants from the cathode could be done via an ion exchange membrane that is stable under these harsh conditions. Further, insight into the influence of the organic phase fraction on FDCA yield could enable a high yield at higher organic fractions in the reactor. On a process level, catalysts for the oxidation that exhibit a high activity at less alkaline pH would also be beneficial. On the one hand, degradation of HMF would be reduced by less harsh conditions. On the other hand, a subsequent pH-shift crystallization for FDCA purification would require lower amounts of acid.

5 Paired Electrolysis for Electrochemical Biomass Valorization on the Example of 2,5-Furandicarboxylic acid and 2-Butanone

Parts of this chapter are in preparation for publication:

The Membrane Matters in Paired Electrolysis: Synthesis of 2,5-Furandicarboxylic Acid and 2-Butanone

Tobias Harhues, Saskia Fischer, Matthias Wessling, Robert Keller

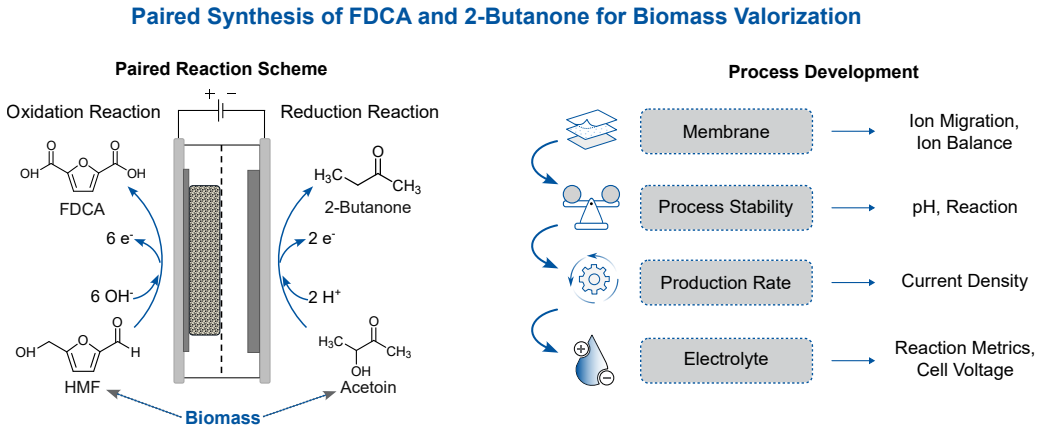

5.1 Introduction

The continuously rising CO_2 emissions fuel climate change with dramatic global consequences. Defossilization of carbon sources for the chemical industry can enable the sustainable production of chemicals and decrease CO_2 emissions. Renewable carbon sources are imperative, especially for the production of polymers and solvents, where the carbon molecules are indispensable for functionality in many cases [Wint2022]. Sustainable carbon can, for example, be supplied directly from atmospheric CO_2 or biomass [Meys2021]. Polymers based on biomass, so-called biopolymers, are often structurally different from conventional polymers as they consist of different monomers than their fossil counterparts [Reic2020]. One prominent example of a bio-based monomer is 2,5-furandicarboxylic acid (FDCA), which can be polymerized to polyethylenfuronate (PEF) [Jong2012a]; [Pand2021]. PEF and other FDCA co-polymers have been researched extensively and are potentially critical building blocks and polymers for the future of the polymer industry. [Eerh2012]; [Zhan2021]; [Jong2012a].

Next to bio-based polymers, widely used and established solvents, such as ethanol or 2-butanone (also known as methyl ethyl ketone (MEK)), also depend on carbon. They can be produced via sustainable pathways from renewable carbon sources, which enables their usage in a fossil-free future [Ocho2019]; [Gray2006]; [Harh2022]. Independent of the product, carbon from biomass must be utilized as efficiently as possible as renewable carbon will be a limited resource in the future [Bidd2023]; [Meys2021].

The biorefinery established a concept to efficiently use all fractions of biomass while aiming for efficiency in highly integrated processes [Cher2010]. Advances in the field of electrochemical reactions and engineering, especially for the synthesis of FDCA, allow for the introduction of electrochemical conversion into the biorefinery, which coined the term e-refinery [Tang2021]. The interest to move from catalyst research towards process integration and intensification has recently gained momentum, especially for the synthesis of FDCA [Lats2018]; [Harh2023]. Simultaneously,

process integration for the sustainable synthesis of 2-butanone from glucose via the coupling of fermentation and electrochemical conversion has been advanced [Harh2022]. Nevertheless, process conditions such as current density and reactant concentration often remain far from the required values for an economical feasible process [Pate2022]; [Mass2022].

To close the gap towards economical viability, efforts to increase energy efficiency have been employed to decrease the cell voltage and direct energy consumption [Qian2023]. Additionally, process intensification has moved to couple two value-adding reactions via paired electrolysis to utilize both the reduction and the oxidation reaction in an electrochemical cell to generate value-added products. The resulting paired electrolysis can decrease power consumption in electrochemical processes and has been extensively discussed in research [Iban2016] and illustrated for biomass valorization [Liu2021]. Pairing an electrochemical oxidation reaction with the HER has been identified as a substantial hydrogen source in the future and has been demonstrated for FDCA experimentally [Leow2023]; [Yang2021]; [Gao2023]. However, electrochemical hydrogen generation must be conducted at very low overpotential and in vast quantities to be economically competitive, which impairs HER as an efficient paired reaction for the valorization of biomass. Therefore, other reaction couples for the oxidation of HMF to FDCA have been investigated. HMF can yield value-added products on both the anode and cathode in divergent electrolysis. This has been demonstrated with the reduction of HMF to 2,5-bis(hydroxymethyl)furan (BHMF), for example [Chad2019]. Further, other reduction reactions, such as nitrate reduction to ammonia [Yang2023] or the oxygen reduction reaction (ORR) to operate in fuel cell mode [Qian2023] have been demonstrated as an example of parallel paired electrolysis. Recently, the reduction of CO_2 to CO has been paired with HMF oxidation utilizing a bipolar membrane (BPM) [Hauk2023] and with glycerol oxidation with a cation exchange membrane (CEM) to decrease power consumption and replace the rather sluggish oxygen evolution reaction (OER) [Vehr2023]. The literature provides a more detailed overview [Gao2023]; [Yang2021]. While these studies showed remarkable yields and paired Faraday efficiencies

of up to 190%, most focus on catalyst design and demonstrate the reactions in small cells and low overall reaction rates. Therefore, the pressing issue of process stability considering the often inherently unstable conditions through ion migration that strongly influence the pH, electrosmotic drag through the membrane [Pärn2021]; [Baes2023], and charge balance remains mostly unaddressed. These challenges are heavily influenced by the choice of the ion exchange membrane (IEM) [Xu2023]; [Pärn2021].

IEMs determine the migration of ions in an electrochemical cell - anion exchange membranes (AEMs) allow the migration of anions from cathode to anode. In contrast, CEMs restrict the migration of anions and allow the migration of cations from the anode to the cathode [Jian2021]; [Drio2016]. The ion migration heavily influences the process as it is not restricted to protons and hydroxide ions participating in the oxidation or reduction reactions. It extends to the co-migration of other ions, for example from the background electrolyte with a typical concentration between 0.1 and 1 mol L^{-1}. The concentration exceeds that of protons and hydroxide ions by several orders of magnitude in neutral pH. Additionally, diffusion or co-migration through the membrane can result in reactant crossover or drastic changes in pH, which can heavily influence process economics or lead to unstable process conditions [Xu2023]; [Salv2021]; [Venn2019]. Further, IEMs do not exhibit a selectivity of 100%, so that co-ions also migrate through the membrane. Next to process stability, the crossover of ions and reactants can heavily influence subsequent downstream processes for product purification and recycling of the electrolyte. BPMs can mitigate ion migration through the membrane as water diffuses into the membrane, where it dissociates into protons and hydroxide ions, which migrate to the respective electrode [Xu2023]; [Blom2020]. BPMs are known for their application in electrodialysis (ED) or capacitive deionization (CDI) [Drio2016]. BPMs consist of laminated pairs of AEM and CEM, which frequently employ a catalyst in the junction layer to facilitate water dissociation. Yet, BPMs suffer from disadvantages, such as additional water diffusion and dissociation resistance, which increases the required voltage [Blom2021]. This detrimental overvoltage increases with increasing current density so that the

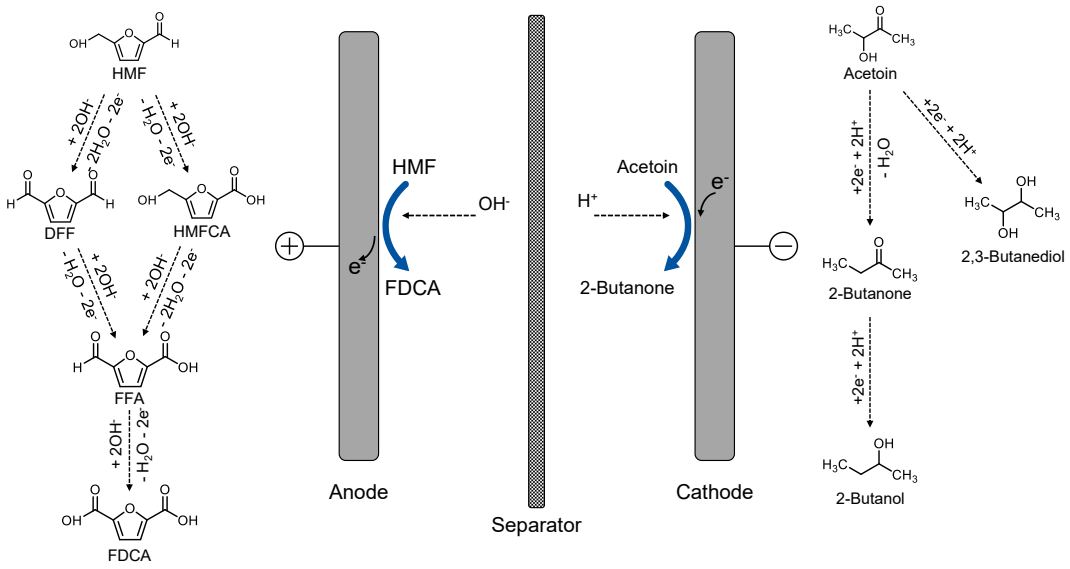

Figure 5.1: Reaction mechanisms in the paired electrolysis. On the anode, HMF is oxidized to FDCA via two possible routes. On the cathode, acetoin is reduced to 2-butanone or the side product 2,3-butanediol. 2-butanone can be reduced further to 2-butanol.

existing applications are limited in current density [Xu2023]; [Pärn2023]. Co-ions, especially multivalent ions that migrate into the membrane where they accumulate, are another challenge for BPMs, especially in long-term operations. Another challenge is the non-ideal separation performance of BPMs that leads to unwanted ion migration between the compartments has been the subject of extensive research [Blom2021].

This work develops a paired electrolysis process for the efficient valorization of HMF and acetoin. A schematic of the paired electrolysis process with the respective reaction mechanisms is displayed in Figure 5.1. In the first step, the three different types of IEMs are explored, and the resulting direction of migration and implications for the reactions are assessed. Secondly, the BPM as the most promising option is studied in more detail to develop a stable process. Once a stable process is established, it is driven towards higher current densities with increasing reactant concentrations to achieve industrially relevant conditions. Subsequently, the feasibility to exchange the potassium-based with a sodium-based electrolyte to decrease the direct costs is discussed. The impact of the different electrolyte systems

is assessed with respect to their influence on yield, Faraday efficiency (FE), and resulting cell voltage.

5.2 Materials and Methods

5.2.1 Materials

Nickel foam (grade 4753) was purchased from Recemat NL, HMF (>99%) from AVA-Biochem. Nickelnitrate hexahydrate ($Ni(NO_3)_2 \cdot 6H_2O$), titanium foil (99.7%, thickness 0.89 mm) and lead electrodes (>99%, thickness 1.12 mm) were purchased from Alpha Aesar. Sulfuric acid (H_2SO_4, 1 mol L^{-1}), nitric acid (HNO_3, 65 wt%), hydrochloric acid (HCL, 1 mol L^{-1}), FDCA (97%), 5-Hydroxymethyl-2-furancarboxylic acid (HMFCA) (>95%), acetoin (>96%), potassium dihydrogenphosphate (K_2HPO_4) (>98%), and Furan-2,5-dicarbaldehyde (DFF) (>97%) were purchased from Sigma-Aldrich. Acetone (technical), 2-MTHF (>99%), trifluoroacetic acid(TFA) (≥99.9%), potassium hydrogen phosphate (KH_2PO_4) (>99%), and acetic acid (glacial, 100%) were purchased from CarlRoth. 2-formyl-5-furancarboxylic acid (FFCA) (98%) was purchased from TCI chemicals. All chemicals were used as received without further purification.

5.2.2 Preparation of Electrodes

Anode

Electrodes for the planar electrochemical cell were prepared as described in chapter 4.2.4. Here, they were cut to a geometrical surface area of 25 cm^2. The etching procedure remained unchanged, for the coating, the current density was adjusted to the smaller electrode area. The counter electrode was a platinized titanium mesh (Umicore, Germany) with 35 cm^2 surface area.

Cathode

A lead plate was used as the cathode as described in chapter 3.2.4 with an electrode area of 25 cm^2. It was cleaned before each experiment by polishing with sandpaper and immersed in 1 mL HCL in an ultrasonic bath for 10 min. Subsequently, it was rinsed with DI-water.

5.2.3 Flow Cell Composition

For the flow cell, the commercially available flex-E-cell (FXC Engineering GmbH, Germany) with a geometrical electrode surface area of 25 cm^2 was used. The interior design is displayed in Figure 5.2.

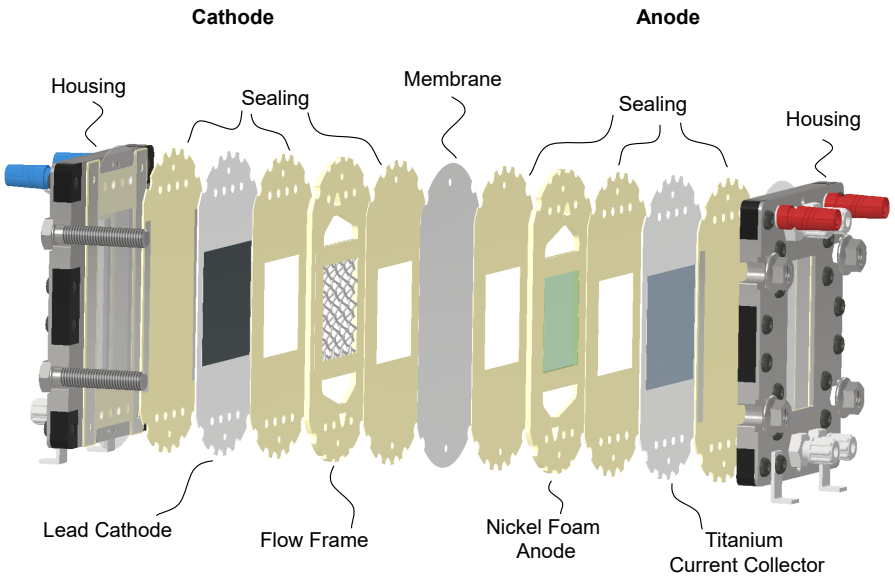

Figure 5.2: Design and setup of the electrochemical flow cell.

The anode side was designed as a zero-gap-assembly; a titanium current collector contacted a stack of two nickel foam electrodes (grade 4753, Recemat NL, Netherlands) through which the anolyte was pumped. The foam electrodes were directly in contact with the IEM.

On the cathode side, a 3 mm electrolyte gap was present between the IEM and the lead plate electrode. The flow channel was filled with a polymeric 3D-printed spacer to keep the electrolyte gap constant.

For sealing all compartments, ethylene propylene diene rubber (EPDM) frames were used. The cell was assembled with 4 screws and tightened to a compression ratio of 10% of the original thickness of the EPDM frames.

5.2.4 Experimental Setup

The experimental Setup is depicted in Figure 5.3. The electrolyte was circulated by two gear pumps (MCP Standard, Ismatec, Germany) at a flow rate of 500 ml min^{-1}. The pH of the anolyte and the catholyte was monitored continuously by a pH sensor (SE 555, Knick, Germany). Manual pH control was done by feeding of 10 mol L^{-1} KOH on the anode side and 10 mol L^{-1} phosphoric acid on the cathode side via a multichannel peristaltic pump (Reglo ICC, Ismatec) into the reservoir. At a current density of 100 mA cm^{-2} and above, the electrolyte was cooled to 25 C° using a cryostat (Julabo, Germany). Power was supplied by a potentiostat (GSTAT302N, Metrohm Autolab, Germany) below 100 mA cm^{-2}, and by a power supply (HMP4040, Rohde & Schwarz, Germany) for experiments at 100 mA cm^{-2} and 150 mA cm^{-2}. When the potentiostat was used, a four electrode setup with two reference electrodes (Hydroflex RHE, Gaskatel, Germany) were used to determine the half-cell voltages. All experiments were conducted at constant current with an initial electrolyte volume of 125 ml. Samples were taken from the respective electrolyte reservoirs in intervals of 30 min with duplicates at the start and the end of the experiment. Samples from the anolyte were diluted with a phosphate buffer (7.5 g L^{-1} K_2HPO_4 and 5.5 g L^{-1} KH_2PO_4) to stabilize the pH, samples from the catholyte were diluted with DI-water. The added electrolyte volume through pH control was taken into account to evaluate of the experiments.

Experiments to show the effect of increased reactant concentration in Section 5.3.3 and the influence of the electrolyte in Section 5.3.4 were evaluated for conversion (X), selectivity (S), yield (Y) according to Equations 2.6a-c and Faraday efficiency (FE) according to Equation 2.8. The evaluation always refers to the time of full theoretical conversion (t_{FC}), when

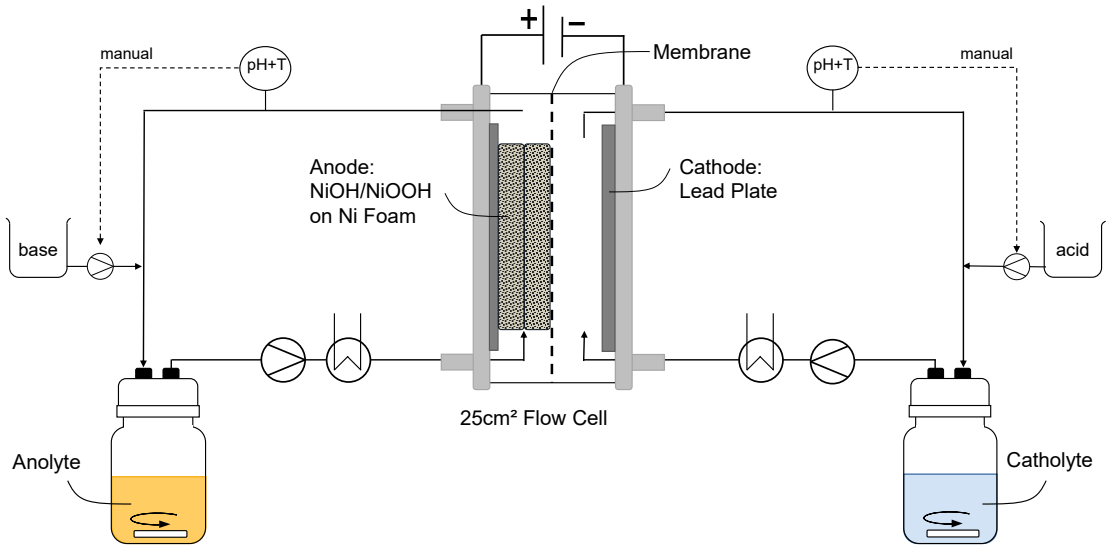

Figure 5.3: Experimental setup with the flow cell in the center and circulating electrolytes on the anode and cathode side.

sufficient charge for the reaction sequence from HMF to FDCA on the anode and acetoin to 2-butanone on the cathode was supplied, calculated after Equation 2.9. The charge transferred couples the reaction on the anode and the cathode, and an identical t_{FC} is desired. The stoichiometric ratio is determined by the respective amount of electrons transferred in the reaction:

$$\frac{c_{HMF}}{c_{Acetoin}} = \frac{z_{Anode}}{z_{cathode}} = \frac{1}{3} \tag{5.1}$$

The initial concentration was varied in the experiments. To identify a suitable membrane and reach a stable process in Figure 5.4 and Figure 5.6, For experiments, the ratio between initial reactant concentration and current density is kept constant at 3 $\frac{mmol_{HMF}L^{-1}}{mAcm^{-2}}$ and 9 $\frac{mmol_{acetoin}L^{-1}}{mAcm^{-2}}$ to minimize the influence of mass transport limitations. The ratio of 1:3 (c_{HMF} to $c_{acetoin}$) is determined by the stoicheometry of the electron transfer in the respective reaction (see Figure 5.1). For example, this results in an initial acetoin concentration of 90 $mmol_{acetoin}$ L^{-1} and 30 $mmol_{acetoin}$ L^{-1}.

5.2.5 Sample Analysis

Quantification of reactants was done via high performance liquid chromatography (HPLC) analysis for the anolyte and the catholyte, separately. The anolyte was analyzed as described in chapter 4.2.9 for the aqueoues samples. The catholyte was analyzed as described in chapter 3.2.3. Additionaly, the anolyte and catholyte were analzyed for reactants from the respective other side after each experiment to identify possible crossover of reactants through the membrane.

Further, ion chromatography (IC) (930 Compact IC Flex, Metrohm, Swiss) was used to reveal ion crossover through the BPM. Cation concentration was determined with the eluent 1.7 mmol L^{-1} pyridine-2,6-dicarboxylic acid and 1.7 mmol L^{-1} nitric acid with a flow rate of 0.7 mL min^{-1}. Anions concentration was determined with the eluent 3.6 mmol L^{-1} sodium carbonate and 1.7 mmol L^{-1} sulfuric acid with a flow rate of 0.9 mL min^{-1}.

5

5.3 Results and Discussion

5.3.1 Membrane Selection

The three different membranes commonly used in electrochemical applications were tested in the paired electrolysis process. For an analysis, the pH of the anolyte and catholyte is displayed in Figure 5.4a and 5.4c, respectively. The resulting amount of FDCA in the anolyte in Figure 5.4b, and the resulting amount of 2-butanone are displayed in Figure 5.4d. The initial amount of HMF in the system was 2.5 mmol, while the initial acetoin amount was 7.5 mmol so that t_{FC} for the two conversions is identical.

The pH in the anolyte drops substantially throughout the experiments when an AEM or a CEM is employed, while it rises in the catholyte simultaneously. The change in pH is caused by migration through the respective IEM; a schematic for the different membranes is displayed in Figure 5.5. In the case of a CEM in Figure 5.5a, the positively charged potassium ions

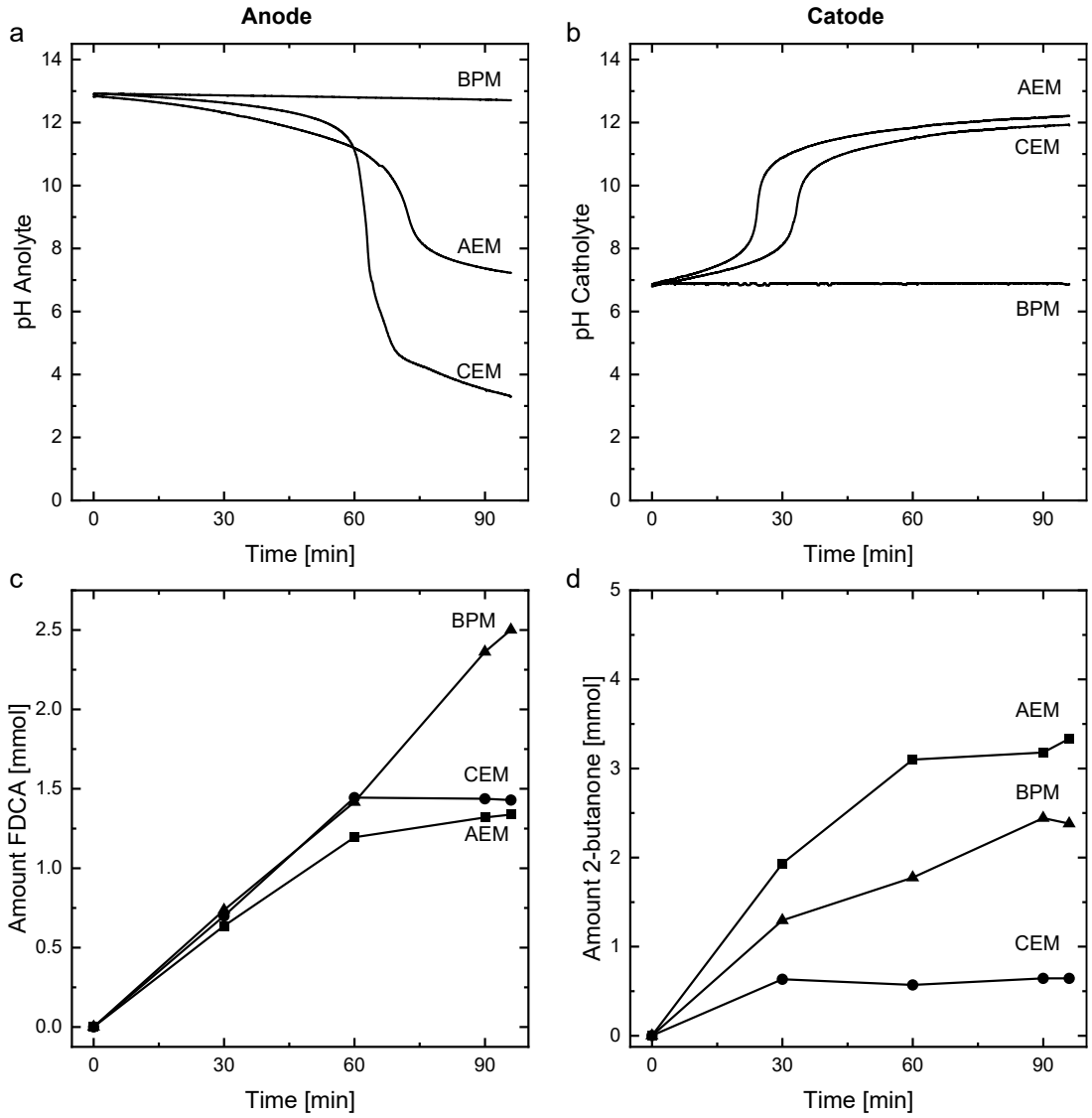

Figure 5.4: Course of the pH and amount of products over the course of the experiment in a, c: the anolyte and b, d: the catholyte with the different types of membranes (BPM, AEM, and CEM) at a current density of 10 mA cm^{-2}.

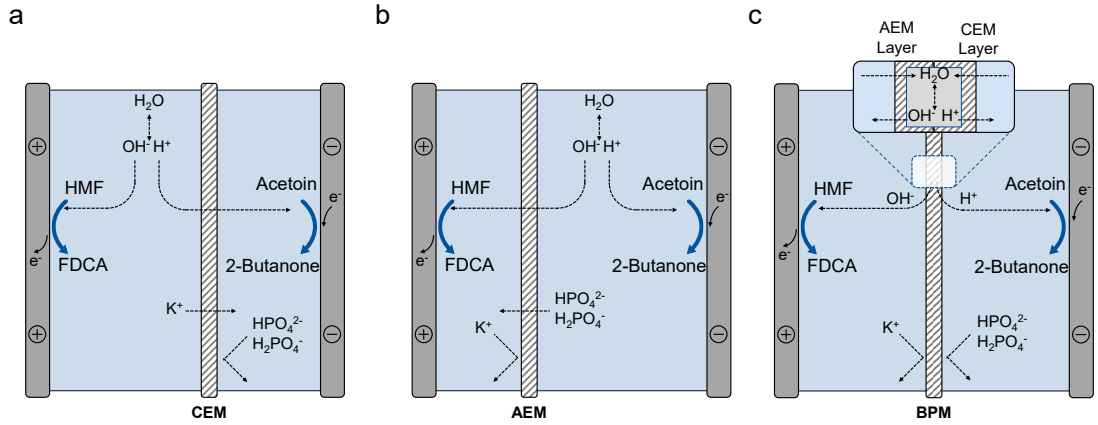

Figure 5.5: Ion movement by migration in the flow cell and through the membrane during the paired reaction with a: a CEM, b: an AEM, and c: a BPM. The movement is displayed for a potassium-phosphate buffer in the catholyte and KOH in the anolyte.

from the anolyte migrate to the catholyte, while hydroxide ions are consumed in the reaction on the anode. At the beginning of the experiment, the concentration of potassium ions in the catholyte exceeds the concentration of protons by more than ten orders of magnitude, so that potassium ions will transport the majority of charge. This interplay strongly decreases the pH of the anolyte so that FDCA synthesis ceases after 60 minutes, as apparent from Figure 5.4b. Additionally, the nickel foam electrodes deteriorated massively due to the decreasing pH, and the acidic interface of the CEM [Pour1974]; [Pärn2021]. The green color of the anolyte indicates dissolved nickel species that migrate through the membrane and precipitate on the cathode and on the spacer in the catholyte. Therefore, only very small amounts of 2-butanone can be detected in the catholyte as shown in Figure 5.4d.

With an AEM, the direction of charge transfer is reversed, and anions migrate from the catholyte to the anolyte, as depicted in Figure 5.5b. The majority of charge is transported via the negatively charged phosphate ions. This leads to a pH drop in the anolyte and a rising pH in the catholyte, which is even more pronounced in the beginning than with a CEM. The course of the pH reflects well in the amount of FDCA in the anolyte in Fig-

ure 5.4b. In the catholyte, more 2-butanone is produced than with a CEM since nickel migration through the membrane is mitigated, and the reaction to 2-butanone is less sensitive to the pH than the oxidation to FDCA.

With a BPM, the pH is much more stable and decreases to 12.66 in the anolyte throughout the experiment, while no change in the pH in the catholyte is visible. Almost all HMF is converted to FDCA during the experiment with an FDCA yield close to 1. The synthesis of 2-butanone synthesis in Figure 5.4d does not benefit from BPM compared to the AEM as the reaction from acetoin to 2-butanone is not pH-sensitive and a more alkaline pH can suppress the competing HER. However, an alkaline pH can lead to condensation reaction acetoin, causing a loss of reactant [Zhu2016]. The nature of the BPM mitigates migration across the membrane, as water dissociates in the middle at the interface of the membrane and only the resulting protons and hydroxide ions can migrate into the respective compartments as depicted in Figure 5.5c. Nevertheless, the pH decrease from 13 to 12.7 throughout the experiment, which will be further investigated in the following section.

5.3.2 Stable process conditions

The most stable process can be established with a BPM. However, the pH still drops from 13 to 12.66, which is a significant decrease by more than 50% on the logarithmic pH scale. Considering the relatively short duration of the experiment and rather low current density, this result questions the stability of the process. The effect becomes even more pronounced when reactant concentration and current density are increased in Figure 5.6. The gray line serves as a reference to the result presented before. When the reactant concentration is increased to 60 mmol $^{-1}_{HMF}$ and 30 mA cm^{-2}, the pH drops significantly throughout the experiment. IC samples show only minimal amounts of phosphate below 1 mmol L^{-1} in the anolyte. However, the concentration is too low to cause such a drastic change in pH. Instead, the pH decrease is caused by the two carboxylic acid groups of the produced FDCA that deprotonate under the alkaline conditions and decrease

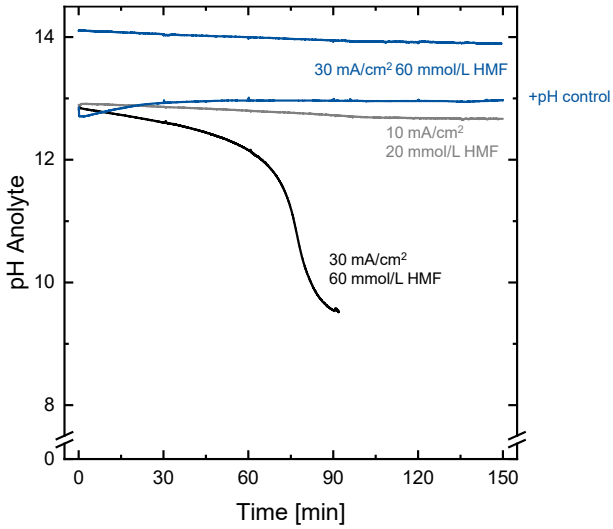

Figure 5.6: pH in the anolyte over the duration of the experiment at increasing reactant concentration and current density as in indicator for the process stability. The blue lines show the course of the pH with a starting pH of 14 and a pH of 13 with applied pH control, respectively.

the electrolyte's pH and conductivity [Harh2023]. Two strategies to counteract this effect can be employed. Either, the initial pH can be increased by increasing the concentration of KOH to 1 mol L^{-1}, as depicted by the blue line in Figure 5.6. However, this approach limits the maximum reactant concentration and does not counteract the instable nature of the process. Further, the increased pH leads to increased HMF degradation, as demonstrated in literature before [Coum2022]; [Lats2018]; [Harh2023].

Alternatively, the pH can be controlled continuously by feeding a base to the electrolyte, as shown in Figure 5.6. The pH control enables a stable process at a more moderate pH of 13. However, it increases the process complexity. To achieve a stable process in subsequent experiments, 10 mol L_{-1} KOH is dosed to stabilize the pH in the anolyte. Since the BPM does not inhibit 100% phosphate or potassium crossover, pH control is also installed for the catholyte and conducted with 10 mol L^{-1} phosphoric acid for future experiments.

5.3.3 Increased Production Rate

The production rate and product concentration need to be increased to increase space-time yield, enable efficient downstream purification, and move the paired electrolysis of FDCA and 2-butanone process towards industrial relevance. The production rate is coupled to the current density, while the initial reactant concentration limits the product concentration. Figure 5.7a shows the resulting yield on the anode and cathode while increasing the reactant concentration and current density.

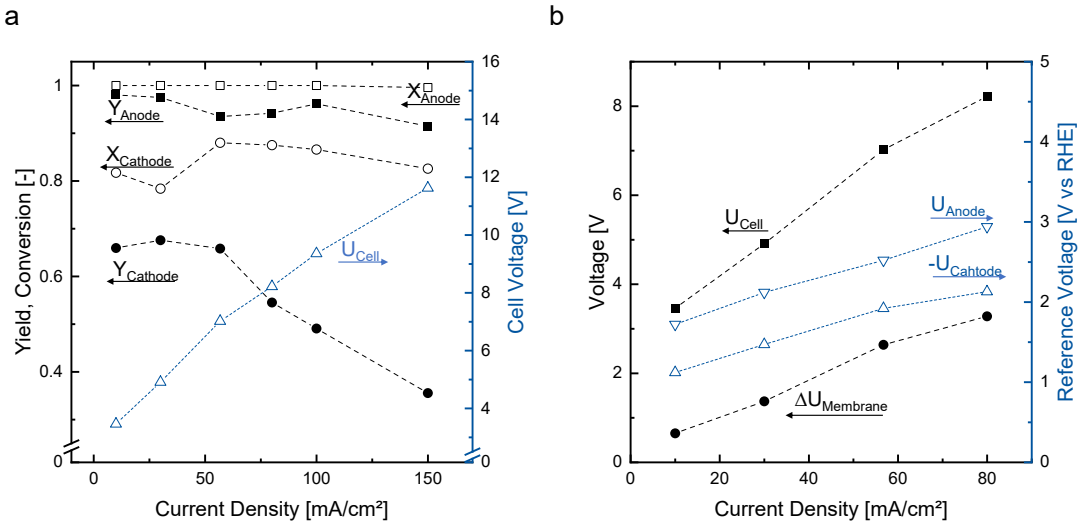

Figure 5.7: a: Yield of FDCA (Y_{Anode},■) and conversion of HMF (X_{Anode},□) on the anode side, yield of 2-butanone ($Y_{Cathode}$,●), and conversion of acetoin ($X_{Cathode}$,○) on the cathode on the left y-axis at increased current density. The resulting cell voltage (U_{Cell}△) is displayed on the right y-axis. b: Absolute cell voltage (U_{Cell},■) and voltage drop over the membrane ($U_{Voltage}$,●) on the left y-axis and half-cell voltage of anode (U_{Anode},▽) and cathode ($-U_{Cathode}$,△) over the current density up to 80 mA cm^{-2}. The initial reactant concentration was increased linearly with the current density (3 $\frac{mmol L^{-1}}{mA cm^{-2}}$). Dashed lines serve to increase readability.

The oxidation of HMF shows a high conversion of nearly 100% at any current density, and the yield remains well above 90%, independent of the current density. The reduction of acetoin to 2-butanone shows less favorable reaction metrics. While the conversion remains high between 80% and 90%, the yield remains close to 70% until the current density of 55 mA cm^{-2}.

Here, the paired process has a combined yield and Faraday efficiency of close to 170%. When the current density is increased further, the yield decreases below 40% at the highest current density of 150 mA cm^{-2}. Nevertheless, the combined yield and Faraday efficiency is 130% at this elevated current density. The overall lower yield of 2-butanone is in agreement with previous findings in Chapter 3.3.2, where an over-reduction of 2-butanone to 2-butanol is apparent. It is most likely caused by the rather unspecific lead catalyst [Ocho2019]; [Harh2022]. As the over-reduction occurs prominently at higher 2-butanone concentration, it could be circumvented by *in-situ* product separation or through operation at a lower acetoin conversion.

In addition to the increased production rate and product concentration, limiting the cell voltage is necessary to drive an electrochemical process towards industrial feasibility. In Figure 5.7, the cell voltage increased significantly from 3.4 V at 10 mA cm^{-2} to over 11 V at 150 mA cm^{-2}. The additionally energy dissipates into thermal energy. The overall cell voltage is comprised of the half-cell potentials and the additional ohmic resistance of the membrane and the electrolyte.

Figure 5.7b shows the individual contributions to the resulting cell voltage of the two half-cell reactions and the membrane. It reveals that both half-cell voltages increase linearly with the increasing current density with a comparable slope. However, the absolute voltage drop over the membrane on the left y-axis shows a far steeper slope than the half-cell voltages. Therefore, the detrimental impact of the resistance of the BPM is outweighs that of the individual reactions at elevated current densities. This is in agreement with Literature [Xu2023] where the high overvoltage is attributed to limited water diffusion into the membrane [Xu2023]; [Blom2021]. Next to the membrane, the electrolyte exhibits an ohmic drop that is regarded in more detail in the following section.

5.3.4 Adapting the Electrolyte

Ohmic losses in the electrolyte increase the cell voltage and the direct energy consumption of the reaction. Additionally, the electrolytes are associated with with direct costs, especially when the reactants and products are dissolved within the electrolyte, so the entire aqueous phase is subject to downstream processing. This is even more pronounced in the production of FDCA, as the produced organic acid complexes with cations from the electrolyte and the electrolyte need to be dosed continuously, as shown in Figure 5.6. Possibilities to recycle the electrolyte are subject to research but need to be adjusted and trialed for any specific case [Rabi2020]. The number of different ionic species in the electrolyte should be limited as much as possible to simplify downstream processing. Therefore, an additional background electrolyte should comprised the same species as the original electrolyte.

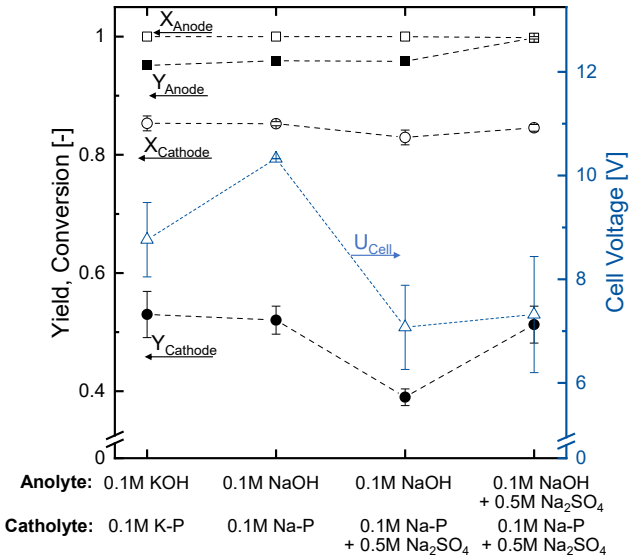

Figure 5.8: Yield of FDCA (Y_{Anode},■) and conversion of HMF (X_{Anode}□) on the anode side, yield of 2-butanone ($Y_{Cathode}$●) and conversion of acetoin ($X_{Cathode}$○) on the cathode on the left y-axis for different compositions of anolyte and catholyte. Cell voltage (U_{Cell}△) on the right y-axis. The current density was 100 mA cm^{-2} and the inital reactant concnetration was 0.3 mol L^{-1} HMF and 0.9 mol L^{-1} acetoin. Values were recorded at t_{FC}. Dashed lines serve to increase readability.

In the case of FDCA synthesis, the substitution of potassium with sodium has been identified as beneficial for economic feasibility [Pate2022]; [Mass2022]. Figure 5.8 shows the effect of substituting potassium with sodium and the introducing a background electrolyte on yield and conversion on both electrodes and the resulting cell voltage. Replacing potassium with sodium at constant electrolyte concentrations does not influence the reaction specific figures of merit for either of the paired reactions. However, the cell voltage increases by more than 25% to over 10 V, which is caused by the decreased conductivity of the electrolyte, due to the lower mobility of sodium compared to potassium ions. Especially in the catholyte, the conductivity decreases by more then 25% from 15.7 mS cm^{-1} in the potassium phosphate buffer to 11.4 mS cm^{-1} in the sodium-based buffer, before the addition of acetoin. The increasing cell voltage decreases the economic prospect of the cheaper electrolyte through the increased energy consumption. Yet, this can be counteracted by the addition of a background electrolyte. Na_2SO_4 was added as an additional background electrolyte with a concentration of 0.5 mol L^{-1} to the catholyte. The voltage decreased significantly to below 7 V, substantially lower than the cell voltage with the potassium-based electrolytes, limiting the detrimental effect of the reduced conductivity.

Adding the background electrolyte to the anode side only slightly impacts the cell voltage. Due to the zero-gap assembly on the anode side, the conductivity of the anolyte is less critical for the overall cell voltage than that of the catholyte. The additional sulfate in the anolyte does not impact the catalyst's performance throughout the experiment. However, if a background electrolyte is desired on the anode side, the effect of sulfate on the long-term performance of the catalyst should be assessed in long term experiments.

5.4 Conclusion and Outlook

This work developed a structured approach for the paired electrochemical valorization of biomass on the example of the oxidation of HMF to FDCA

and the reduction of acetoin to 2-butanone in a flow cell with an electrode area of 25 cm^2. The evaluation of the different types of IEMs revealed that a stable process is possible only with a BPM. Due to the non-ideal nature of the BPM and the carboxylic acid groups of the oxidation product FDCA, pH control is necessary in both the anolyte and the catholyte. With the established, stable process, the current density and reactant concentration were increased to move the process towards industrial applicability. The oxidation of HMF to FDCA excelled with a yield of above 90% even at the highest current density of 150 mA cm^{-2} and a reactant concentration of up to 0.45 mol L^{-1} HMF, resulting in a final FDCA concentration of 0.4 mol L^{-1}. Synthesis of 2-butanone was less efficient, with a yield of 65% up to a current density of 55 mA cm^{-2}, which then dropped to below 40% at 150 mA cm^{-2}, mainly due to overreduction of 2-butanone to 2-butanol. Accordingly, the combined Faraday efficiency was 160% at 55 mA cm^{-2} and decreased to 130% at 150 mA cm^{-2}. Subsequently, we showed that it is possible to replace the potassium-based electrolyte with a cheaper sodium-based electrolyte without impairing the yield of the reaction. Adding a background electrolyte relieved the detrimental effect of the lower conductivity of the electrolyte on the cell voltage. Finally, the paired synthesis showed promising figures of merit, such as a yield of above 90% for FDCA and close to 50% for acetoin at a current density of 100 mA cm^{-2} with a sodium-based electrolyte and a cell voltage of around 6 V.

While this work showed a structured development of a paired synthesis process, it revealed an imbalance between the oxidation and reduction reaction. The synthesis of FDCA runs at a very high yield, independent of the current density, while the reduction of acetoin to 2-butanone deteriorated at the elevated current density, which could be counteracted by the *in-situ* separation of 2-butanone from the electrolyte. Future work should apply the structured approach presented herein to pair a different reduction reaction to the oxidation of HMF to FDCA. In addition to the practical aspects discussed in this work, reactions performing well at similar current densities should be considered, such as the reduction of CO_2 to formic acid or CO.

6 Conclusion and Perspective

This thesis presented the integration of electrochemical reactions into two process chains, from glucose to 2-butanone and fructose to 2,5-furandicarboxylic acid (FDCA). It demonstrated the integration on a horizontal level to mitigate intermediate purification steps by combining biocatalytic and chemocatalytic reactions with the subsequent electrochemical reduction and oxidation, respectively. Additionally, a structured approach to establish a paired electrolysis was developed and carried out to integrate the electrochemical reduction and oxidation reaction vertically to increase energy efficiency.

The **horizontal process integration** for the synthesis of **2-butanone from glucose** showed how process integration can mitigate purification of the intermediate acetoin from the complex fermentation medium of the microbial conversion. With the complex fermentation supernatant from *B. Licheniformis* as the electrolyte, the electroreduction showed close to 50% yield for 2-butanone. The adaptation of the fermentation to a minimal media fermentation with the highly efficient *L. Lactis* increased the yield of the subsequent electrochemical conversion to above 50% without intermediate purification. These results highlight the importance of experimental evaluation of consecutive processes within their process chain. The experimental assessment provided results that cannot be supplied by process models, since these usually do not account for the complex mixture of species in the fermentation broth. In the future, experimental evaluation could move beyond the integration of two processes and incorporate the extraction of 2-butanone from the product mixture. Likewise, the substrate could be extended to hemicellulosic biomass instead of glucose for the

microbial fermentation, in which the titer of acetoin should be increased to achieve higher overall product concentrations.

The **biphasic integrated synthesis of FDCA from fructose** presented an approach that mitigates the need for intermediate purification **through horizontal process integration** and simultaneously stabilizes the highly reactive intermediate hydroxymethylfurfural (HMF). This could be achieved through the novel biphasic electrochemical process in which the raw organic product phase of HMF synthesis was used without any intermediate purification. The electrochemical conversion with HMF from the raw organic product phase resulted in a yield of 70% FDCA from HMF, which is only slightly lower than with a model solution. The high yield demonstrates the feasibility of the biphasic electrochemical oxidation. Further, this chapter explored different reactor geometries for the biphasic electrochemical oxidation. Especially the high specific surface to volume ratio of the swiss roll reactor showed promising results for a future continuous and scaleable single pass process. Future work could develop a continuous, biphasic process that physically interlinks the two unit operations of HMF synthesis and its oxidation to FDCA in a continuous production on a pilot plant scale.

The **paired electrolysis** of FDCA and 2-butanone showed the possibility for **vertical process integration** of two different value chains. This work developed a structured approach towards the development of such a paired reaction. A stable process using a bipolar membrane BPM was established. The results demonstrate a combined yield of above 150% at a current density of 55 mA cm^{-2}, which decreases to 130% at higher current densities of 150 mA cm^{-2}. Further, in a product concentration of 0.4 mmol L^{-1} was achieved, which is a reasonable starting concentration to investigate the efficiency of downstream processes in the future. Additional, economical considerations were extended to the used electrolyte and potassium was replaced with more economical sodium. The detrimental effect on the cell voltage from the inherently lower ion mobility could be more than compensated by the addition of a background

electrolyte.
The structured approach to design a paired process presented herein provide guidelines to establish paired electrolysis processes which can readily be applied to other reactions. The oxidation of HMF to FDCA could, for example, be coupled to other value added reactions, such as the reduction of nitrate to ammonia or the reduction of CO_2.

All three approaches showed the successful integration of electrochemical reactions into value chains based on sustainable carbon sources. Techno-economic analysis (TEA) and Life cycle assessments (LCA) of the processes in their respective arrangement based on experimental results in this thesis and other work will reveal the most promising approaches to be pursued. Their demonstration in pilot plants will encounter challenges in up-scaling of the respective processes and will reveal if biomass will pose additional challenges in larger electrochemical reactors. This work showed that electrochemical processes are ready to move towards their application in the toolbox of the biorefinery.

Bibliography

[Agha2014] M. Aghazadeh et al. “Electrochemical preparation of a-Ni(OH)2 ultrafine nanoparticles for high-performance supercapacitors”. *Journal of Solid State Electrochemistry* 18.6 (2014). DOI: 10.1007/s10008-014-2381-7 (cit. on p. 54).

[Aign2020] M. Aigner et al. “Model–based equipment design for the biphasic production of 5–hydroxymethylfurfural in a tubular reactor”. *AIChE Journal* 66.4 (2020). DOI: 10.1002/aic.16849 (cit. on pp. 50, 60).

[Al G2021] A. Al Ghatta, J. D. E. T. Wilton-Ely, and J. P. Hallett. “From sugars to FDCA: a techno-economic assessment using a design concept based on solvent selection and carbon dioxide emissions”. *Green Chemistry* 23.4 (2021). DOI: 10.1039/D0GC03991H (cit. on p. 51).

[Alhe2013] N. A. Alhebshi, R. B. Rakhi, and H. N. Alshareef. “Conformal coating of Ni(OH)2 nanoflakes on carbon fibers by chemical bath deposition for efficient supercapacitor electrodes”. *Journal of Materials Chemistry A* 1.47 (2013). DOI: 10.1039/c3ta12936e (cit. on p. 55).

[Anas2010] P. Anastas and N. Eghbali. “Green chemistry: principles and practice”. *Chemical Society reviews* 39.1 (2010). DOI: 10.1039/b918763b (cit. on pp. 26, 50).

[Armb2020] S. Armbruster et al. “Short and spaced twisted tapes to mitigate fouling in tubular membranes”. *Journal of Membrane Science* 595 (2020). DOI: 10.1016/j.memsci.2019.117426 (cit. on p. 51).

[Azap2013] A. Azapagic et al. *Carbon Footprints of Recycled Solvents: Study for the European Solvent Recycler Group (ESRG)*. Manchester, England, 2013 (cit. on p. 26).

[Aziz2020] M. B. A. Aziz, ed. *Fossil free fuels: Trends in renewable energy*. Boca Raton: CRC Press, 2020 (cit. on p. 20).

[Bae2016] S.-J. Bae, S. Kim, and J.-S. Hahn. “Efficient production of acetoin in Saccharomyces cerevisiae by disruption of 2,3-butanediol dehydrogenase and expression of NADH oxidase”. *Scientific reports* 6 (2016). DOI: 10.1038/srep27667 (cit. on p. 28).

[Baes2023] J. Baessler et al. “Paired Electrosynthesis of Formic Acid from CO 2 and Formaldehyde from Methanol”. *ACS Sustainable Chemistry & Engineering* 11.18 (2023). DOI: 10.1021/acssuschemeng.2c07523 (cit. on p. 78).

[Baiz1984] M. M. Baizer et al. “Electrochemical conversion of 2,3-butanediol to 2-butanone in undivided flow cells: a paired synthesis”. *Journal of Applied Electrochemistry* 14.2 (1984). DOI: 10.1007/BF00618738 (cit. on p. 28).

[Bard2000] A. J. Bard and L. R. Faulkner. *Electrochemical Methods: Fundamentals and Applications*. 2nd Edition. [s.l.]: John Wiley & Sons Inc, 2000 (cit. on p. 11).

[Bawa2018] B. Bawareth et al. “Unravelling Electrochemical Lignin Depolymerization”. *ACS Sustainable Chemistry & Engineering* 6.6 (2018). DOI: 10.1021/acssuschemeng.8b00335 (cit. on p. 52).

[Bell2019] S. Bello et al. “Environmental sustainability assessment of HMF and FDCA production from lignocellulosic biomass through life cycle assessment (LCA)”. *Holzforschung* 73.1 (2019). DOI: 10.1515/hf-2018-0100 (cit. on p. 51).

[Bend2022] M. T. Bender et al. “Electrochemical Hydrogenation, Hydrogenolysis, and Dehydrogenation for Reductive and Oxidative Biomass Upgrading Using 5-Hydroxymethylfurfural as a Model System”. *ACS Catalysis* 12.19 (2022). DOI: 10.1021/acscatal.2c03606 (cit. on pp. 22, 51).

[Bhow2018] G. de Bhowmick, A. K. Sarmah, and R. Sen. “Lignocellulosic biorefinery as a model for sustainable development of biofuels and value added products”. *Bioresource technology* 247 (2018). DOI: 10.1016/j.biortech.2017.09.163 (cit. on p. 22).

[Bidd2023] E. J. Biddinger and P. J. A. Kenis. “Current and Emerging Electrochemical Approaches for Chemical Manufacturing”. *The Electrochemical Society Interface* 32.2 (2023). DOI: 10.1149/2.F08232IF (cit. on pp. 1, 76).

[Blom2020] M. A. Blommaert et al. “Reduced Ion Crossover in Bipolar Membrane Electrolysis via Increased Current Density, Molecular Size, and Valence”. *ACS Applied Energy Materials* 3.6 (2020). DOI: 10.1021/acsaem.0c00687 (cit. on pp. 18, 78).

[Blom2021] M. A. Blommaert et al. “Insights and Challenges for Applying Bipolar Membranes in Advanced Electrochemical Energy Systems”. *ACS energy letters* 6.7 (2021). DOI: 10.1021/acsenergylett.1c00618 (cit. on pp. 19, 78, 79, 90).

[Chad2019] X. H. Chadderdon et al. “Paired electrocatalytic hydrogenation and oxidation of 5-(hydroxymethyl)furfural for efficient production of biomass-derived monomers”. *Green Chemistry* 21.22 (2019). DOI: 10.1039/C9GC02264C (cit. on p. 77).

[Chen2015] Z. Chen et al. “Metabolic Engineering of Klebsiella pneumoniae for the Production of 2-Butanone from Glucose”. *PloS one* 10.10 (2015). DOI: 10.1371/journal.pone.0140508 (cit. on p. 27).

[Cher2010] F. Cherubini. “The biorefinery concept: Using biomass instead of oil for producing energy and chemicals”. *Energy Conversion and Management* 51.7 (2010). DOI: 10.1016/j.enconman.2010.01.015 (cit. on pp. 20–22, 76).

[Coum2022] F. J. A. G. Coumans et al. “Protection Strategies for the Conversion of Biobased Furanics to Chemical Building Blocks”. *ACS Sustainable Chemistry & Engineering* 10.10 (2022). DOI: 10.1021/acssuschemeng.1c06723 (cit. on p. 88).

[Cui2018] X. Cui, X. Zhao, and D. Liu. “A novel route for the flexible preparation of hydrocarbon jet fuels from biomass-based platform chemicals: a case of using furfural and 2,3-butanediol as feedstocks”. *Green Chemistry* 20.9 (2018). DOI: 10.1039/C8GC00292D (cit. on p. 27).

[Dahm2016] M. Dahmen and W. Marquardt. “Model-Based Design of Tailor-Made Biofuels”. *Energy & Fuels* 30.2 (2016). DOI: 10.1021/acs.energyfuels.5b02674 (cit. on p. 26).

[Dai2021] J. Dai, Y. Sun, and Z. Xiu. “Ionic liquid-based salting-out extraction of bio-chemicals”. *Chinese Journal of Chemical Engineering* 30.1 (2021). DOI: 10.1016/j.cjche.2020.11.004 (cit. on p. 27).

[Deli2014] I. Delidovich, K. Leonhard, and R. Palkovits. “Cellulose and hemicellulose valorisation: an integrated challenge of catalysis and reaction engineering”. *Energy & Environmental Science* 7.9 (2014). DOI: 10.1039/C4EE01067A (cit. on p. 27).

[Deng2016] H. Deng et al. “Probing Ion Transfer across Liquid-Liquid Interfaces by Monitoring Collisions of Single Femtoliter Oil Droplets on Ultramicroelectrodes”. *Analytical chemistry* 88.15 (2016). DOI: 10.1021/acs.analchem.6b01747 (cit. on p. 51).

[Di M2017] D. Di Marino et al. “Emulsion electro-oxidation of kraft lignin”. *Green Chemistry* 19.20 (2017). DOI: 10.1039/C7GC02115A (cit. on pp. 14, 51).

[Dick2014] J. E. Dick et al. “Electrogenerated chemiluminescence of common organic luminophores in water using an emulsion system”. *Journal of the American Chemical Society* 136.39 (2014). DOI: 10.1021/ja507198r (cit. on p. 51).

[Drab2017] P. Drabo et al. “Anionic Extraction for Efficient Recovery of Biobased 2,3-Butanediol-A Platform for Bulk and Fine Chemicals”. *ChemSusChem* 10.16 (2017). DOI: 10.1002/cssc.201700899 (cit. on p. 27).

[Drio2016] E. Drioli and L. Giorno. *Encyclopedia of Membranes*. Berlin, Heidelberg: Springer Berlin Heidelberg, 2016. DOI: 10.1007/978-3-662-44324-8 (cit. on pp. 16, 17, 78).

[Du2020] X. Du et al. “Electrochemical Lignin Conversion”. *ChemSusChem* 13.17 (2020). DOI: 10.1002/cssc.202001187 (cit. on p. 20).

[Eerh2012] A. J. J. E. Eerhart, A. P. C. Faaij, and M. K. Patel. “Replacing fossil based PET with biobased PEF; process analysis, energy and GHG balance”. *Energy & Environmental Science* 5.4 (2012). DOI: 10.1039/c2ee02480b (cit. on p. 76).

[Emer1982] R. R. Emerson, M. C. Flickinger, and G. T. Tsao. “Kinetics of dehydration of aqueous 2,3-butanediol to methyl ethyl ketone”. *Industrial & Engineering Chemistry Product Research and Development* 21.3 (1982). DOI: 10.1021/i300007a025 (cit. on p. 28).

[Fuhr2019] L. Fuhr. *Plastic atlas 2019: Facts and figures about the world of synthetic polymers*. Berlin: Heinrich Böll foundation, 2019 (cit. on p. 50).

[Gao2023] Y. Gao et al. “Electrocatalytic Refinery of Biomass-Based 5-Hydroxymethylfurfural to Fine Chemicals”. *ACS Catalysis* (2023). DOI: 10.1021/acscatal.3c02272 (cit. on p. 77).

[Gaus2020] M. Gausmann et al. “Recovery of succinic acid by integrated multiphase electrochemical pH-shift extraction and crystallization”. *Separation and Purification Technology* 240 (2020). DOI: 10.1016/j.seppur.2019.116489 (cit. on p. 52).

[Ge2022] R. Ge, J. Li, and H. Duan. “Recent advances in non-noble electrocatalysts for oxidative valorization of biomass derivatives”. *Science China Materials* 488 (2022). DOI: 10.1007/s40843-022-2076-y (cit. on p. 51).

[Geye2017] R. Geyer, J. R. Jambeck, and K. L. Law. “Production, use, and fate of all plastics ever made”. *Science advances* 3.7 (2017). DOI: 10.1126/sciadv.1700782 (cit. on p. 50).

[Grab1991] G. Grabowski, J. Lewkowski, and R. Skowroński. “The electrochemical oxidation of 5-hydroxymethylfurfural with the nickel oxide/hydroxide electrode”. *Electrochimica Acta* 36.13 (1991). DOI: 10.1016/0013-4686(91)85084-K (cit. on p. 51).

[Gray2006] K. A. Gray, L. Zhao, and M. Emptage. “Bioethanol”. *Current opinion in chemical biology* 10.2 (2006). DOI: 10.1016/j.cbpa.2006.02.035 (cit. on p. 76).

[Grde2012] M. Grdeń, M. Alsabet, and G. Jerkiewicz. “Surface science and electrochemical analysis of nickel foams”. *ACS applied materials & interfaces* 4.6 (2012). DOI: 10.1021/am300380m (cit. on p. 54).

[Grüt2023] C. Grütering et al. “Acetoin production by resting cells of Lactococcus lactis for direct electrochemical synthesis of 2-butanone”. *Green Chemistry* 25.22 (2023). DOI: 10.1039/D3GC02513F (cit. on pp. 32, 45).

[Hame2020] S. Hameed et al. “Recent Developments in Metal-Based Catalysts for the Catalytic Aerobic Oxidation of 5-Hydroxymethyl-Furfural to 2,5-Furandicarboxylic Acid”. *Catalysts* 10.1 (2020). DOI: 10.3390/catal10010120 (cit. on p. 50).

[Harh2022] T. Harhues et al. “Direct Electrosynthesis of 2-Butanone from Fermentation Supernatant”. *ACS Sustainable Chemistry & Engineering* 10.19 (2022). DOI: 10.1021/acssuschemeng.2c01971 (cit. on pp. 76, 77, 90).

[Harh2023] T. Harhues et al. “Integrated Biphasic Electrochemical Oxidation of Hydroxymethylfurfural to 2,5-Furandicarboxylic Acid”. *ACS Sustainable Chemistry & Engineering* 11.23 (2023). DOI: 10.1021/acssuschemeng.3c01403 (cit. on pp. 76, 88).

[Hauk2023] P. Hauke, S. Brückner, and P. Strasser. “Paired Electrocatalytic Valorization of CO 2 and Hydroxymethylfurfural in a Noble Metal-free Bipolar Membrane Electrolyzer”. *ACS Sustainable Chemistry & Engineering* 11.37 (2023). DOI: 10.1021/acssuschemeng.3c03144 (cit. on p. 77).

[Hege2018] S. Heger et al. “Comparative ecotoxicity of potential biofuels to water flea (Daphnia magna), zebrafish (Danio rerio) and Chinese hamster (Cricetulus griseus) V79 cells”. *The Science of the total environment* 631-632 (2018). DOI: 10.1016/j.scitotenv.2018.03.028 (cit. on p. 26).

[Hege2021] S. Heger et al. “Green toxicological investigation for biofuel candidates”. *The Science of the total environment* 764 (2021). DOI: 10.1016/j.scitotenv.2020.142902 (cit. on p. 26).

[Heym2020] B. Heyman et al. “Online monitoring of the respiratory quotient reveals metabolic phases during microaerobic 2,3-butanediol production with Bacillus licheniformis”. *Engineering in life sciences* 20.3-4 (2020). DOI: 10.1002/elsc.201900121 (cit. on pp. 28, 30, 32).

[Hoel2011] D. Hoell et al. “2-Butanone”. In*Ullmann’s encyclopedia of industrial chemistry*. Ed. by B. Elvers and F. Ullmann. Vol. 5. Weinheim: Wiley-VCH, 2011. P. 225. (Cit. on p. 26).

[Holz2017] F. J. Holzhäuser et al. “Electrocatalytic upgrading of itaconic acid to methylsuccinic acid using fermentation broth as a substrate solution”. *Green Chemistry* 19.10 (2017). DOI: 10.1039/C6GC03153F (cit. on p. 29).

[Holz2020] F. J. Holzhäuser, J. B. Mensah, and R. Palkovits. “(Non-)Kolbe electrolysis in biomass valorization – a discussion of potential applications”. *Green Chemistry* 22.2 (2020). DOI: 10.1039/C9GC03264A (cit. on p. 22).

[Hopp2016] F. Hoppe et al. “Tailor-Made Fuels from Biomass: Potentials of 2-butanone and 2-methylfuran in direct injection spark ignition engines”. *Fuel* 167 (2016). DOI: 10.1016/j.fuel.2015.11.039 (cit. on p. 26).

[Iban2016] J. G. Ibanez, B. A. Frontana-Uribe, and R. Vasquez-Medrando. “Paired Elecrochemical Processes: Overview, Systematizations, Selection Criteria, Design Strategies and Projection”. *J. Mex. Chem. Soc.* 60 (2016). (Cit. on pp. 13, 14, 77).

[Jens2020] M. H. Jensen and A. Riisager. “Advances in the synthesis and application of 2,5-furandicarboxylic acid”. In*Biomass, Biofuels, Biochemicals*. Elsevier, 2020. Pp. 135–170. (Cit. on pp. 50, 51).

[Jia2017] X. Jia et al. “Conversion of cellulose and hemicellulose of biomass simultaneously to acetoin by thermophilic simultaneous saccharification and fermentation”. *Biotechnology for biofuels* 10 (2017). DOI: 10.1186/s13068-017-0924-8 (cit. on p. 28).

[Jian2021] S. Jiang et al. “A comprehensive review on the synthesis and applications of ion exchange membranes”. *Chemosphere* 282 (2021). DOI: 10.1016/j.chemosphere.2021.130817 (cit. on p. 78).

[Jong2012a] E. de Jong et al. “Furandicarboxylic Acid (FDCA), A Versatile Building Block for a Very Interesting Class of Polyesters”. In*Biobased Monomers, Polymers, and Materials*. Ed. by P. B. Smith and R. A. Gross. Vol. 1105. ACS Symposium Series. Washington, DC: American Chemical Society, 2012. Pp. 1–13. (Cit. on p. 76).

[Jong2012b] E. de Jong et al. “Product developments in the bio-based chemicals arena”. *Biofuels, Bioproducts and Biorefining* 6.6 (2012). DOI: 10.1002/bbb.1360 (cit. on pp. 21, 50).

[Jong2022] E. de Jong et al. “The Road to Bring FDCA and PEF to the Market”. *Polymers* 14.5 (2022). DOI: 10.3390/polym14050943 (cit. on p. 50).

[Kand2016] V. Kandasamy et al. “Synthesis of (3R)-acetoin and 2,3-butanediol isomers by metabolically engineered Lactococcus lactis”. *Scientific reports* 6 (2016). DOI: 10.1038/srep36769 (cit. on pp. 28, 45).

[Kiat2022] W. Kiatkittipong et al. “Bioresources and biofuels—From classical to perspectives and trends”. In*A-Z of Biorefinery*. Elsevier, 2022. Pp. 165–220. (Cit. on p. 20).

[Kim2016] W. Kim et al. “2,3-Butanediol dehydration catalyzed by silica-supported sodium phosphates”. *Applied Catalysis A: General* 511 (2016). DOI: 10.1016/j.apcata.2015.11.043 (cit. on p. 26).

[Krol1998] J. Krol et al. “Behaviour of bipolar membranes at high current densityWater diffusion limitation”. *Separation and Purification Technology* 14.1-3 (1998). DOI: 10.1016/S1383-5866(98)00058-6 (cit. on p. 19).

[Lats2018] R. Latsuzbaia et al. “Continuous electrochemical oxidation of biomass derived 5-(hydroxymethyl)furfural into 2,5-furandicarboxylic acid”. *Journal of Applied Electrochemistry* 48.6 (2018). DOI: 10.1007/s10800-018-1157-7 (cit. on pp. 51, 52, 61, 66, 76, 88).

[Leow2023] W. R. Leow et al. “Electrified hydrocarbon-to-oxygenates coupled to hydrogen evolution for efficient greenhouse gas mitigation”. *Nature communications* 14.1 (2023). DOI: 10.1038/s41467-023-37382-3 (cit. on pp. 50, 77).

[Limp2022] A. Limper et al. “Additive manufacturing of composite porosity mixer electrodes”. *Electrochemistry Communications* 134 (2022). DOI: 10.1016/j.elecom.2021.107176 (cit. on pp. 51, 54, 69).

[LIU2006] Z. LIU et al. “Development and Commercial Application of Methyl-ethyl-ketone Production Technology”. *Chinese Journal of Chemical Engineering* 14.5 (2006). DOI: 10.1016/S1004-9541(06)60134-1 (cit. on p. 26).

[Liu2017] C. Liu et al. “Single Organic Droplet Collision Voltammogram via Electron Transfer Coupled Ion Transfer”. *Analytical chemistry* 89.17 (2017). DOI: 10.1021/acs.analchem.7b02072 (cit. on pp. 51, 63).

[Liu2020] X. Liu, D. C. Y. Leong, and Y. Sun. “The production of valuable biopolymer precursors from fructose”. *Green Chemistry* 22.19 (2020). DOI: 10.1039/D0GC02315A (cit. on p. 51).

[Liu2021] H. Liu et al. “Paired electrolysis of 5-(hydroxymethyl)furfural in flow cells with a high-performance oxide-derived silver cathode”. *Green Chemistry* 23.14 (2021). DOI: 10.1039/D1GC00988E (cit. on p. 77).

[Luo2023] J. Luo and T. L. Liu. “Electrochemical valorization of lignin: Status, challenges, and prospects”. *Journal of Bioresources and Bioproducts* 8.1 (2023). DOI: 10.1016/j.jobab.2022.11.003 (cit. on p. 22).

[Ma2009] C. Ma et al. “Enhanced 2,3-butanediol production by Klebsiella pneumoniae SDM”. *Applied microbiology and biotechnology* 82.1 (2009). DOI: 10.1007/s00253-008-1732-7 (cit. on p. 27).

[Main2021a] S. Maina et al. “Bioprocess Development for 2,3-Butanediol Production from Crude Glycerol and Conceptual Process Design for Aqueous Conversion into Methyl Ethyl Ketone”. *ACS Sustainable Chemistry & Engineering* 9.26 (2021). DOI: 10.1021/acssuschemeng.1c00253 (cit. on pp. 27, 29).

[Main2021b] S. Maina et al. “Prospects on bio-based 2,3-butanediol and acetoin production: Recent progress and advances”. *Biotechnology advances* (2021). DOI: 10.1016/j.biotechadv.2021.107783 (cit. on pp. 27, 29).

[Main2021c] S. Maina et al. “Volumetric oxygen transfer coefficient as fermentation control parameter to manipulate the production of either acetoin or D-2,3-butanediol using bakery waste”. *Bioresource technology* 335 (2021). DOI: 10.1016/j.biortech.2021.125155 (cit. on pp. 28, 29).

[Mass2022] M. C. Massaro and A. H. A. Monteverde. “Techno-Economic Analysis of FDCA Production through Electrocatalytic Processes”. *Journal of The Electrochemical Society* 169.5 (2022). DOI: 10.1149/1945-7111/ac6bc0 (cit. on pp. 51, 61, 77, 92).

[Mehr2019] C. R. Mehrer et al. “Growth-coupled bioconversion of levulinic acid to butanone”. *Metabolic engineering* 55 (2019). DOI: 10.1016/j.ymben.2019.06.003 (cit. on pp. 26, 27).

[Meys2021] R. Meys et al. “Achieving net-zero greenhouse gas emission plastics by a circular carbon economy”. *Science (New York, N.Y.)* 374.6563 (2021). DOI: 10.1126/science.abg9853 (cit. on pp. 1, 22, 50, 76).

[Mohd2017] M. Z. Mohd Yusoff et al. “Production of acetoin from hydrothermally pretreated oil mesocarp fiber using metabolically engineered Escherichia coli in a bioreactor system”. *Bioresource technology* 245.Pt A (2017). DOI: 10.1016/j.biortech.2017.08.131 (cit. on p. 28).

[Mukh2015] A. Mukherjee, M.-J. Dumont, and V. Raghavan. “Review: Sustainable production of hydroxymethylfurfural and levulinic acid: Challenges and opportunities”. *Biomass and Bioenergy* 72 (2015). DOI: 10.1016/j.biombioe.2014.11.007 (cit. on p. 50).

[Mult2012] A. Multer et al. “Production of Methyl Ethyl Ketone from Biomass Using a Hybrid Biochemical/Catalytic Approach”. *Industrial & Engineering Chemistry Research* 22 (2012). DOI: 10.1021/ie3007598 (cit. on p. 27).

[Naka1998] Y. Nakashimada, K. Kanai, and N. Nishio. “Optimization of dilution rate, pH and oxygen supply on optical purity of 2, 3-butanediol produced by Paenibacillus polymyxa in chemostat culture”. *Biotechnology Letters* 20.12 (1998). DOI: 10.1023/A:1005324403186 (cit. on pp. 32, 37).

[Ocho2019] J. R. Ochoa-Gómez et al. “Electrosynthesis of 2,3-butanediol and methyl ethyl ketone from acetoin in flow cells”. *Green Chemistry* 21.1 (2019). DOI: 10.1039/C8GC03028F (cit. on pp. 28–30, 35, 41, 43, 76, 90).

[Pand2021] S. Pandey et al. “Biobased 2,5-furandicarboxylic acid (FDCA) and its emerging copolyesters’ properties for packaging applications”. *European Polymer Journal* 160 (2021). DOI: 10.1016/j.eurpolymj.2021.110778 (cit. on p. 76).

[Pärn2021] R. Pärnamäe et al. “Bipolar membranes: A review on principles, latest developments, and applications”. *Journal of Membrane Science* 617 (2021). DOI: 10.1016/j.memsci.2020.118538 (cit. on pp. 18, 19, 78, 86).

[Pärn2023] R. Pärnamäe et al. “Origin of Limiting and Overlimiting Currents in Bipolar Membranes”. *Environmental science & technology* 57.26 (2023). DOI: 10.1021/acs.est.2c09410 (cit. on p. 79).

[Pate2022] P. Patel et al. “Technoeconomic and Life-Cycle Assessment for Electrocatalytic Production of Furandicarboxylic Acid”. *ACS Sustainable Chemistry & Engineering* 10.13 (2022). DOI: 10.1021/acssuschemeng.1c08602 (cit. on pp. 51, 77, 92).

[Penn2017] D. Penner et al. “Conceptual Design of Methyl Ethyl Ketone Production via 2,3-Butanediol for Fuels and Chemicals”. *Industrial & Engineering Chemistry Research* 56.14 (2017). DOI: 10.1021/acs.iecr.6b03678 (cit. on p. 27).

[Pere2016] N. Perez. *Electrochemistry and Corrosion Science*. Cham: Springer International Publishing, 2016. DOI: 10.1007/978-3-319-24847-9 (cit. on p. 8).

[Pour1974] M. Pourbaix. *Atlas of electrochemical equilibria in aqueous solutions*. 2d English ed. Houston, Tex.: National Association of Corrosion Engineers, 1974 (cit. on p. 86).

[Qian2023] Y. Qiang et al. “Liquid flow fuel cell with an electrodeposition-modified nickel foam anode for efficient oxidation of 5-hydroxymethylfurfural to produce 2, 5-furandicarboxylic acid with co-generation of electricity”. *Chemical Engineering Journal* 469 (2023). DOI: 10.1016/j.cej.2023.143832 (cit. on p. 77).

[Rabi2020] J. A. Rabinowitz and M. W. Kanan. “The future of low-temperature carbon dioxide electrolysis depends on solving one basic problem”. *Nature communications* 11.1 (2020). DOI: 10.1038/s41467-020-19135-8 (cit. on p. 91).

[Rait2022] M. Raita et al., eds. *Lignocellulosic biomass and its potential derivative products*. Elsevier, 2022. DOI: 10.1016/B978-0-12-819248-1.00016-6 (cit. on p. 21).

[Reic2020] C. L. Reichert et al. “Bio-Based Packaging: Materials, Modifications, Industrial Applications and Sustainability”. *Polymers* 12.7 (2020). DOI: 10.3390/polym12071558 (cit. on p. 76).

[Ronc2017] T. Roncal et al. “Efficient production of acetoin by fermentation using the newly isolated mutant strain Lactococcus lactis subsp. lactis CML B4”. *Process Biochemistry* 58 (2017). DOI: 10.1016/j.procbio.2017.04.007 (cit. on p. 27).

[Rose2020] C. Rosenfeld et al. “Current Situation of the Challenging Scale-Up Development of Hydroxymethylfurfural Production”. *ChemSusChem* 13.14 (2020). DOI: 10.1002/cssc.202000581 (cit. on p. 50).

[Saha2014] B. Saha and M. M. Abu-Omar. “Advances in 5-hydroxymethylfurfural production from biomass in biphasic solvents”. *Green Chem* 16.1 (2014). DOI: 10.1039/C3GC41324A (cit. on p. 50).

[Saji2018] M. Sajid, X. Zhao, and D. Liu. “Production of 2,5-furandicarboxylic acid (FDCA) from 5-hydroxymethylfurfural (HMF): recent progress focusing on the chemical-catalytic routes”. *Green Chemistry* 20.24 (2018). DOI: 10.1039/C8GC02680G (cit. on p. 50).

[Salv2021] D. A. Salvatore et al. “Designing anion exchange membranes for CO2 electrolysers”. *Nature Energy* 6.4 (2021). DOI: 10.1038/s41560-020-00761-x (cit. on p. 78).

[Sánc2021a] E. Sánchez-Ramírez et al. “Intensified alternative to purify methyl-Ethyl ketone in a framework of green process”. *Energy* 220 (2021). DOI: 10.1016/j.energy.2020.119641 (cit. on p. 27).

[Sánc2021b] E. Sánchez-Ramírez et al. “Synthesis and Optimization of Sustainable Processes Based on Liquid-Liquid Extraction to Purify Methyl Ethyl Ketone”. *Chemical Engineering and Processing - Process Intensification* 86 (2021). DOI: 10.1016/j.cep.2021.108522 (cit. on p. 27).

[Schm2003] V. M. Schmidt. *Elektrochemische Verfahrenstechnik: Grundlagen, Reaktionstechnik, Prozeßoptimierung*. Weinheim: Wiley-Blackwell, 2003 (cit. on pp. 1, 8–12, 14–16, 18).

[Schr2015] U. Schröder, F. Harnisch, and L. T. Angenent. “Microbial electrochemistry and technology: terminology and classification”. *Energy & Environmental Science* 8.2 (2015). DOI: 10.1039/C4EE03359K (cit. on p. 29).

[Schw2022] K. Schwabe. *Physikalische Chemie: Band 2: Elektrochemie*. 3., bearbeitete und erweiterte Auflage, Reprint 2021. Vol. Band 2. Physikalische Chemie. Berlin and Boston: De Gruyter, 2022. DOI: 10.1515/9783112480403 (cit. on p. 14).

[Shen2022] T. Shen et al. “Production of 100% bio-based semi-aromatic nylon by aerobic oxidation of 5-hydroxymethylfurfural to 2,5-furandicarboxylic acid with bio aliphatic diamine”. *Chemical Engineering Journal* 437 (2022). DOI: 10.1016/j.cej.2022.135361 (cit. on p. 50).

[Shin2020] S. H. Shinde, A. Hengne, and C. V. Rode. “Lignocellulose-derived platform molecules”. In*Lignocellulose-derived platform molecules*. Ed. by S. H. Shinde, A. Hengne, and C. V. Rode. Elsevier, 2020. Pp. 1–31. (Cit. on pp. 1, 19–21).

[Shol2016] D. S. Sholl and R. P. Lively. “Seven chemical separations to change the world”. *Nature* 532.7600 (2016). DOI: 10.1038/532435a (cit. on p. 23).

[Smit2007] T. J. Smith and K. J. Stevenson. “Reference Electrodes”. (2007). DOI: 10.1016/B978-044451958-0.50005-7 (cit. on p. 9).

[Smit2023] S. M. de Smit et al. “Trace metals from microbial growth media form in situ electro-catalysts”. *Electrochimica Acta* 462 (2023). DOI: 10.1016/j.electacta.2023.142722 (cit. on pp. 29, 47).

[Stie2015] S. Stiefel et al. “Controlled depolymerization of lignin in an electrochemical membrane reactor”. *Electrochemistry Communications* 61 (2015). DOI: 10.1016/j.elecom.2015.09.028 (cit. on p. 51).

[Sun2020] Z. Sun et al. “Downstream Processing Strategies for Lignin-First Biorefinery”. *ChemSusChem* 13.19 (2020). DOI: 10.1002/cssc.202001085 (cit. on p. 20).

[Tafe1905] J. Tafel. “Über die Polarisation bei kathodischer Wasserstoffentwicklung”. *Zeitschrift für Physikalische Chemie* 50U.1 (1905). DOI: 10.1515/zpch-1905-5043 (cit. on p. 10).

[Tait2019] B. J. Taitt, D.-H. Nam, and K.-S. Choi. “A Comparative Study of Nickel, Cobalt, and Iron Oxyhydroxide Anodes for the Electrochemical Oxidation of 5-Hydroxymethylfurfural to 2,5-Furandicarboxylic Acid”. *ACS Catalysis* 9.1 (2019). DOI: 10.1021/acscatal.8b04003 (cit. on p. 51).

[Tanb2020] N. Tanbouza, T. Ollevier, and K. Lam. “Bridging Lab and Industry with Flow Electrochemistry”. *iScience* 23.11 (2020). DOI: 10.1016/j.isci.2020.101720 (cit. on p. 2).

[Tang2021] C. Tang et al. “Electrocatalytic Refinery for Sustainable Production of Fuels and Chemicals”. *Angewandte Chemie (International ed. in English)* 60.36 (2021). DOI: 10.1002/anie.202101522 (cit. on pp. 22, 76).

[Thio2017] S. Thion et al. “An experimental study in a jet-stirred reactor and a comprehensive kinetic mechanism for the oxidation of methyl ethyl ketone”. *Proceedings of the Combustion Institute* 36.1 (2017). DOI: 10.1016/j.proci.2016.05.022 (cit. on p. 26).

[Thon2022] N. Thongchul et al. “Overview of biorefinery”. In*A-Z of Biorefinery*. Elsevier, 2022. Pp. 3–32. (Cit. on pp. 21, 22).

[Toki2018] M. Tokic et al. “Discovery and Evaluation of Biosynthetic Pathways for the Production of Five Methyl Ethyl Ketone Precursors”. *ACS synthetic biology* 7.8 (2018). DOI: 10.1021/acssynbio.8b00049 (cit. on p. 27).

[Torr2020] L. Torres-Vinces et al. “Methyl Ethyl Ketone Production through an Intensified Process”. *Chemical Engineering & Technology* 43.7 (2020). DOI: 10.1002/ceat.201900664 (cit. on p. 26).

[Urba2017] C. Urban et al. “Production of drop-in fuels from biomass at high selectivity by combined microbial and electrochemical conversion”. *Energy & Environmental Science* 10.10 (2017). DOI: 10.1039/C7EE01303E (cit. on p. 29).

[Vehr2023] J. Vehrenberg et al. “Paired electrochemical synthesis of formate via oxidation of glycerol and reduction of CO2 in a flow cell reactor”. *Electrochemistry Communications* 151 (2023). DOI: 10.1016/j.elecom.2023.107497 (cit. on p. 77).

[Venn2019] J.-B. Vennekötter et al. “The electrolyte matters: Stable systems for high rate electrochemical CO2 reduction”. *Journal of CO2 Utilization* 32 (2019). DOI: 10.1016/j.jcou.2019.04.007 (cit. on pp. 14, 78).

[Wang2014] Z. Wang et al. “Improvement of acetoin reductase activity enhances bacitracin production by Bacillus licheniformis”. *Process Biochemistry* 49.12 (2014). DOI: 10.1016/j.procbio.2014.08.017 (cit. on p. 27).

[Werp2004] T. Werpy and G. Petersen. “Top Value Added Chemicals from Biomass: Volume I – Results of Screening for Potential Candidates from Sugars and Synthesis Gas”. 2004 (2004). DOI: 10.2172/15008859 (cit. on pp. 21, 50).

[Wint2022] B. Winter et al. “Sugar-to-What? An Environmental Merit Order Curve for Biobased Chemicals and Plastics”. *ACS sustainable chemistry & engineering* 10.48 (2022). DOI: 10.1021/acssuschemeng.2c03275 (cit. on pp. 1, 19, 22, 76).

[Xiao2012] Z. Xiao et al. “Thermophilic fermentation of acetoin and 2,3-butanediol by a novel Geobacillus strain”. *Biotechnology for biofuels* 5.1 (2012). DOI: 10.1186/1754-6834-5-88 (cit. on p. 28).

[Xiao2014] Z. Xiao and J. R. Lu. “Strategies for enhancing fermentative production of acetoin: a review”. *Biotechnology advances* 32.2 (2014). DOI: 10.1016/j.biotechadv.2014.01.002 (cit. on pp. 27, 29).

[Xu2023] Z. Xu et al. “Continuous ammonia electrosynthesis using physically interlocked bipolar membrane at 1000 mA cm-2”. *Nature communications* 14.1 (2023). DOI: 10.1038/s41467-023-37273-7 (cit. on pp. 18, 19, 78, 79, 90).

[Yang2017] T. Yang et al. “Metabolic engineering strategies for acetoin and 2,3-butanediol production: advances and prospects”. *Critical reviews in biotechnology* 37.8 (2017). DOI: 10.1080/07388551.2017.1299680 (cit. on p. 29).

[Yang2021] Y. Yang and T. Mu. “Electrochemical oxidation of biomass derived 5-hydroxymethylfurfural (HMF): pathway, mechanism, catalysts and coupling reactions”. *Green Chemistry* 23.12 (2021). DOI: 10.1039/D1GC00914A (cit. on p. 77).

[Yang2023] M. Yang et al. “Bifunctional bimetallic oxide nanowires for high-efficiency electrosynthesis of 2,5-furandicarboxylic acid and ammonia”. *Journal of colloid and interface science* 652.Pt A (2023). DOI: 10.1016/j.jcis.2023.08.079 (cit. on p. 77).

[Yone2014] H. Yoneda, D. J. Tantillo, and S. Atsumi. “Biological production of 2-butanone in Escherichia coli”. *ChemSusChem* 7.1 (2014). DOI: 10.1002/cssc.201300853 (cit. on p. 27).

[Yuan2020] H. Yuan et al. “Biocatalytic production of 2,5-furandicarboxylic acid: recent advances and future perspectives”. *Applied microbiology and biotechnology* 104.2 (2020). DOI: 10.1007/s00253-019-10272-9 (cit. on p. 50).

[Zhan2016a] B. Zhang et al. “Production of Acetoin through Simultaneous Utilization of Glucose, Xylose, and Arabinose by Engineered Bacillus subtilis”. *PloS one* 11.7 (2016). DOI: 10.1371/journal.pone.0159298 (cit. on p. 28).

[Zhan2016b] L. Zhang et al. “Biotechnological production of acetoin, a bio-based platform chemical, from a lignocellulosic resource by metabolically engineered Enterobacter cloacae”. *Green Chemistry* 18.6 (2016). DOI: 10.1039/C5GC01638J (cit. on p. 28).

[Zhan2017] H. Zhang et al. “Electrochemistry of single droplets of inverse (water-in-oil) emulsions”. *Physical chemistry chemical physics : PCCP* 19.24 (2017). DOI: 10.1039/c7cp03300a (cit. on p. 63).

[Zhan2021] H. Zhang et al. “Development of High-Molecular-Weight Fully Renewable Biopolyesters Based on Oxabicyclic Diacid and 2,5-Furandicarboxylic Acid: Promising as Packaging and Medical Materials”. *ACS Sustainable Chemistry & Engineering* 9.19 (2021). DOI: 10.1021/acssuschemeng.1c01055 (cit. on pp. 50, 76).

[Zhen2019] J. Zheng and S. Suh. “Strategies to reduce the global carbon footprint of plastics”. *Nature Climate Change* 9.5 (2019). DOI: 10.1038/s41558-019-0459-z (cit. on p. 50).

[Zhou2018] X. Zhou et al. “Improving the performance of cell biocatalysis and the productivity of acetoin from 2,3-butanediol using a compressed oxygen supply”. *Process Biochemistry* 64 (2018). DOI: 10.1016/j.procbio.2017.09.027 (cit. on p. 28).

[Zhu2016] C. Zhu et al. “Production of liquid hydrocarbon fuels with acetoin and platform molecules derived from lignocellulose”. *Green Chemistry* 18.7 (2016). DOI: 10.1039/C5GC02414E (cit. on pp. 43, 87).